

Alma Mater Studiorum – Università di Bologna

DOTTORATO DI RICERCA IN  
INGEGNERIA ELETTROTECNICA

Ciclo XXIX

**Settore Concorsuale di afferenza: 09E1**

**Settore Scientifico disciplinare: INGIND/31**

Sterilization by means of a surface Dielectric Barrier Discharge: effects of  
Electro-Hydro-Dynamics and reactive species.

**Presentata da: Paolo Seri**

**Coordinatore Dottorato**  
**Prof. Domenico Casadei**

---

**Relatore**  
**Prof. Carlo Angelo Borghi**

---

**Esame finale anno 2017**



DOTTORATO DI RICERCA IN 1

**1 PLASMA: A QUICK GUIDE** **1**

---

**1.1 BASIC PLASMA INTERACTIONS** **3**

1.1.1 COLLISIONAL PROCESS 3

1.1.2 ELECTRONIC SOURCES 5

1.1.3 RECOMBINATIONS 5

1.1.4 NEUTRALS EXCITATION AND DISSOCIATION 6

**1.2 DIFFERENT TEMPERATURES OF A NON-THERMAL PLASMA** **7**

**2 DIELECTRIC BARRIER DISCHARGES** **9**

---

**2.1 DISCHARGE DYNAMIC** **10**

**2.2 DBD DISCHARGES POWERED BY A SINUSOIDAL VOLTAGE** **12**

2.2.1 FIRST QUARTER 12

2.2.2 SECOND QUARTER 13

2.2.3 THIRD AND FOURTH QUARTERS 13

**2.3 ATMOSPHERIC PRESSURE GLOW DISCHARGES** **14**

**3 PLASMA CHEMISTRY OF DBD PLASMAS IN AIR** **15**

---

**3.1 O<sub>3</sub> SYNTHESIS** **15**

**3.2 NO SYNTHESIS** **15**

**3.3 O<sub>3</sub> AND NO<sub>x</sub> INTERACTION** **16**

**4 PLASMA STERILIZATION** **18**

---

**4.1 CONVENTIONAL METHODS** **18**

4.1.1 TEMPERATURE BASED STERILIZATION 18

4.1.2 CHEMICAL STERILIZATION 18

4.1.3 RADIATION STERILIZATION 18

4.1.4 MECHANICAL METHODS 19

**4.2 COLD PLASMA STERILIZATION** **19**

4.2.1 DIRECT AND INDIRECT TREATMENTS 19

4.2.2 EFFECTS OF NEUTRAL SPECIES 20

4.2.3 EFFECTS OF CHARGED PARTICLES 20

4.2.4 EFFECTS OF THE ELECTRIC FIELD 22

4.2.5 THERMAL EFFECTS 23

4.2.6 UV RADIATION EFFECTS 23

**4.3 AIM OF THIS WORK** **23**

<b>5</b>	<b>VARIABLES OF A PLASMA STERILIZATION SYSTEM</b>	<b>25</b>
5.1	ELECTRO-HYDRO-DYNAMIC EFFECTS	25
5.2	EFFECTS OF METHODS AND MATERIALS	26
5.3	EFFECTS OF PLASMA'S CHEMICAL COMPOSITION	28
<b>6</b>	<b>GEOMETRICAL EFFECTS ON THE ELECTRO-HYDRO-DYNAMIC EFFECT</b>	<b>29</b>
6.1	INTRODUCTION TO THE ELECTRO-HYDRO-DYNAMIC EFFECT	29
6.2	ANNULAR DESIGN	32
6.3	EXPERIMENTAL SETUP AND RESULTS	34
6.3.1	POWER MEASUREMENT	34
6.3.2	STREAMERS LENGTH AND PLASMA AREA	36
6.3.3	SCHLIEREN INVESTIGATION	38
6.3.4	VELOCITY PROFILES	40
6.4	CONCLUSIONS	41
6.5	FINAL REACTOR'S GEOMETRY	42
<b>7</b>	<b>A REFERENCE PROTOCOL</b>	<b>43</b>
7.1	REFERENCE BIOLOGICAL AGENT	43
7.1.1	PREPARATION OF THE B. SUBTILIS SPORES STOCK	44
7.1.2	PREPARATION OF MRSA CULTURES	44
7.2	COMPARISON OF RESULTS FROM FILTRATION AND PIPETTING PROCEDURES	45
7.2.1	FILTERING PROTOCOL	45
7.2.2	PIPETTING PROTOCOL	47
7.2.3	COMPARISON OF THE FILTERING AND PIPETTING PROCEDURES	49
7.3	CELLS RECOVERY	50
7.4	UV INACTIVATION OF B. SUBTILIS AND MRSA	51
7.5	PLASMA INACTIVATION OF B. SUBTILIS AND MRSA	53
7.5.1	DBD REACTOR DESIGN	53
7.5.2	PLASMA SOURCE AND ELECTRIC MEASUREMENTS	53
7.5.3	REACTOR'S TEMPERATURES	54
7.5.4	RESULTS OF THE PLASMA INACTIVATION TESTS	54
7.6	CONCLUSIONS	55
<b>8</b>	<b>INFLUENCE OF DIFFERENT PRODUCTS ON ATMOSPHERIC AIR DBD PLASMA STERILIZATION</b>	<b>57</b>
8.1	REACTOR'S DISCHARGE CHARACTERIZATION	58
8.1.1	DEFINITION OF TWO OPERATING CONDITIONS	59
8.1.2	INFLUENCE OF POWER ON TEMPERATURE	59
8.1.3	INFLUENCE OF POWER ON CHEMISTRY	59
8.1.4	FTIR MEASUREMENTS	60
8.1.5	CHEMICAL DOSES	64
8.2	PLASMA SANITIZATION PROCESS	67

**8.3 CONCLUSIONS 68**

**9 CONCLUSIONS 69**

---

**10 BIBLIOGRAPHY 71**

---

## CHAPTER 1

### 1 PLASMA: A QUICK GUIDE

This section is *not* a complete review of plasma physics and chemistry. It will however be more than enough to allow any reader to understand the following chapters.

Plasma is defined as a globally neutral volume of ionized gas. It is a state of the matter resulting from the introduction of a proper amount of energy inside a gaseous system (Figure 1).

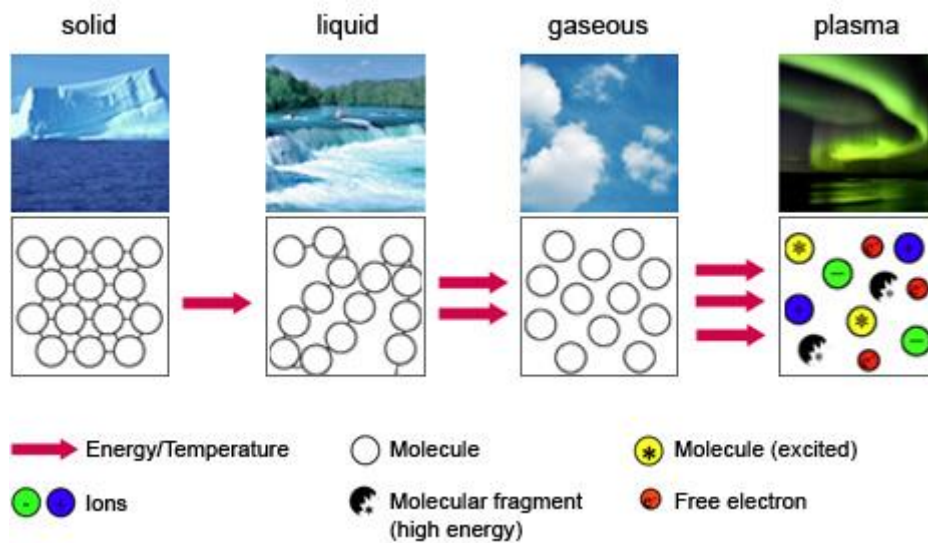


Figure 1 – How a plasma is formed and composed

Plasma is firstly present in nature. Stars and nebulas are made of plasma, and most of the known universe is made out of it. Its abundance on earth is relatively small, but it can still be observed in thunders and auroras.

Since not *all* the particles inside a gas must necessarily be in an ionized state for it to be defined as a plasma, we can distinguish various types of plasmas, from weakly to heavily ionized.

Another fundamental parameter that defines a plasma is the mean energy of its elements<sup>1</sup>. We usually refer to energy as a temperature, since temperature is a concept strictly linked with the agitation of a particle on the atomic or molecular level.

Inside a plasma we can distinguish two main categories of particles: electrons (low weight) and heavy weight particles. Therefore, we can also define two different temperatures describing their respective energy levels:  $T_e$  and  $T_H$ .

---

<sup>1</sup> In three-dimensional space an atom or a molecule can be associated with a set of so-called degrees of freedom, that defines their freedom of movement. Those sets can always be affiliated to translations, rotations, and vibrations. We can determine the amount of energy associated with each one of those movements, and then define the internal energy as the sum of the average energies associated with each degree of freedom.

The huge mass difference between electrons and other heavier particles means that their respective dynamics have profoundly different time scales. Inside a plasma, energy from an electric field is almost exclusively used to accelerate electrons. They will in turn transfer such energy to heavier particles via different mechanisms. This is why electrons can be found at higher energy levels than the heavy particles. We therefore define a hot (or thermal) plasma when  $T_e = T_H$  and a cold (or non-thermal) plasma when  $T_e \gg T_H^2$ .

The energetic (and thermal) equilibrium can be reached only maintaining constant conditions for a proper amount of time while preventing any energy removal (i.e. cooling) from the plasma volume.

Since the global temperature of any medium is defined by the mean temperature weighted on the mass of each particle inside said volume, a non-thermal plasma has actually relatively cold global temperatures ( $300 \div 1000$  K) if compared to the hot plasmas ones ( $10^4 \div 10^8$  K). This is why cold plasmas are usually preferred when working with biological or microbiological materials, despite their lower energetic content and density. In general, hot plasmas are usually more powerful, while cold plasmas allow for more selective treatments (Figure 2).

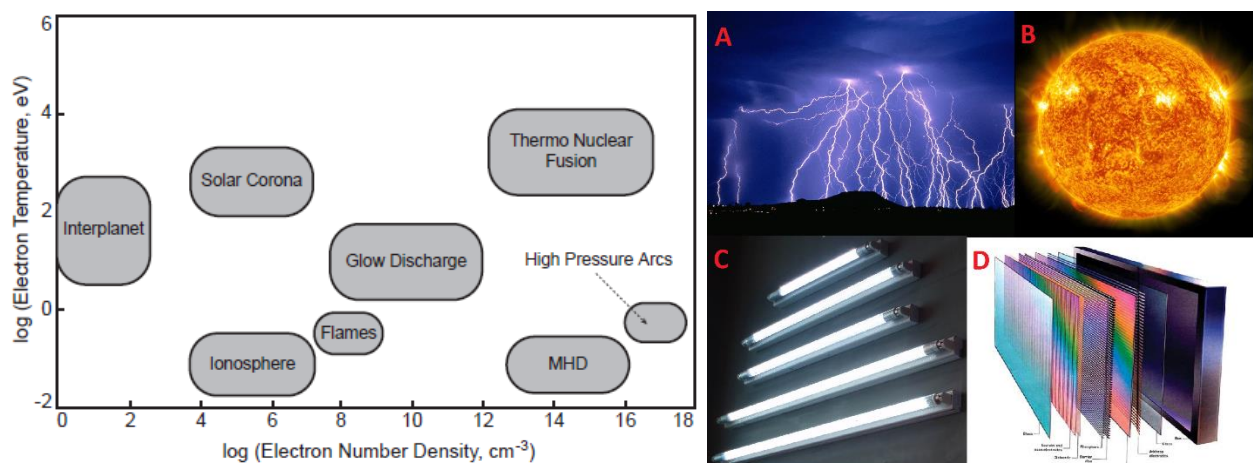


Figure 2 – On the left, different kind of plasmas are defined as a function of temperature and electron density. On the right, common natural hot plasmas (pictures A: thunders and B: stars) and artificial cold plasmas (pictures C: fluorescent lights and D: plasma monitors) are displayed.

The generation of a discharge inside a chemically inert gas produces a relevant quantity of chemically active ionic and atomic species. Free electrons and ions inside a plasma can easily break the atomic bonds keeping the reagents' molecules and atoms together, inducing several chemical reactions or atomic processes that would usually require high activation energies. Those reactive species can strongly interact with surfaces modifying their superficial energy and the properties connected with it (i.e. wettability). Plasma can also induce the formation of thin polymeric film layers or other nanostructures (plasma deposition and nanofabrication). Another application of plasma discharges can be found in visible or UV light emitting sources, such as in fluorescent lamps or old plasma monitors.

<sup>2</sup> This concept will be further discussed in section 1.2.

The interaction of a discharge with a surface can also remove certain impurities or inactivate microorganisms, allowing for plasma cleaning and sterilization processes, which is the main topic of this thesis.

There are several ways we can introduce energy into a system in order to generate plasma, but all of them can be indexed to either thermal or electrical processes. In this study we will only focus on the latter. The mechanism behind plasma generation involves the acceleration of naturally occurring free electrons by an electric field. Such electrons will in turn collide with heavier particles (atoms and molecules), eventually causing their ionization. Rules and limits of this system will be discussed in the next section.

## 1.1 BASIC PLASMA INTERACTIONS

The most important process needed to generate any plasma is ionization. It occurs from the interaction between electrons and atoms or molecules. Ionization is possible whenever electrons gather enough energy from an electric field  $E$ , interacting with gaseous atoms or molecules.

We can define the Electron Energy Distribution Function (EEDF)  $f(\varepsilon)$  as the *probability* for a given electron to be sitting at a certain energy level (Figure 3).  $f(\varepsilon)$  is influenced by the chemical composition of the plasma and its typology. Cold atmospheric plasmas are characterized by electron energies ranging from 1 to 10 eV, with mean values around 1 eV (Figure 3).

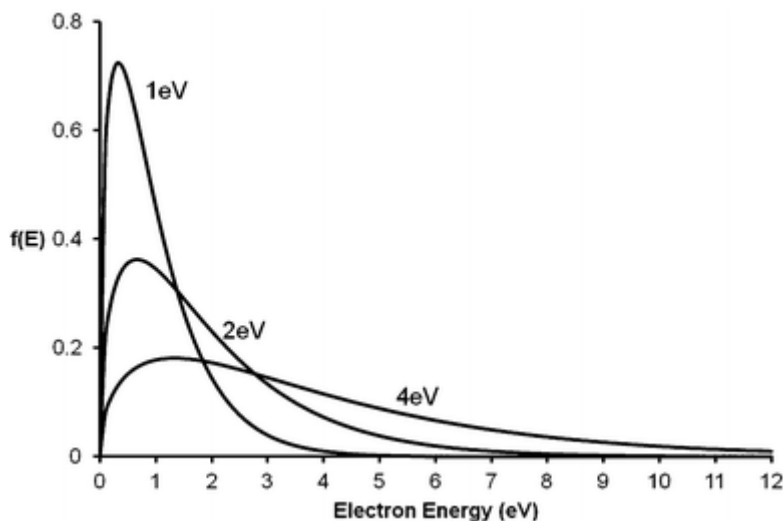


Figure 3 – Typical EEDF used in plasma modelling for plasmas of different average electron energy [1].

Those energy levels are capable of triggering chemical reactions via the excitation of atomic and molecular species, they can break chemical links and cause radiative UV emissions. This is possible thanks to a number of possible interactions and processes, listed below.

### 1.1.1 Collisional process

Collisions can be elastic and inelastic. Both of them involve a redistribution of the kinetic energy and scattering, but only the latter allows for *internal* energy exchange, which is fundamental for an ionization to occur. In fact, every time an electron gathers and transfers an amount of energy  $\Delta\varepsilon$  higher than the atomic or molecular ionization potential  $I$ , a so-called direct ionization will occur<sup>3</sup>. This mechanism is the main player in the generation of all the cold plasmas we will study, where a high electric field and low energy heavy particles are usually involved.

-Cross section  $\sigma(\varepsilon)$

It is related to the *probability* for a given particle to interact with a target. It has the measurement unit of an area since it can be seen as the area around a target particle inside of which the presence of another particle (i.e. an electron) will surely generate an interaction between them. Cross section is strongly influenced by a particle's internal energy<sup>4</sup>.

-Mean free path  $\lambda$

It is the distance a particle A needs to travel in order to statistically have the chance to meet and interact with a particle B. This distance is inversely related to both the cross section and the B particle density.

-Interaction frequency  $\nu$

Is defined by the ratio between the velocity of a particle and its mean free path.

-Reaction rate  $w_{A+B}$

Is the number of collisions between A and B per time and volume unit. It is given by the product of the particle density and its interaction frequency.

-Transferred energy fraction  $\gamma$

It tells how energy is redistributed after a collision among two particles.  $\gamma$  is the fraction of energy that can be transferred from a high energy to a low energy particle. It can be demonstrated that this fraction depends from each particle's mass, following this formula:

$$\gamma = \frac{2m_a m_b}{(m_a + m_b)^2} \quad Eq. (1)$$

Since atoms are extremely light weighted if compared to atoms or ions nuclei, the only way for electronic collisions to effectively transfer energy is colliding with another electrode<sup>5</sup>. This way, part of the kinetic

---

<sup>3</sup> Thomson model describes the direct ionization probability as a cross section:  $\sigma_i = Z_v \frac{1}{(4\pi\varepsilon_0)^2} \frac{\pi e^4}{\varepsilon} \left( \frac{1}{I} - \frac{1}{\varepsilon} \right)$  [2]

Where  $Z_v$  is the valence electrons number. It can be noticed how this function reaches its maximum for  $\varepsilon = 2I$ . This means that higher electron energies will not necessarily increase the direct ionization phenomenon.

<sup>4</sup> In order to explain this phenomenon, let's consider a simplified case. Two charged particles can meet only if their kinetic energy  $\varepsilon$  is at least equal to the coulombian repulsion  $U$  they experience at a distance  $b$ . Therefore, only if:

$$U = \frac{q^2}{4\pi\varepsilon_0 b} \sim \varepsilon; \quad b \sim \frac{q^2}{4\pi\varepsilon_0 \varepsilon}$$

An interaction can occur also whenever one of those particles is found inside the other's cross section. This defines a relationship between  $\sigma$  and  $b$  that in turn describes how cross sections are usually influenced by particles' internal energy:  $\sigma = \pi b^2 = \frac{\pi q^4}{(4\pi\varepsilon_0 \varepsilon)^2}$

<sup>5</sup> Ionizations from a collision of an electrode with a heavy weighted particle is possible, but requires very high electron energy levels and it is statistically irrelevant in our typical applications.

energy from a free, accelerated electron, can be transferred into the excitation energy of a second electron that will in turn interact with other particles inside the plasma volume.

When the impacting electrons energy levels are not sufficient to generate direct ionization, stepwise ionization can occur. In this case, electrons firstly rise the atoms and molecules energy levels to their excited states, allowing for a *second* electronic impact to eventually induce the ionization of the excited particle. Lower mean energies are necessary to enable this process, since the ionization potential of an already excited atom or molecule is lower than the ionization potential of the same non-excited particle. This process goes by the name of “Penning effect” and is typically involved in thermal plasmas.

We can define four parameters to describe the collision and interaction between two particles (A and B):

Another interesting ionization mechanism is photoionization. It occurs when a photon with the correct amount of energy gets absorbed by a neutral atom or molecule. If the energy associated with the photon is higher than the neutral’s ionization potential, ionization can occur. It must be noticed that photons are not necessarily produced from an external source, but they’re often emitted by the disexcitation energy of an excited particle inside the plasma itself.

### 1.1.2 Electronic sources

Apart from naturally occurring free electrons, there are several additional sources that can be triggered inside a plasma volume.

One of those is thermionic emission. If a metallic surface is heated and reaches a relatively high temperature, a cloud of free electrons (with a negative spatial charge) is formed around it, up to the point when the negative spatial charge itself prevents further emissions. An electric field can accelerate this cloud towards the anode at a certain rate<sup>6</sup> (the higher the electric field, the higher this rate will be), preventing the saturation of this electronic emission.

Another important mechanism is secondary emission. It is mostly caused by the ionic bombardment of any surface. Anytime an ion strikes a surface, it can transfer some energy (always related to eq.(1)) to those superficial particles. If this energy fraction overcomes the particle’s ionization potential, electrons can be freed from the surface. Secondary emissions can be also given from the photoionization of a surface. Also electrons can give the same effect, but energies required make this path important only for low pressure, high frequency plasmas.

### 1.1.3 Recombinations

Free electrons and ions can recombine with other particles inside the plasma. There are three main possible paths.

-Electron-Ion recombinations

---

<sup>6</sup> The electric current  $j$  resulting from the displacement of this charge can be related to the electric field  $E$ , as  $j \propto \exp\left(-\frac{W}{T}\right)$ ;  $W \propto -\sqrt{E}$ , where  $W$  is the energy required to remove an electron from the metallic surface. Notice how  $W$  is decreased with increasing electric fields (Schottky effect), in turn increasing  $j$ .

With this recombination, an electron gets absorbed by an ion, resulting in one or more neutral particles which can be excited or not, depending on the energy balance. This recombination is common inside a molecular gas<sup>7</sup>.



This recombination removes a free electron from the plasma volume.

-Three-body recombinations

It involves two electrons and an ion. One electron is absorbed by the ion, elevating it to its excited state.



Excess energy can also be converted to an electron's kinetic energy. This recombination is prevalent in high temperature, high density plasmas.

-Radiative recombinations



It typically has a very low cross sections, and can substitute the three-body recombination (commonly in high temperature, low pressure plasmas).

#### 1.1.4 Neutrals excitation and dissociation

Atoms and molecules can be excited via translational, vibrational and rotational modes. Translational and vibrational excitations are respectively related to a particle's constant and periodic motion. *Rotational* excitation, as the name suggests, refers to the energy related to the angular momentum of a rotating particle (i.e. an ion). On the other hand, electrons trade their energy colliding with molecules and exciting their *vibrational* modes. The energy from those modes will in turn be converted into *translational* energy via collisional mechanisms, eventually resulting in the Joule heating of the gas. "Time scales of this energy transfer in atmospheric air are  $10 \div 100 \mu\text{s}$ . Cold plasmas are generated keeping typical discharge times lower than such values, preventing this conversion to happen" [5].

-Vibrational excitation

Molecular excitation from a vibrational state  $v_1$  to a higher level,  $v_2$ , does not happen purely via a collisional process, since Eq.(1) clearly shows it is not an efficient mechanism, due to the high difference in masses. In order for an excitation to happen, *resonant* processes<sup>8</sup>

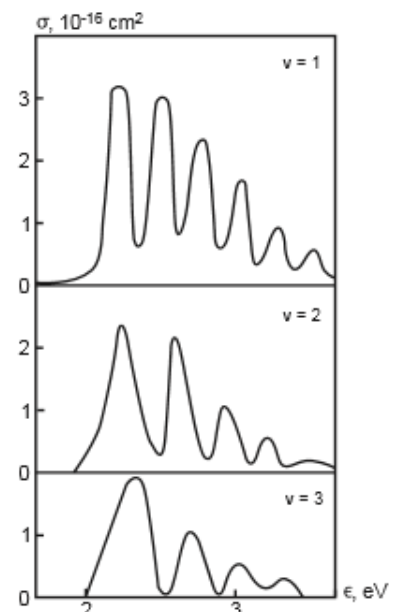


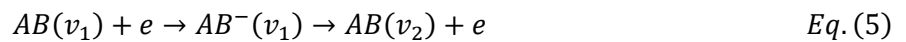
Figure 4 - Cross sections of vibrational excitation as a function of electron energy for different vibrational levels [2]

<sup>7</sup> Electron-ion recombinations can also occur inside an atomic gas, via an additional mechanism involving the atomic ions:  $A^+ + A + A \rightarrow A_2^+ + A$ ;  $e + A_2^+ \rightarrow A + A^*$

Electron-Ion recombination rate is inversely proportional to the electronic temperature:  $k_r^{ei} \propto \frac{1}{T_0 \sqrt{T_e}}$  [2]

<sup>8</sup> Especially high cross sections are found if the incoming particle transfers exactly the energy of a discrete state of the system. Resonances are found at such energies.

must be triggered (Figure 4), via a metastable negative ion and the following mechanism:



Typical resonant energy levels are found between 1 ÷ 3 eV: common levels for low-temperature plasmas.

-Rotational excitation

On the other hand, rotational excitation is usually a non-resonant mechanism happening at low energy levels (<1 eV). It can also follow resonant processes suit for higher energies, but in a less prevalent manner.

Excitation by electronic impact can also occur, but energies as high as 10 eV are needed. Electron impact is able to dissociate molecules by vibrational and electronic excitation. Dissociations of vibrationally excited neutrals are usually multi-step processes. It involves the energy exchange between particles that will eventually gather a sufficient *vibrational* energy level for a dissociation to happen. Rotationally excited particles undergo through direct electronic impact dissociations.

The general contribution of each excitation channel, for different reduced electric fields<sup>9</sup> (and therefore electron energy levels), is given in Figure 5<sup>10</sup>. In cold plasmas, vibrational excitation is preferred, and the majority of the input power eventually ends up being funnelled into this channel. Chemical reactions that are dependent on such kind of excitation are enhanced by the generation of a plasma.

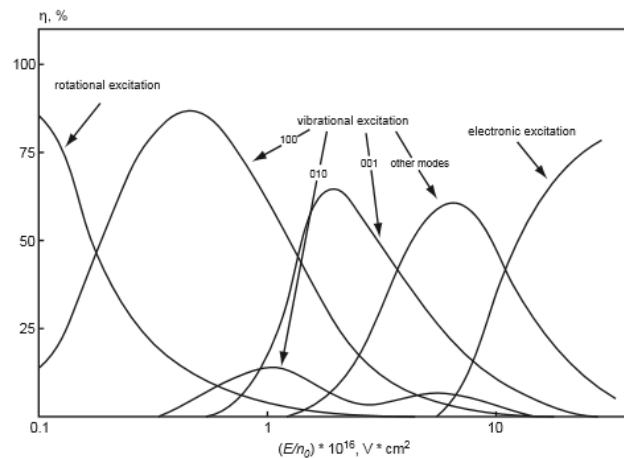


Figure 5 - Typical electron energy distribution between excitation channels as a function of the reduced electric field [2]

## 1.2 Different temperatures of a non-thermal plasma

*Temperature* is a parameter describing a particular distribution of states among various energy levels. Referring to it with only one intensity can be correct only when *all* degrees of freedom are equilibrated.

<sup>9</sup> The reduced field E/N is the ratio between the electric field E and the concentration of neutral particles N. It is often used because the mean energy of electrons (and therefore the discharge properties connected with it) is a function of E/N. Its unit of measurement is V cm<sup>2</sup>, but the Townsend unit (Td= 10<sup>-17</sup> V cm<sup>2</sup>) is frequently used. Typical values of E/N capable of triggering a breakdown are circa 100-200 Td, which means that for atmospheric pressure discharges we have to generate an electric field in the order of 10<sup>4</sup> V/cm.

<sup>10</sup> Different gasses have different behaviours, generally in agreement with this figure.

When different degrees of freedom are related to different energy levels, one can refer to different temperatures as well.

Since rotations and translations are strictly coupled (the energy exchange needed to establish a thermal equilibrium among them takes only a few collisions), they are often treated as having the same temperature: the “*rotational*” temperature  $T_{rot}$ . This temperature can sometimes be measured via emission spectroscopy<sup>11</sup>, and since the temperature of a gas is a measure of the average translational kinetic energy of the molecules, it is also considered to be equal to the macroscopic gas temperature<sup>12</sup>,  $T_{gas}$ . Non-equilibrium plasmas are characterized by gas temperatures very close to room temperatures:

$$T_{gas} \sim 300 \text{ K}$$

(when using room temperature working gases to begin with) and this is extremely useful and sometimes necessary when working with heat sensitive materials such as biologic matter or biomaterials.

On the other hand, we’ve already discussed how vibrational energy exchange with the environment is more difficult. Vibrations take longer to equilibrate thermally with the rotations and translations, thus are often treated as being at a different temperature: the “*vibrational*” temperature  $T_{vib}$ . Non-equilibrium plasmas have typically:

$$T_{vib} \sim 3000 \text{ K}$$

Since in cold plasmas electronic energy levels are different again (and can have complicated energy exchange mechanisms), an “*electronic* temperature”  $T_{el}$  can also be identified, which describes the distribution of the electronic energy levels. In non-equilibrium plasmas common values are found to be:

$$T_{el} \sim 9000 \text{ K}$$

In conclusion, in non-equilibrium plasmas one can always suppose that:

$$T_{gas} \sim T_{tr} = T_{rot} < T_{vib} < T_{el}$$

---

<sup>11</sup> “The gas temperature in non-equilibrium plasmas is often obtained from the plasma-induced emission by measuring the rotational temperature of a diatomic molecule in its excited state. This is motivated by both tradition and the availability of low budget spectrometers” [3].

<sup>12</sup> “However, non-thermal plasmas do not automatically guarantee that the rotational distribution in the monitored vibrational level of the diatomic molecule is in equilibrium with the translational (gas) temperature” [3].

## CHAPTER 2

### 2 DIELECTRIC BARRIER DISCHARGES

During the last years, plasma applications had the tendency to migrate from low-pressure discharges towards atmospheric pressure ones. This is due to the high financial and practical burden a vacuum system usually carries. Low pressure plasmas are more thermally stressful on materials, and the maximum treatable volume is limited by the vacuum chamber's dimensions (therefore its cost).

Atmospheric pressure plasmas are free from such issues. Treating large and complex geometries with this kind of plasmas remains an engineering challenge, but the solutions often found are cheaper and have an easier setup and layout than the low-pressure alternative. As previously discussed (section 1.2), low macroscopic temperatures and high electronic ones allow for the production of high reactive particles' density (higher than low-pressure plasmas) with no thermal stresses for materials in contact with the plasma.

However, this technology has also its drawbacks. Non-thermal plasmas are more difficult to control in terms of their internal parameters and stability (they are, by definition, *non-equilibrium* plasmas). Higher pressures also involve higher "breakdown" voltages (which is the voltage needed in order to initiate a discharge in a given gaseous gap<sup>13</sup>) and plasma frequencies (a parameter that defines the tendency of the plasma to re-establish each particles' neutrality<sup>14</sup>).

Physicists and engineers developed several different atmospheric plasma sources (i.e. corona discharges, RF discharges, etc...), but this chapter will focus only on the Dielectric Barrier Discharges (DBDs), since those are the ones used throughout this thesis.

First reported by Ernst Werner von Siemens in 1857 as a novel type of electrical gas discharge that could generate ozone from atmospheric-pressure oxygen or air [4], DBDs were historically used for industrial ozone production. Nowadays they have a vast field of interest, ranging from polymers and textiles surface treatments for improved wettability, to pollutant reduction, biomedical applications, excimer UV sources, high-power CO<sub>2</sub> lasers and plasma TVs.

As the name suggests, a DBD is generated by two electrodes facing each other with one or more dielectric and gaseous layers between them. The fundamental role of the dielectric layer will be cleared in section 2.1.

---

<sup>13</sup> For each gas or gas mixture, breakdown voltages are related to the pressure of the gas and the dimension of the gaseous gap one wants to ignite a discharge into.

<sup>14</sup> As seen in section 1.1.1, collisions can neutralize a particle's charge, and plasma frequency is related to the collisions' frequency. A more collisional plasma, like atmospheric pressure ones, have higher chances to neutralize its particles in a shorter time period [2].

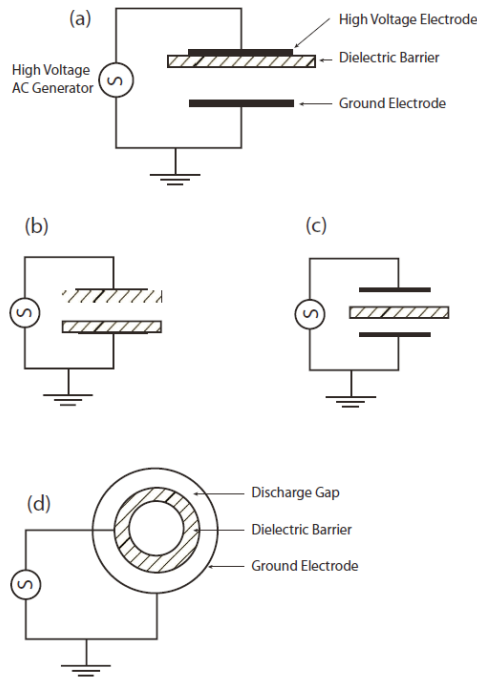


Figure 6 - Common configurations of the dielectric-barrier discharges (DBDs): planar (a,b,c), cylindrical (d).

Several common geometries are shown in Figure 6. The simplest DBD configuration is the same as a parallel plates capacitor: two parallel electrodes with a hollow discharge gap ( $d_g$ ) filled with a gas and at least one dielectric layer in between ( Figure 7).

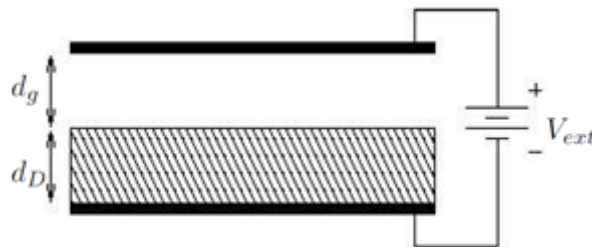


Figure 7 – Simple parallel plates DBD device

## 2.1 Discharge dynamic

As soon as the electrodes are powered with a voltage overcoming the breakdown  $V_b$ ,

$$V_{ext} > V_b = E_b \cdot d_g ; E_b \sim 30 \frac{kV}{cm} \text{ in air} \quad Eq. (6)$$

the discharge will ignite inside the gap. The main purpose of the dielectric barrier is to limit the electric current intensity during the discharge in a non-dissipative way.

We can imagine the DBD dynamics as a series of the following steps:

-Local discharge ignition: wherever the electric field overcomes the breakdown conditions, due to its intensity fluctuation, or a local electrodes' imperfection, ionizations start to happen. A cloud of negative electrons and positive ions is formed near the cathode surface.

-Spatial charge separation: since electrons have a higher mobility due to their lower mass, they are rapidly accelerated towards the anode by the electric field, while ions remain in a relatively stationary position. A spatially non uniform charge distribution will start to grow inside the ionized gap.

-Streamer formation: such non-uniform charge distribution will distort the initial electric field, locally increasing it in the proximity of the negative side of this charged cloud, generating more ionization. This positive feedback will generate an ionization wave, or "streamer", that will proceed like an avalanche towards the anode, with extremely fast dynamics.

-Streamer propagation: streamers are linked to non-uniformities in the spatial charge distribution. They can propagate from the cathode towards the anode as discussed, but also the opposite can happen. While the negative head of the streamer travels towards the anode, a positively charged region near the cathode is left behind. This positive non-uniformity will trigger a cathode-oriented streamer with similar dynamics as the ones already discussed (Figure 8).

-Charge build up and discharge quenching: charges from the streamer are deposited onto the dielectric superficial layer. While charges rapidly build up and arrange themselves on the dielectric, the resulting reduction of the local electric, to the point that  $V_{locally} < V_b$ , eventually quenching the discharge and preventing the discharge formation in the vicinity.

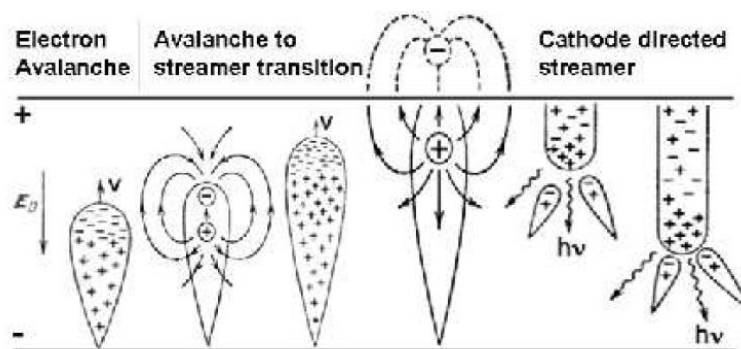


Figure 8 – Time evolution of a DBD microdischarge showing the electronic avalanche generation near the cathodic region, followed by a streamer towards the anode, and a cathode directed streamer afterwards [7].

In this discussion, micro-discharges have been considered as a single entity. In reality a DBD has thousands of them even inside a limited cross section (< 100  $\mu\text{m}$  in diameter [2]). Different micro-discharges will rapidly develop (circa 10 ns) and interact with each other, competing in charge deposition. They are also influenced by how the charge deposition happens in space [8]. Each micro-discharge will tend to generate in a different position, since the deposited charge from previous discharges have lowered the electric field in a stochastic way. Additionally, the superficial charge deposition and self-rearrangement happens on a spatially bigger dimension. This will help creating a more homogeneous plasma. In a similar way, dielectric regions where a bigger charge build up is present, become a preferential site of charge ignition during the negative slope of an AC voltage.

## 2.2 DBD discharges powered by a sinusoidal voltage

The same rules are typically followed even supplying the electrodes with an alternating voltage, since high voltage power supplies' common frequencies range from 10s to 100s of kHz, while a micro-discharge development is orders of magnitude faster.

An important aspect to be considered is whether the characteristic period of an AC supply,  $T$ , can be comparable with the plasma recombination time,  $\tau_r$ . Plasma recombination progressively reduces the amount of free charges inside the micro-discharge channel, reducing its conductivity. Supposing  $\tau_r \ll T$  we can analyse what happens when an AC supply is used.

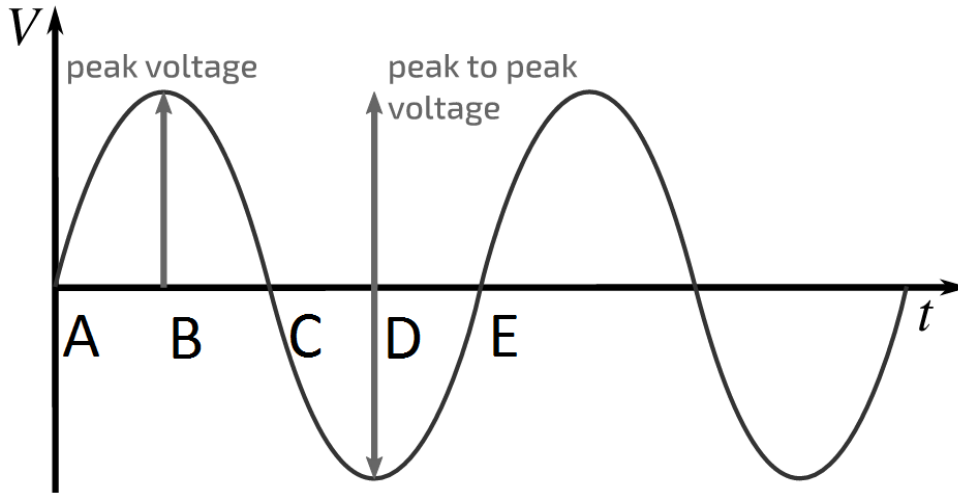


Figure 9 – Sinusoidal voltage and definitions.

When the voltage is rising during the first quarter of the sinusoidal cycle (A-B in Figure 9), the first micro-discharge starts to happen as soon as  $V = V_{min}$ . After the first microdischarge has completely developed, charges will be deposited on the dielectric layer, and recombination will make the gaseous gap a non-conductive medium again. In this instant, the gap, dielectric and supplied voltage are:

$$V_g = 0; V_d = V_{min}; V = V_{min} \quad Eq. (7)$$

$$V_g = V - V_d = V - V_{min} \quad Eq. (8)$$

### 2.2.1 First quarter

During the first quarter, supplied voltage is increasing. A second discharge will happen if  $V_g = V_{min}$ , which corresponds to an electrode voltage  $V = 2V_{min}$ . After the second micro-discharge has completed its life cycle, this mechanism will repeat itself until the voltage will eventually stop increasing, at the end of the first quarter (B). At this instant, applied voltage has reached its maximum  $V_0$ , and a number of microdischarges in the range of

$$N_1 = \frac{V_0 - V_{min}}{V_{min}} \quad Eq. (9)$$

have developed.

### 2.2.2 Second quarter

During the second quarter (B-C in Figure 9), the same events with opposite directions will characterize the discharge. At the instant B, as said,  $V = V_0$ , and a sufficient number of charges have deposited on the dielectric layer so that  $V_g = 0$ . In this quarter, voltage is progressively lowered. A microdischarge event will happen when

$$V_g = V - V_d = V - V_0 = -V_{min} \quad Eq. (10)$$

which is a condition met for:

$$V = V_0 - V_{min} \quad Eq. (11)$$

This time, a discharge will start from the dielectric layer charge buildup towards the cathode. This process will, again, repeat itself until the applied voltage will stop decreasing. During the second quarter,

$$N_2 = \frac{V_0 - V_{min}}{V_{min}} = N_1 \quad Eq. (12)$$

discharges will have been created.

### 2.2.3 Third and fourth quarters

The third and fourth quarters (C-E in Figure 9) will symmetrically reproduce the same flow of events as discussed during the first and second quarters. After one complete sinusoidal cycle,  $4N_1$  discharges will have fully developed. Fast ignition and quenching of the discharge can be inferred by voltage-current time behaviour reported in Figure 10.

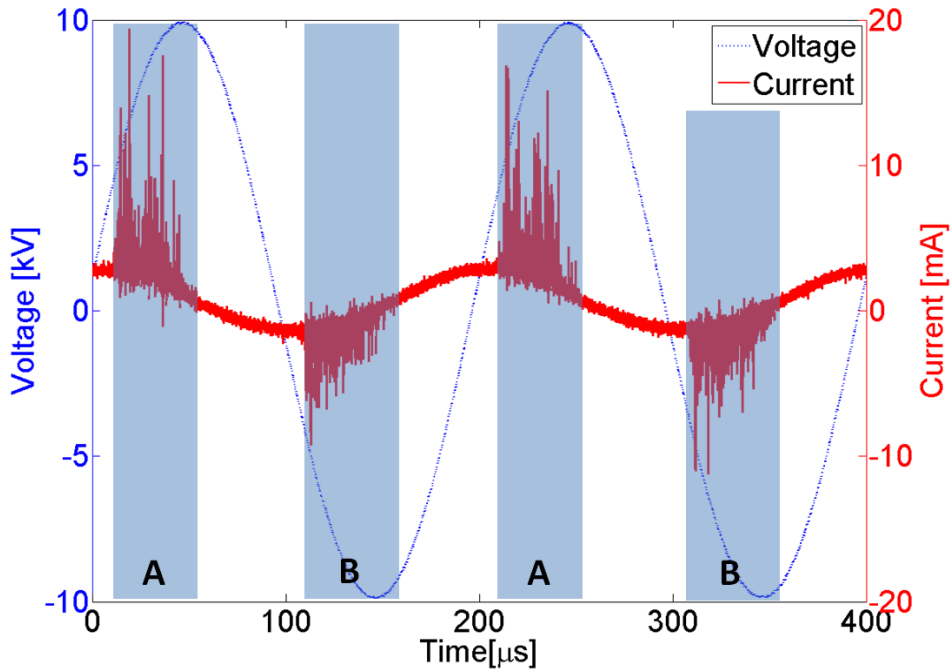


Figure 10 – Plot of voltage and current intensities over time for an atmospheric DBD discharge powered by 20 kV<sub>pp</sub> and a frequency of 5 kHz.

Plasma is ignited during the time intervals in which the absolute value of the voltage increases (time intervals A and B highlighted in Figure 10). Each current pulse is formed by assembly sequence of streamers that are thin filaments, with a diameter of 10-100  $\mu\text{m}$  [9, 10].

This general explanation is not valid for different waveforms (i.e. a square waveform will induce only *two* more intense discharges for each period), or high frequencies. If  $\tau_r \ll T$  the microdischarge channel will always be kept in a conductive state, and the current flow will be characterized by a more continuous behaviour of current flow and charge deposition [11].

### 2.3 Atmospheric Pressure Glow Discharges

A very interesting and often desirable DBD plasma regime is the glow discharge. Atmospheric Pressure Glow Discharges (APGDs) are characterized by a diffused and non-filamentary behaviour, verified for certain conditions. Glow APGDs gathered a big experimental interest, but it is still not completely understood.

The way this kind of discharge supposedly develops involves a minimum pre-ionization level in between each microdischarge event, or a certain free electrons density before the breakdown phase begins. This can bring to the superimposition of several breakdown discharges inside a single microdischarge channel, preventing any intense electric field deformation and the development into a streamer.

A simple criterion to establish whether a discharge will evolve into a diffused or not is based on the necessity for different electronic avalanches to superimpose before the streamer transition can happen. In order to quantitatively estimate the transition threshold to develop a streamer condition, we assume the whole negative charge of the separated electrons inside an avalanche to be concentrated on its head. Assuming an avalanche of length  $z_a$ , we can calculate its radius of diffusion  $r_h$  as:

$$r_h^2 = z_a l_d \quad \text{Eq. (13)}$$

Where  $l_d$  is the electronic diffusion free mean path. The number of free electrons inside the avalanche can be written as:

$$N_a = e^{\alpha z_a} \quad \text{Eq. (14)}$$

Where  $\alpha$  is the Townsend coefficient, defined as the number of ionizing collisions an electron causes per unit length. The electric field generated by this electrons cloud is given by the Gauss theorem:

$$E_a = \frac{1}{4\pi\epsilon_0} \frac{N_a e}{r_h^2} \quad \text{Eq. (15)}$$

The contribution to the global electric field from the ionic tail of an avalanche with  $z_a \gg r_h$  is negligible. An estimation of the critical distance  $z_{cr}$  that an avalanche must travel before developing a streamer can be given imposing  $E_a = E_{breakdown}$ . One can notice several avalanches can superimpose only if  $r_h$  happens to be bigger than the average avalanches spacing, *before* reaching the critical distance. Since an estimation of the avalanche spacing can be given by  $n_{e0}^{-1/3}$ , where  $n_{e0}$  is the initial free electrons density (pre-ionization density), a higher pre-ionization level (i.e. an external ionization source, as a UV radiation source) will surely be beneficial for the development of an APGD [12].

### 3 PLASMA CHEMISTRY OF DBD PLASMAS IN AIR

Plasmas can be ignited in several different gasses and gas mixtures, usually depending on the chemical or physical effect one is trying to achieve. Common working gases are Helium, Argon, Oxygen or Nitrogen. Each one of those gases can be dangerous because of its asphyxiation or flammability potential, and the need for a high pressure vessel to contain them. In this work, air is the gas of choice: a common, cheap, easy to access gas with no health and safety issues.

Air is mostly composed by Nitrogen (79%) and Oxygen (21%). Another relevant compound is water vapour, that varies in quantity depending on the humidity level. After the ignition of a plasma, several more or less stable reactive species are formed from the original composition of the working gas. Reactive Nitrogen Species (RNS) and Reactive Oxygen Species (ROS) are the most useful products of a non-thermal discharge in air [6]. This chapter will explore the main paths followed by chemistry inside the plasma that will deliver such compounds.

#### 3.1 O<sub>3</sub> SYNTHESIS

When the possibility of generating toxic by-products via the chlorination of drinking water has motivated the research for different disinfection mechanisms. "Ozone is a strong oxidizing molecule that is capable to sterilize water and later decompose itself into non-toxic elements. Common Ozone generating devices are all based on DBD technologies" [15]. The global reaction leading to the generation of ozone is the following endothermic process:



In an electrical discharge this can happen in two separate steps: the production of atomic Oxygen via electronic interaction and a three-body recombination.



Ozone production is competing with its recombination and destruction mechanisms, that can happen in two ways:



The presence of water vapour can also reduce the amount of produced Ozone via the following path:



#### 3.2 NO SYNTHESIS

NO synthesis is an endothermic process:



Atomic nitrogen can be delivered as a product of the Zeldovich mechanism, commonly known in combustion chemistry and relevant at high temperatures ( $T_{gas} > 1850 K$ ):



Or can be triggered by an electronic collision, as a result of the dissociation of an excited nitrogen molecule:



The latter is prevalent in cold plasmas, since the minimum temperature that is necessary for the Zeldovich mechanism to be relevant is one order of magnitude higher than the ones found in a typical cold DBD (see section 1.2).

Other NO production mechanisms in plasmas are:



Once NO is formed, further oxidative processes can transform it into NO<sub>2</sub>.

### 3.3 O<sub>3</sub> AND NO<sub>x</sub> INTERACTION

Nitrogen oxides (NO<sub>x</sub>) molecules can help producing atomic oxygen thanks to the following reactions:



However this alternative path is much slower than the direct process of Eq.24:

NO<sub>2</sub> is formed destroying a molecule of ozone, via the following catalytic process:



Those two reactions show why the presence of NO<sub>x</sub> can strongly influence the Ozone production rate one can achieve with a DBD plasma in air.

The interaction of O<sub>3</sub>, NO<sub>x</sub> and OH• from the presence of water vapour will subsequently result in the formation of other molecules like N<sub>2</sub>O, N<sub>2</sub>O<sub>5</sub>, NO<sub>3</sub> and HNO<sub>3</sub> [15]. Each one of those products of the discharge plays a role in common sterilization processes (see section 4.2).

Table 1 summarizes the most important reactions inside a plasma in air. Complete sets comprising hundreds of equations can be used for simulating the full chemistry of a discharge and can be found in the literature.

Process	Rate Coefficient [ $\text{cm}^6 \text{ molec}^{-2} \text{ s}^{-1}$ ]	Reference
$O + O_2 + M \rightarrow O_3 + M$	$M = O_2 ; k = 5,58 \cdot 10^{-29} T^{-2}$ $M = N_2 ; k = 8,6 \cdot 10^{-31} T^{-1,25}$	[16]
$O + O + O_2 \rightarrow O_2 + O_2$	$k = (3,8/T) \cdot 10^{-30} T^{-1} \exp(-170/T)$	[17]
$O_2 + O_3 \rightarrow O_2 + O_2 + O$	$k = 7,3 \cdot 10^{-10} \exp(-11400/T)$	[17]
$N + O_2 \rightarrow NO + O$	$k = 4,4 \cdot 10^{-12} \exp(-3219/T)$	[18]
$O + N + M \rightarrow NO + M$	$k = 5,46 \cdot 10^{-33} \pm 4,96 \cdot 10^{-34} \exp(-1,29/RT)$	[19]
$N + O_3 \rightarrow NO + O_2$	$k = 1 \cdot 10^{-16}$	[20]
$NO + O_3 \rightarrow NO_2 + O_2$	$k = 1,79 \cdot 10^{-12} \exp(-1369/T)$	[20]
$NO_2 + O \rightarrow NO + O_2$	$k = 6,51 \cdot 10^{-12} \exp(120/T)$	[20]
$NO_2 + O_3 \rightarrow NO_3 + O_2$	$k = 1,4 \cdot 10^{-13} \exp(-2470/T)$	[20]
$NO_2 + OH \rightarrow HNO_3$	$k = 2,6 \cdot 10^{-30} (T/298)^{-2,9}$	[20]
$NO_2 + NO_3 + M \rightarrow N_2O_5 + M$	$k = 3,7 \cdot 10^{-30} T^{-4,1}$	[21]
$O(^1D) + N_2 \rightarrow N_2O$	$k = 9,02 \cdot 10^{-37}$	[20]

Table 1 – Summary of the most important reactions in atmospheric pressure air plasma [22]

Since each reaction's kinetic constant is related to temperature, and temperature is also linked to plasma's electronic energy levels, an increase of specific energy input in non-thermal discharges, due to higher power or lower air flow rate, leads to an increase in the concentrations of NO and NO<sub>2</sub>.

“A high concentration of nitrogen oxides completely stops the generation of O<sub>3</sub>. This phenomenon is known as the discharge poisoning effect and is related to fast reactions of O atoms with NO<sub>x</sub>. When NO<sub>x</sub> concentrations exceeds the threshold value of about 0.1%, the atomic oxygen reactions with nitrogen oxides become faster than their reactions with molecular oxygen to form ozone. Even ozone molecules already formed in the non-thermal atmospheric-pressure discharge under conditions of discharge poisoning are converted back to oxygen in the fast low-barrier reactions with nitrogen oxides.”[2]

Nitrogen oxides are not generally consumed in the reactions of discharge poisoning; therefore, they can be interpreted as the catalytic recombination of oxygen atoms and catalytic destruction of ozone in the presence of NO<sub>x</sub>. Ozone and nitrogen oxides don't coexist well in plasma. Non-thermal atmospheric-pressure discharges produce nitrogen oxides at elevated specific energy inputs and temperatures without any ozone formation. Conversely, at low specific energy inputs and temperatures close to room temperature, ozone is effectively produced but not NO<sub>x</sub>, and the discharges can even be used in air purification of NO<sub>x</sub> [2, 15, 22].

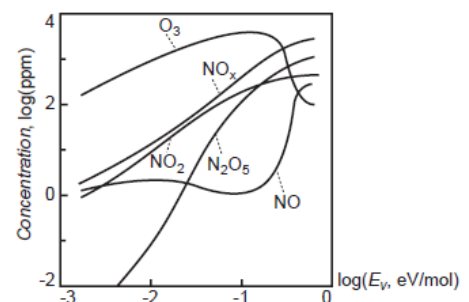


Figure 11 - Concentrations of ozone and nitrogen oxides generated by a DBD air plasma as a function of specific energy levels. [2]

## CHAPTER 4

### 4 PLASMA STERILIZATION

Sterilization is a process that removes or deactivates biological forms of life in a certain region, such as a surface, a volume of fluid, etc... It is a distinct process from disinfection or sanitization.

The efficacy of any pathogen reduction is given by a base-10 logarithm of the reduction ratio:

$$\log\left(\frac{N(t)}{N_0}\right) \quad \text{Eq. (35)}$$

Where  $N_0$  is the initial population and  $N(t)$  is the population for the instant  $t$ . Sterilization is defined as a process that produces a 6-log reduction:  $\log\left(\frac{N(t)}{N_0}\right) = 6$ . This number has been chosen as a safe residual quantity of life, since the survival of an individual microorganism in a colony is never zero.

How fast a process produces a reduction is given by the so-called D-value, defined as the time needed to reduce the population to one tenth of its original value:

$$\log\left(\frac{N(D)}{N_0}\right) = 1 \quad \text{Eq. (36)}$$

#### 4.1 Conventional methods

The efficacy of a sterilization process depends on the type of microorganism to be inactivated and the process. There are several different ways to attempt sterilization. In this section we will discuss the most conventional ones, and how plasmas are capable of summarize most of them with one single technology.

##### 4.1.1 Temperature based sterilization

Microorganisms can be inactivated increasing their temperature for a certain amount of time. This method is relatively simple to perform, but is characterized by long treatment times and can only be used with non-thermally sensitive products (metals, glass, contact lenses, etc...). Dry heat technique (increasing temperature in a dry environment) typically implies temperatures of  $140 \div 170$  °C for  $60 \div 80$  minutes. Steam under pressure can also be used at lower temperatures ( $120 \div 140$  °C) and times ( $30 \div 60$  min).

##### 4.1.2 Chemical sterilization

This is the most common method to sterilize materials that are more susceptible to high temperatures. Products to be sterilized are placed in an atmosphere of a chemical compound: Ethylene Oxide (EtO), for  $18 \div 24$  hours. EtO has very good disinfectant effects on surfaces, but it also has irritating, sensitizing and narcotic effects. Chronic exposure to ethylene oxide is also mutagenic. It is toxic by inhalation and causes acute poisoning, accompanied by a variety of symptoms. For this reason, its usage is usually extremely regulated and limited, resulting in a more expensive process if compared to the heat based method. Other less used chemical agents used are Nitrogen dioxide, Ozone, Glutaraldehyde, formaldehyde, Hydrogen peroxide and peracetic acid.

##### 4.1.3 Radiation sterilization

This is a good alternative to chemical processing. Sterilization can be achieved using electromagnetic radiation such as electron beams, X-rays, gamma rays, or irradiation by subatomic particles. Electromagnetic or particulate radiation can be energetic enough to ionize atoms or molecules (ionizing radiation: gamma rays, x rays...), or less energetic (non-ionizing radiation: UV light). Sterilized materials can be used immediately, no toxic elements are emitted into the atmosphere and it is a low cost process. However, some materials (like Ultra High Molecular Weight Polyethylene) are degraded by radiations and those cannot be sterilized with this technique.

#### 4.1.4 Mechanical methods

Fluids that cannot withstand thermal sterilization can be processed by filtering in a porous media and in aseptic conditions. This is the case for ophthalmic, intravenous and antibiotic solutions. This method's critical limitation is the maximum treatable flow, often requiring several filtering devices operating in parallel or long treatment times.

### 4.2 Cold plasma sterilization

Plasmas are able to deliver a mixture of all the conventional sterilization mechanisms in one single device. As previously seen, plasmas can deliver a certain heat flux, depending on the plasma's operating conditions, can be rich in highly oxidizing chemical species and radiative emissions. Plasmas can pack all those elements in one solution with a negligible amount waste, in an energy efficient and cheap process.

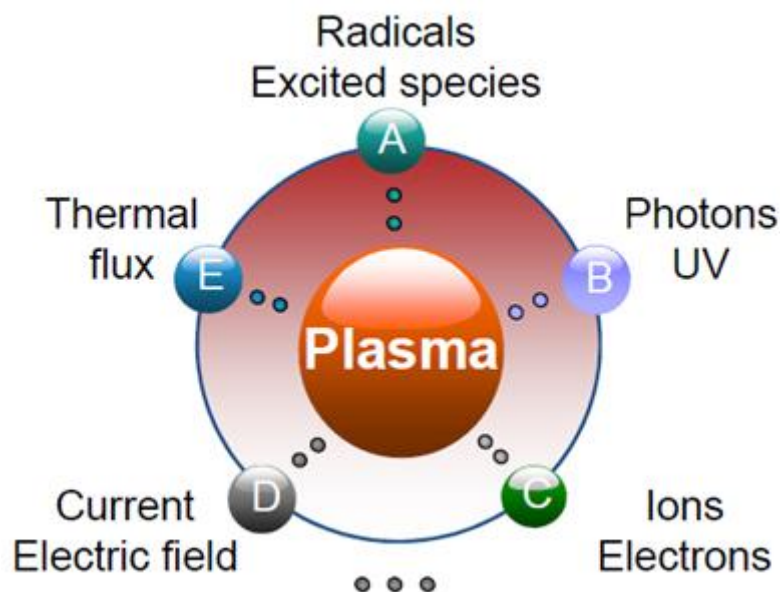


Figure 12 – Plasma components are also the very basic elements of conventional sterilization methods. Cold atmospheric plasmas can be considered as an “all in one” solution that can envelop all the key characteristics of conventional sterilization methods in one single device.

In this section we will analyse the elements inside a plasma that can be useful for sterilization purposes.

#### 4.2.1 Direct and indirect treatments

Neutral elements found inside a plasma can be short living or long living. Things like radicals and metastables ( $O$ ,  $OH$ ,  $O_2^*$ ...) are extremely reactive and their half-life is very short, in the order of ns or  $\mu s$ . When biomaterials are in contact with the plasma and the sterilization process is able to exploit those components constantly produced by the discharge, we define it as a “direct plasma treatment”.

Other molecules such as O<sub>3</sub>, NO, NO<sub>2</sub>... are more stable, but less reactive. Their half-life is longer (from seconds to hours) and they can also be transported to a significant distance from the plasma volume itself. This kind of plasma processing technique will be called “indirect plasma treatment”. Despite being less effective than the direct one, this method is preferred when direct plasma treatments are impractical or impossible to achieve (i.e. large geometries), placing the biomaterial at a distance from the plasma volume.

#### 4.2.2 Effects of neutral species

##### -Effects on membranes

The external membrane surrounding a micro-organism is a gel-like structure made of two layers of lipids<sup>15</sup>, susceptible to oxidation. Oxidation of the membrane is the most important weapon that neutral species use for sterilization purposes. Micro-organisms can repair oxidative damages, but only when it is not excessive.

As an example, OH can easily compromise membranes, attacking organic substrates R- (i.e. the fatty acids that are the membrane’s building blocks), forming a radical:



ROH can be then oxidised by a metallic ion, forming a stable oxide, or interact with another ROH generating an oxidised product [2].

##### -Effects on DNA

Once the membrane is compromised or one of the oxidising species are able to access the inner parts of the structure, DNA<sup>16</sup> can be attacked by them, resulting in the cell’s complete degradation. Crosslinking of the DNA or the glycosidic link oxidation are irreparable damages and fatal [2].

#### 4.2.3 Effects of charged particles

The effects of electrons and ions is particularly important when lifeform that we are trying to inactivate is in direct contact with a plasma volume (i.e. inside a plasma, with a direct treatment). Positive and negative charges are also able to generate highly reactive species, able to sterilize by means of intensive oxidation of biomaterials.

##### -Electrons

Their importance is related to the high-speed electronic flux colliding with the surfaces contained inside a plasma. Free electrons are the most abundant sterilizing specie we can find during a direct treatment. Strongly electronegative<sup>17</sup> gasses can limit this fact, since they will strongly subtract free electrons inside the plasma to form negative anions.

Free electrons can penetrate under a surface (circa 4 μm) before interacting with matter, allowing the inactivation of microorganisms shielded by a liquid layer. An estimation of such distance is given by the

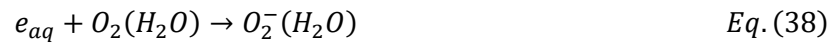
---

<sup>15</sup> Lipids are organic compounds that constitute the whole membrane surrounding bacteria. Damaging them will undermine the structural integrity of the whole cell.

<sup>16</sup> DNA is a nucleic acid that contains all the genetic information necessary to RNA and proteins biosynthesis, necessary for the life of most of living organisms. DNA structures can be found inside a nucleus, or unprotected as it happens in bacteria.

<sup>17</sup> Electronegativity is a chemical property that describes the tendency of an atom or a functional group to attract electrons (or electron density) towards itself.

electronic bio-inactivation cross section. In water, such effect is enhanced by the hydration of the electron<sup>18</sup>:  $e_{aq}$ . If some oxygen is dissolved in the liquid layer, electrons will form the negative superoxide anion  $O_2^-$ :

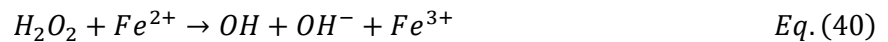


Superoxide is fundamental, since it is a precursor to other strong oxidizing agents, including singlet oxygen and peroxyxynitrite. It is interesting to mention that certain cells in the human body produce superoxide as an antibiotic “weapon” to kill invading micro-organisms.

For sufficient acidity levels, superoxide is converted into hydrogen peroxide via the so-called “superoxide dismutation”:



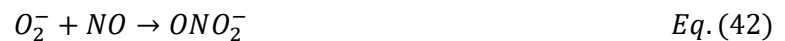
The superoxide also stimulates the conversion of  $H_2O_2$  into OH radicals, which are extremely strong oxidizers very effective in sterilization through a chain oxidation mechanism. This conversion is known as the Fenton reaction and is possible by the oxidation of metal ions (i.e.  $Fe^{2+}$ ):



$Fe^{3+}$  will then reduce back to  $Fe^{2+}$  thanks to the superoxide anions:



Especially with plasmas in air, superoxide can react with NO, generating peroxyxynitrate, another important oxidizing radical:



-Ions

Effects of negative anions like  $O_2^-$  have already been discussed in the previous section. Positive ions  $M^+$  (i.e.  $N_2^+$ ) are usually more abundant near a surface. Their interaction with water is always initiated by a fast charge transfer, producing a water ion:



Water ion reacts with water molecules, producing an acidifying product and OH radicals (as seen, very important for sterilization).



The subsequent decrease of pH<sup>19</sup> will help preventing or limiting the existence of microbiological life in the solution in contact with the plasma. In fact, bacteria, single celled eukaryotes and other microbes, can only live and reproduce within a certain range of environmental conditions. Microbes, such as bacteria are sensitive to the hydrogen ion concentration they find in their environment. Large proteins, such as enzymes, are affected by pH. Usually, their catalytic properties are lost and metabolism is halted. Most

<sup>18</sup> The presence of a polar molecule that can surround the electron, increasing its mean free path.

<sup>19</sup> pH defines the molar concentration of  $H^+$ . Such quantity defines the acidity or basicity of a solution.

bacteria grow best around neutral pH values (6.5 ÷ 7), but some thrive in very acid conditions and some can even tolerate a pH as low as 1.0<sup>20</sup> [23].

-Ionic bombardment

The lipidic layer of a microbiological membrane can be damaged by ionic bombardment. The mean electrons energy in a Cold Atmospheric Pressure Plasma (CAPP),  $\langle \varepsilon_i \rangle$ , can be written as the energy transferred from the electric field  $E$  to an electron  $e$  inside a free mean path  $\lambda$ <sup>21</sup>.

$$\varepsilon_i = e E \lambda \tag{Eq. (45)}$$

As previously stated, this value is typically circa 1 eV, and it is high enough to break the hydrogen bonds of the lipidic layers of a membrane, causing its structural damage. Therefore, even though high pressure plasmas are not associated with high ionic kinetic energies, sterilization via ionic bombardment can happen [2].

4.2.4 Effects of the electric field

The direct effect of an electric field on a micro-organism is electroporation, which is the temporary or permanent generation of pores on a membrane thanks to electrostatic forces from an intense electric field across it. However, in normal circumstances,  $E$  is not high enough to generate such effect.

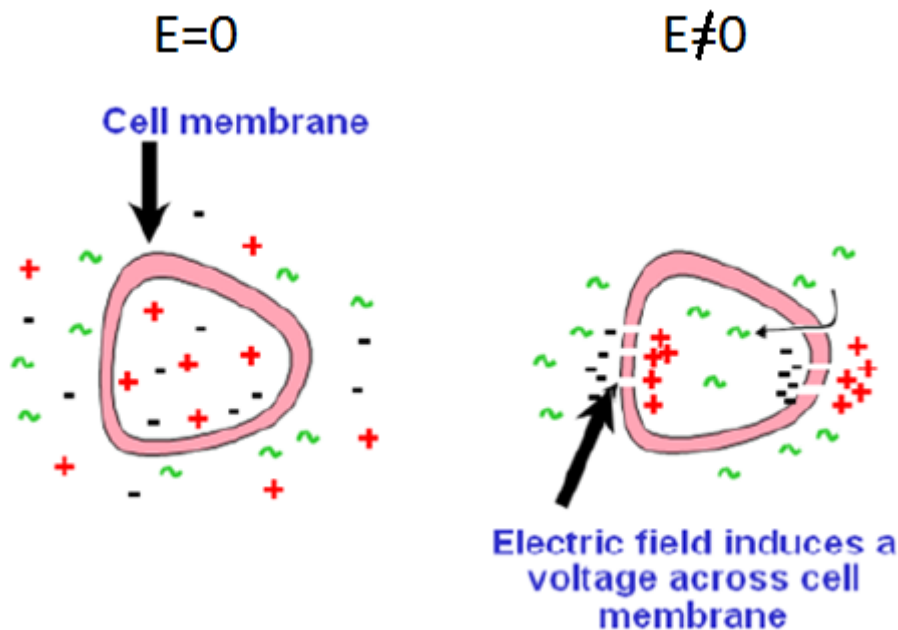


Figure 13 – Effect of an electric field on cellular membranes.

On the other hand, the indirect effects of charge depositions are very important. Electrostatic forces caused by the charge buildup on a membrane can overcome the highest shear stress allowable, causing its rupture.

<sup>20</sup> Even though those ones can live in very acid environments, their internal pH is much closer to neutral values.

<sup>21</sup> That can also be written as a function of temperatures:  $\varepsilon_i = T_{gas} + T_{el}\sqrt{\delta}$ , where  $\delta \sim 0.1$  is the the mean energy lost by an electron colliding with a neutral particle.

Since the electric field is intensified by sharp edges<sup>22</sup>, rough and irregular membranes are more susceptible to this inactivation mechanism.

Another similar contribution can come from the head of a developing streamer, that profoundly increases the local electric field<sup>23</sup>.

#### 4.2.5 Thermal effects

This inactivation mechanism is the most conventional one (as seen in section 4.1.1) and it usually involves temperatures of 120 ÷ 170°C to achieve the sterilization. Cold plasmas don't reach such high temperatures (usually they're up to 70°C) and cold plasma is not a thermally sterilizing process. Some higher temperature micro-regions (1000°C) can be present, and in this case it is possible to thermally sterilize a target, but this is usually a limited side-effect that can actually be undesirable, especially when treating heat sensitive materials.

Most of the thermal effects one can appreciate in a cold plasma is the change of chemical kinetics due to a change in temperature (see Table 1) that can massively stimulate the production of a reactive species. This is a typical example of the possible synergies one can find when working with plasmas.

#### 4.2.6 UV radiation effects

UV-C radiation (100-280 nm) is already used as another effective common sterilization method, and plasmas can emit UV radiations as well, especially the low pressure ones. A dose in the range of mJ/cm<sup>2</sup> is enough to kill a cell thanks to the damage induced in the DNA structure.

### 4.3 Aim of this work

Since the 1970s, plasma's capability to increase gases sterilizing potential has been demonstrated. During the 2000s some studies started to investigate the possibility to use plasmas to add sterilizing properties to non-germicidal gases (air, helium...). At that time, high costs linked to the usage of low-pressure plasmas limited this technology's development.

Cold atmospheric plasmas have now replaced low-pressure ones. Years of studies and development have shown how they can be useful to inactivate different bacteria, spores, fungi and yeasts.

Some of those microbiological elements are extremely resistant and can be safely inactivated only via thermal or chemical processing. Materials that are sensitive to either heat or specific chemical compounds were impossible to sterilize, but cold plasmas have unlocked this possibility with a safe, reliable and cost effective solution.

Interest in the use of non-thermal, atmospheric pressure gas plasmas for inactivating micro-organisms has grown rapidly in recent years [24, 25, 26]. The majority of such applications are related to food [27, 28, 29] and medicine [30, 31, 32] but are by no means restricted solely to these. Plasmas can also be able to

---

<sup>22</sup> If we define  $\phi$  as the superficial potential,  $r$  as the curvature radius,  $\Delta$  the layer thickness,  $F_t$  the maximum tensile stress; a rupture is caused by  $|\phi| > 0.2 \sqrt{r\Delta F_t}$

<sup>23</sup> A streamer with length  $l$  and a head with curvature radius  $r$  will cause a local electric field  $E_m$  by the law:

$$\frac{E_m}{E_0} = 3 + \left(\frac{l}{r}\right)^{0.92} ; 10 < \left(\frac{l}{r}\right) < 20000$$

sanitize complex or big geometries and temperature sensitive materials, with little to no possibilities for bacteria to develop a resistance against this treatment.

For this reason, plasmas have been successfully used to successfully inactivate several kinds of microorganisms, both in-vitro and in-vivo<sup>24</sup>.

The high amount of variables influencing a plasma bring to big differences in the effects it can have on a biological payload. As previously seen, there are several different chemical compounds one can find in a plasma, depending on the kind of gas one is using and the operating conditions one is igniting the plasma with.

In this thesis my work was focused on trying to better understand the differences in sterilizing efficacy of different chemical compounds found inside an atmospheric pressure DBD plasma in air. In particular, the relative importance of NO<sub>x</sub> production and concentrations over the O<sub>3</sub> is investigated. The results gathered from those experiments can seriously influence the design choices of any DBD air plasma device and the optimization of its operating conditions during the sterilization process.

---

<sup>24</sup>In vitro refers to studies performed with microorganisms, cells, or biological molecules outside their normal biological context, usually in test tubes, flasks or Petri dishes. In vivo studies are those conducted in animals and whole plants.

## 5 VARIABLES OF A PLASMA STERILIZATION SYSTEM

A variety of plasma-generating devices has been described in the scientific literature [33-35] and numerous tests to inactivate a wide range of micro-organisms have been conducted. This has led to the generation of a large data resource which could in principle serve in the design of gas plasma-based disinfection processes.

Establishing and keeping as a constant a certain set of electrical parameters supplied to the electrodes of a device and the chemical composition of a working gas is not a problem. This does not mean, though, that reliable results have to be necessarily expected as well. Other variables can play a significant role on plasma's sterilization efficacy.

### 5.1 Electro-Hydro-Dynamic effects

The introduction of *fluid dynamic* consequences from Electro-Hydro-Dynamic (EHD) effect<sup>25</sup> into any experimental setup can really influence results and conclusions. The convective mechanism induced is generating a region with a negative pressure gradient above the exposed electrodes (Figure 14). This region will constantly introduce new air into the plasma volume, significantly influencing its chemistry. Fresh air would also lower plasma's macroscopic temperature, again manipulating the chemical yield of a given device.

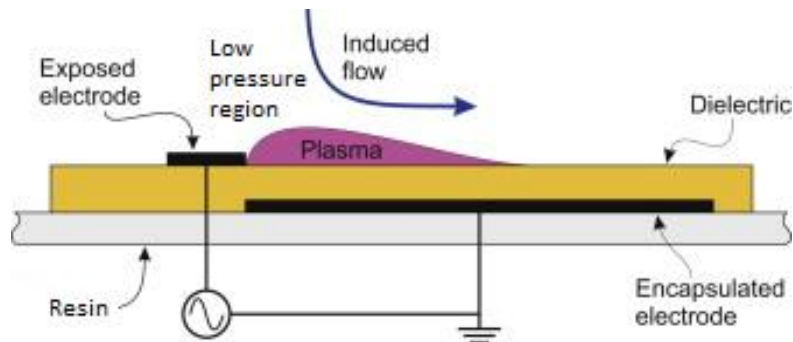


Figure 14 – EHD effect of a surface DBD device.

This was recently demonstrated by Taglioli, et al.[40], who found that an enhanced degradation of indigo solutions due to an increased delivery velocity of the reactive species rather than the increase in their concentration. The enhanced transport caused by the formation of an EHD jet perpendicular to the surface of the device causes the efficacy of the S-DBD in degrading an indigo solution to increase by a factor of 3 from what would otherwise be expected from power and plasma size considerations.

<sup>25</sup> EHD effect is the generation of an ionic wind in the vicinity of the plasma region. See section 6.1 for an introduction to this physical phenomenon affecting any surface DBDs.

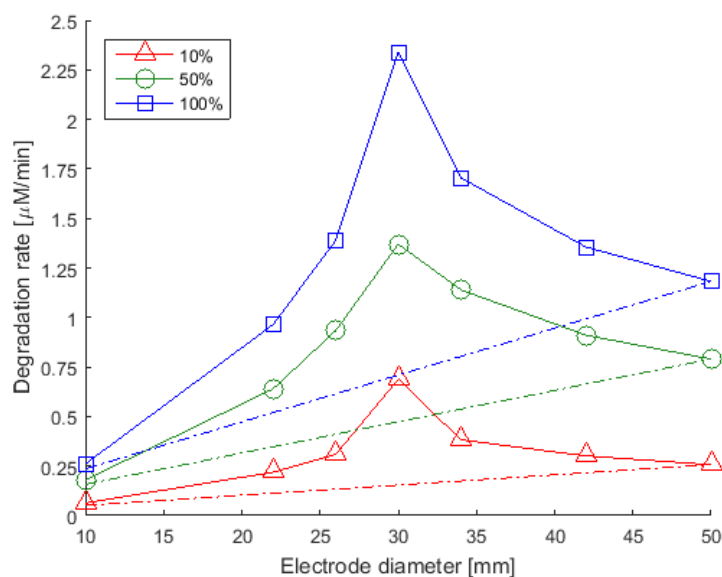


Figure 15 - Degradation rate of 2  $\mu\text{M}$  potassium indigotrisulfonate solutions as a function of the electrode diameter of the S-DBD. Discharges sustained at various duty cycles with a modulation frequency of 5Hz. Dash-dotted lines represent linear increases that can be attributed to the longer plasma formed in larger devices [40].

The EHD effect certainly brings several additional variables capable to radically influence the chemical production of a plasma. Since reliable and constant operating conditions are strongly desired, a method to quench the EHD effect on a surface DBD discharge was needed first.

## 5.2 Effects of methods and materials

Another thing that has remained elusive is a *method* of rigorously comparing the biocidal performance of different plasma devices. Even determining the true biocidal potential of plasma-generating devices of apparently identical configuration is not straightforward.

This can be illustrated with reference to a couple of examples. In the first of these, Xingmin et al. [36] and Miao and Yun [37] using direct DBDs which were produced using similar reactor configurations (Figure 16), investigated the inactivation of *E. coli*.

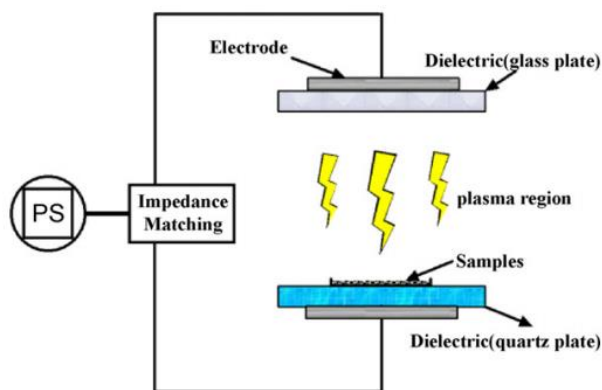


Figure 16 - Reactor configuration used by both Xingmin et al. [36] and Miao and Yun [37].

Employing similar sample preparation methods, the former achieved a single log reduction in viability at a measured energy input of  $50 \text{ J cm}^{-2}$ , whilst the latter achieved the same result with the much reduced energy input of  $4 \text{ J cm}^{-2}$ . In the case of inactivation of *Staphylococcus aureus*, also using DBDs, Xingmin et al.

[36] achieved a single log reduction at an energy expenditure of just under  $6 \text{ J cm}^{-2}$ , whereas Sun et al [38] required approximately  $4.2 \text{ J cm}^{-2}$ , and Ma et al. [39] only  $1 \text{ J cm}^{-2}$ .

That the results from these studies are carefully obtained and valid in their own right is not contested here. Rather, the point being made is that it is difficult to compare results from different studies. It is almost certain that small differences in the operation of the devices would have had an influence on the composition of the plasma and this would have contributed to some extent to the disparity in the results of the examples cited above.

Achieving stable and quantifiable plasma operation is obviously desirable, and in a recent study Pavlovich et al. [41] put forward procedures designed to achieve this. This is an important aspect of experimentation with gas plasmas and one that until recently has not been given due attention. Another welcome initiative in this direction is that undertaken by the “Plasma Sources for Biomedical Applications” workgroup of the European COST action MP1101 “Biomedical Applications of Atmospheric Pressure Plasma Technology” [42], which have been working on the design and characterisation of a reference plasma source.

Notwithstanding such compositional differences, the other major factor contributing to the discrepancies in the data mentioned above arises from differences in the physical and physiological state of the bacteria presented to the plasmas. Evidence for the importance of such factors comes from a variety of previous studies. The life cycle of most micro-organisms comprises four phases; the lag phase, the exponential or log phase, the stationary phase and the death phase (Figure 17).

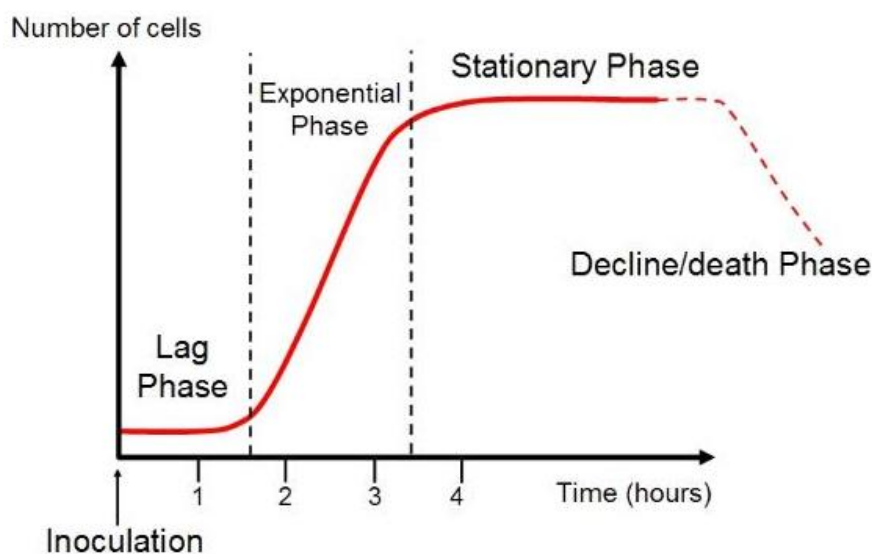


Figure 17 - Bacteria population growth curve

Due to the expression of specific stress response genes, most bacteria possess their highest resistance against external stresses during the stationary phase [43]. That this also holds true in the case of plasma treatment was demonstrated by Yu et al. [44], who reported differences in the inactivation rate constants for *E. coli* at mid-log, late log and stationary phases of growth.

Even when different research groups employ the same species of micro-organisms, the differences that exist between strains of that species can result in wide variations in responses to specific external stresses and this can lead to apparent discrepancies in the data obtained similar to those illustrated above. This was demonstrated, for example, in the case of the UV irradiation of different strains of *Bacillus pumilus* [45] where differences in UV resistance of up to in excess of 300 times that of the reference strain were

exhibited by environmental isolates. Similarly, Bayliak et al. [46] found differences in the resistance of different strains of *Saccharomyces cerevisiae* to hydrogen peroxide, whilst more recently, Kossakowska et al. [47] documented differences in the responses of *Staphylococcus aureus* strains to oxidative stress.

Although the different susceptibility of strains and even mutants can be exploited to gain insights into plasma inactivation mechanisms [48], these differences indicate that for a meaningful comparison to be made, trials should be performed with not only the same species but also with the same strain.

Another important factor in determining microbial survival is the physical state in which the organisms are presented to the gas plasma. The nature of the substrate itself can have a major impact on microbial survival. This was demonstrated by Noriega et al. [49] who found that *Listeria innocua* survived better the effects of plasma treatment when applied to the skin of chicken than on chicken flesh. This was attributed to differences in surface topography; chicken skin is characterised by the existence of feather follicles inside which the bacteria are able to avoid the lethal effects of the plasma, whereas bacteria on the surface of the chicken flesh are more exposed to the chemical species present in the gas plasma. However, even when identical substrates are employed the spatial arrangements of the cells on the substrate can also affect survival. For *E. coli*, Yu et al. [44] observed an approximate 20-fold reduction in the inactivation rate constant as the surface cell concentration was increased from  $10^7$  to  $10^{11}$ .

### **5.3 Effects of plasma's chemical composition**

It is clearly understood and most of the authors agree that air DBD plasmas' chemical compounds active in the sterilization process, especially for an indirect treatment, are ROS and RNS.

While Laroussi, et al. [50] claim that "highly reactive species such as O, OH, and NO<sub>2</sub> that play the most crucial role in the destruction of microorganisms", other authors such as Choi, et al. [51] suggest that "ozone molecules were the dominant germicidal species". Other studies from Mastanaiah, et al. [52] show that while ozone plays a primary role in the process of plasma sterilization, it is not the only agent responsible for sterilization, without any clear indication on the relative importance of those other components.

It would be interesting to try and examine the role ROS and RNS have on plasma sterilization processes more in depth.

On a first thought one could think to try and replicate the plasma's chemical yield mixing the stable compounds of a discharge, without the need of a plasma. However in a plasma "when all of the agents are present simultaneously one can expect some level of synergy to exist" [53], and the only way to exactly reproduce the effects of plasma chemical compounds on micro-organisms is by means of an actual plasma discharge.

The final aim of this work will therefore focus on the importance different chemical products of a DBD device have on plasma sterilization processes analysing the microbiological effects of a plasma operated in two different conditions and different chemical yields. Any differences from those results will indicate and evaluate the relative importance ROS and RNS have in plasma sterilizations.

## 6 GEOMETRICAL EFFECTS ON THE ELECTRO-HYDRO-DYNAMIC EFFECT

### 6.1 INTRODUCTION TO THE ELECTRO-HYDRO-DYNAMIC EFFECT

Electro-Hydro-Dynamic (EHD) interaction is a physical phenomenon that has a strong connection with the so-called ionic wind.

Ionic wind is produced when high electric fields locally ionize the air surrounding an electrode, producing a number of charged particles. The presence of an electric field will lead to the acceleration of those particles, inducing a macroscopic air flow towards the opposite electrode by means of collisions with the surrounding neutral molecules. Since DBDs are providing both a high concentration of charged particles and high electric fields, they are also able to induce the EHD effect.

The force per unit volume within the discharge can be reduced to the following expression:

$$F_{EHD} = (n_i - n_e) E \quad Eq. (46)$$

where  $E$  is the electric field,  $n_i$  and  $n_e$  are ion and electron number density respectively.

First studies were conducted using direct current (DC) corona discharges<sup>26</sup> [54]. This technology was however disadvantageous because of the natural tendency of this cold plasma to evolve into a thermal DC arc, producing irreversible damage to the materials in contact with the plasma and the corona generating device itself.

Today the largest part of EHD devices are based on DBDs, since they allow to use several electrodes geometries, different supplied voltage waveforms and it prevents the transition into the arc regime, as previously discussed in section 2.1.

The most basic way to generate a DBD-based EHD device is via a dissymmetric electrode pair separated by a dielectric slab (Figure 18).

---

<sup>26</sup> A corona discharge is an electrical discharge brought on by the ionization of gas surrounding a conductor that is electrically charged, when the strength of the electric field around a conductor is high enough to form a conductive region, but not high enough to cause electrical breakdown or arcing to nearby objects.

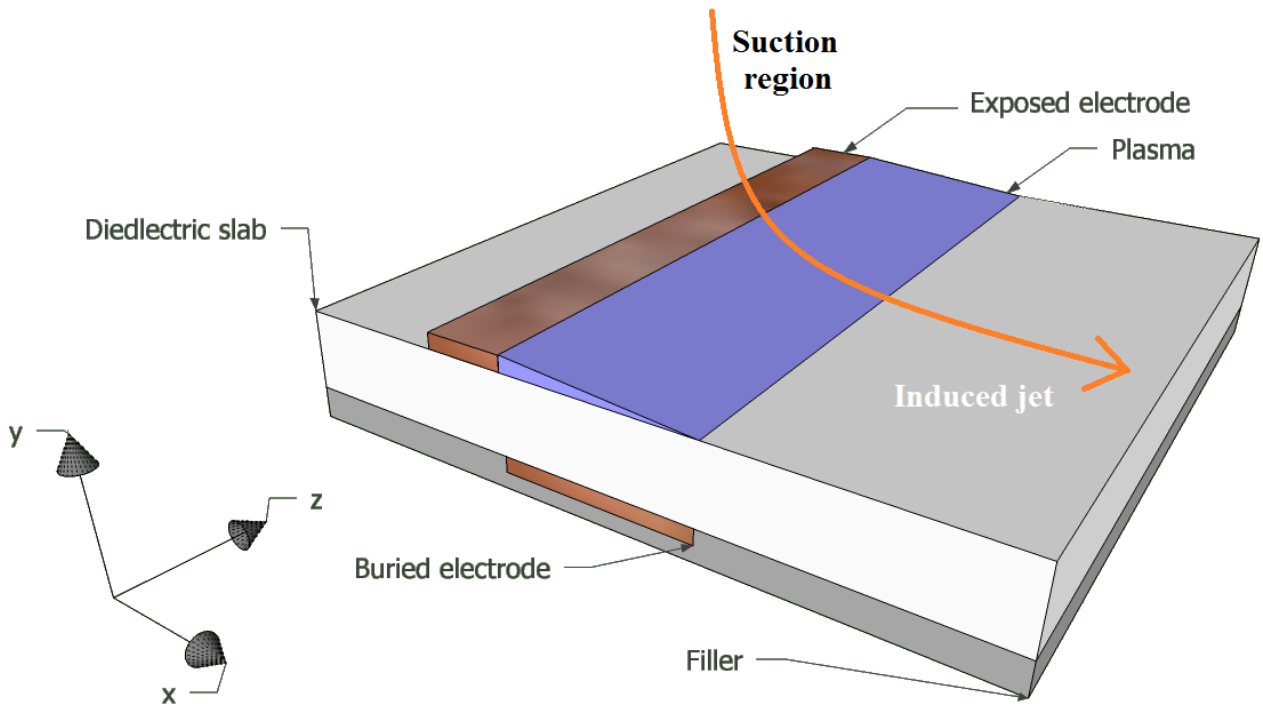


Figure 18 - Design of a common EHD actuator with a dissymmetric electrode pair inducing an air flow along the x axis.

The surface discharge produced applying high AC voltages to the electrodes is able to produce an air flow tangentially to the dielectric wall. Due to the asymmetric electrode arrangement, a suction region is generated above the exposed electrode [55]. Air enters this depression region and experiences a unidirectional thrust tangentially to the actuator surface.

A typical velocity profile induced by the tangential wall jet is shown in Figure 19. Maximum air velocities around 5÷6 m/s are commonly reached.

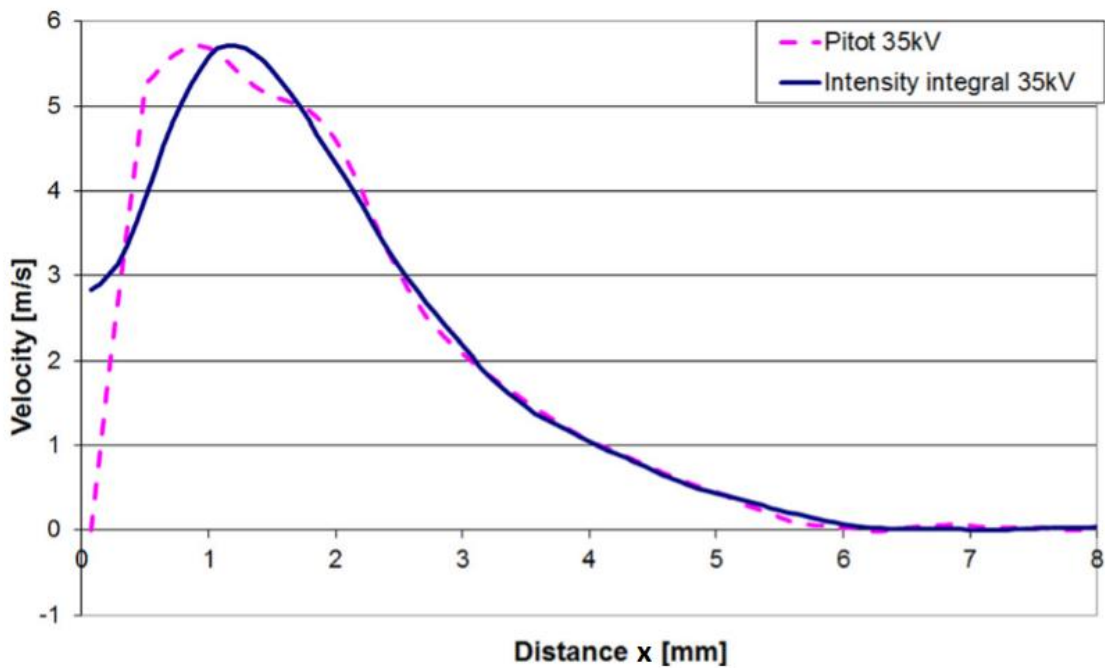


Figure 19 - Common Pitot velocity profile (dashed line) and discharge intensity integral (solid line) along the x axis for y = 0 of an EHD plasma actuator (Cristofolini, et al. [56]).

EHD dynamics are in the order of milliseconds long, which is two orders of magnitude slower than the ones observed inside the plasma (ns scale). Schlieren images of the induced tangential jet's development in time is shown in Figure 20.

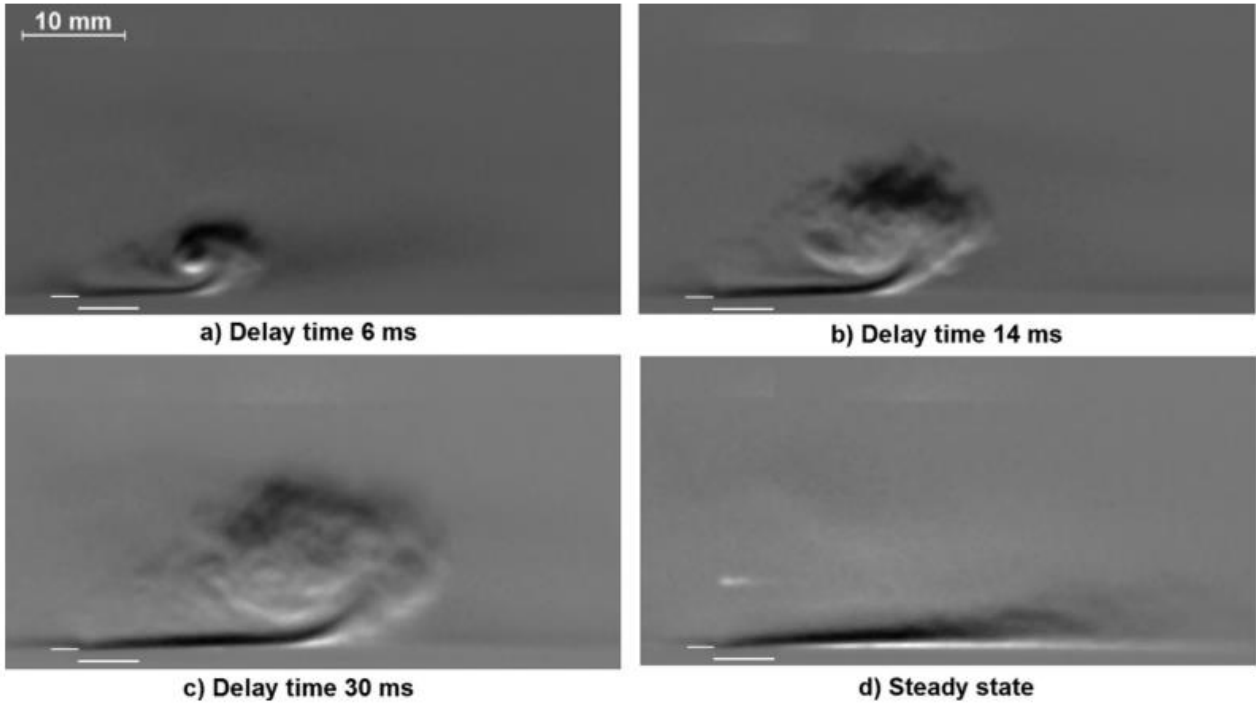


Figure 20 - Schlieren images of the induced tangential jet's development in time (Cristofolini, et al. [56]).

The EHD effect can also be used to generate perpendicular convective flows. This so-called vectorized jet, perpendicular to the actuator surface, can be produced by two tangential jets acting in opposite directions, colliding with each other (Figure 21).

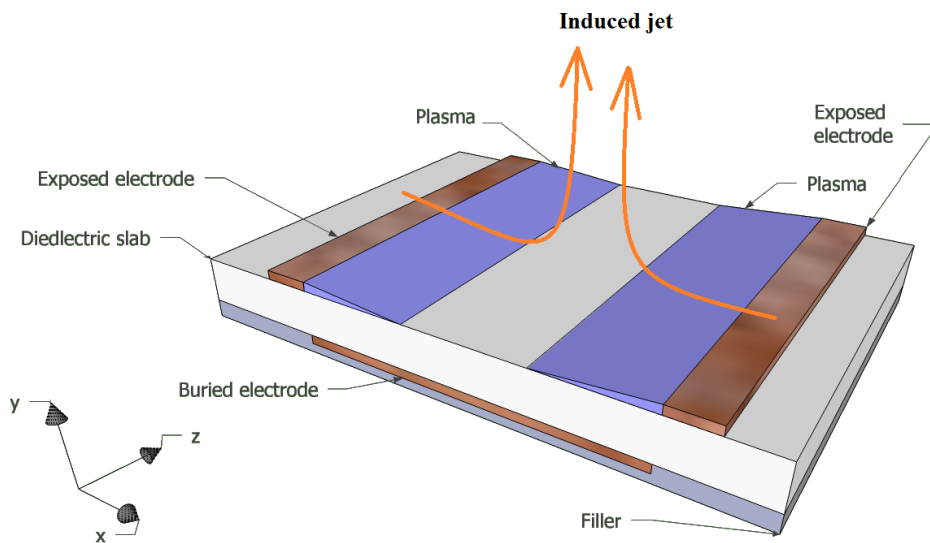


Figure 21 – Design of an EHD actuator capable of producing a vectorized jet perpendicular to the actuator surface.

Such a feature can be exploited to enhance indirect plasma treatments, increasing the delivery of plasma reactive species onto surfaces or liquids, thereby increasing their efficacy (sterilization, ozonisation, surface treatments, etc.) [57, 58].

These jets are currently studied mostly in the aeronautics and aerodynamics field for boundary layer modification, extraterrestrial micro-propulsion [59], and active cooling of electronics with no moving parts [60].

A large number of experimental [61-63] and numerical [64-66] works have been done to exactly understand the mechanisms involved in the EHD interaction, but this goes beyond the aim of this work and will not be detailed. Those works demonstrate the capability of DBD plasma to thrust the surrounding gas in a desired direction.

Different operating conditions (input power, peak voltage, frequency and waveforms) have a strong influence on the EHD effect as well as on plasma's temperatures and chemistry [67-77]. As an example, the maximum speed is limited by the highest intensity of the electric field generated in the discharge. A less diffused morphology of the discharge, with stronger and longer streamers, is less efficient from the EHD effect point of view [67].

Electrical parameters were set and kept constant as:

- Waveform: sinusoidal
- Voltage: 11.5 kV<sub>p</sub>
- Frequency: 5 kHz

This choice provides a non-thermal plasma and a good matching between the power supply (see section 6.3) and the plasma load.

## **6.2 Annular design**

Other known parameters are able to increase the ionic wind speed. An important factor influencing the EHD effect is also geometry [78-80]. The chosen DBD configuration provides two circular electrodes separated by a dielectric barrier that is able to produce a perpendicular vectorized air jet, pictured in Figure 22.

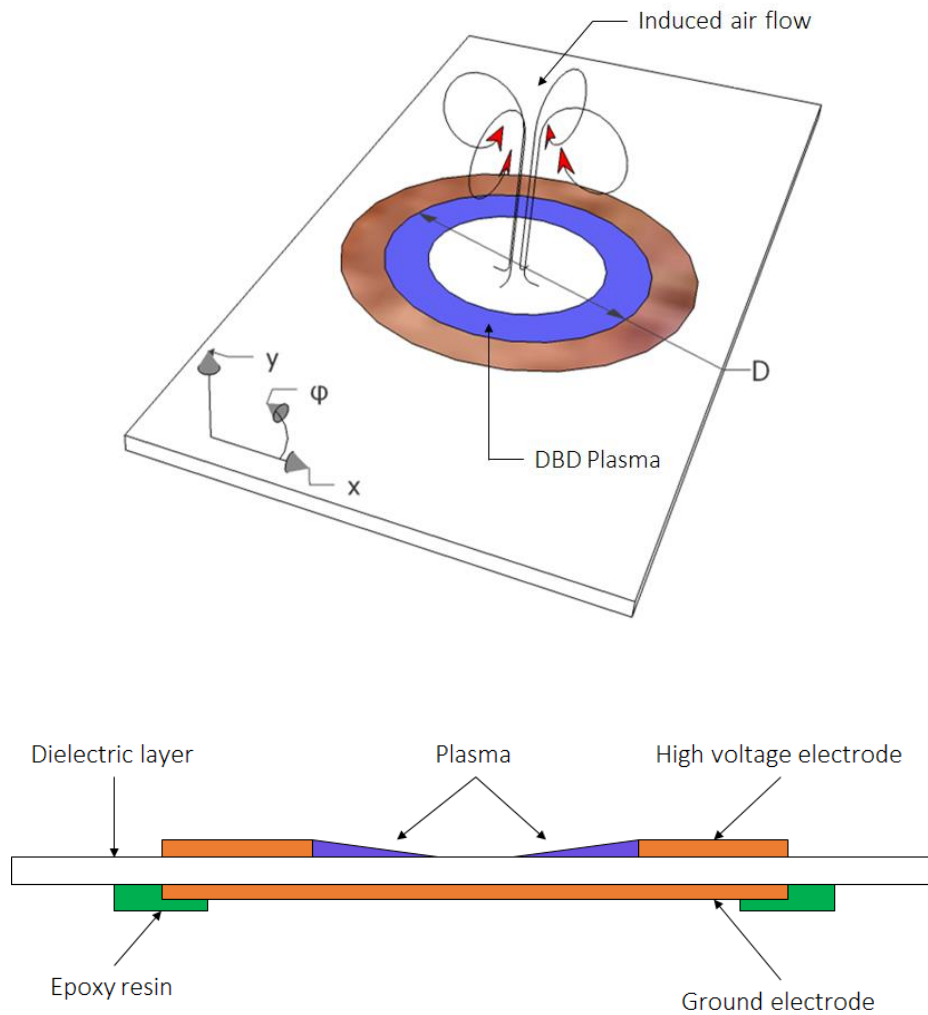


Figure 22 – Single annular actuator (top) and its cross section along the  $x$ - $y$  plane (bottom). Only one of the two circular copper electrodes are visible from this 3D rendering. The other one is a full circular electrode on the opposite face of the dielectric layer. The dielectric barrier, represented as a white slab, is 1.5 mm thick glass epoxy. Plasma is pictured in violet.

We then decided that a good approach to the problem of EHD effect minimization would be to investigate on the influence different hole diameters  $D$  would have on it. Electrodynamics and fluid dynamic measurements have been performed to characterize the plasma and the EHD effect intensity for different diameters.

A series of single-hole, axisymmetric DBD devices (named “annular actuators”), producing jets perpendicularly to the actuator surface, have been fabricated on common 2-layer PCBs, with 35  $\mu\text{m}$  thick copper electrodes and 1.5 mm thick glass epoxy (FR-4) as dielectric. The high voltage electrode has a width of 5 mm and the tested inner diameters were 5, 10, 14, 18, 22, 26, 30, 34, 38, 42, 46, and 50 mm.

### 6.3 Experimental setup and results

Experiments were performed in still air at atmospheric pressure. The power supply feeding the actuator was constituted by a signal generator, an amplifier, and a transformer, as shown in Figure 23<sup>27</sup>. This setup is able to produce a sinusoidal voltage with a peak value of 11.5 kV and 5 kHz frequency.

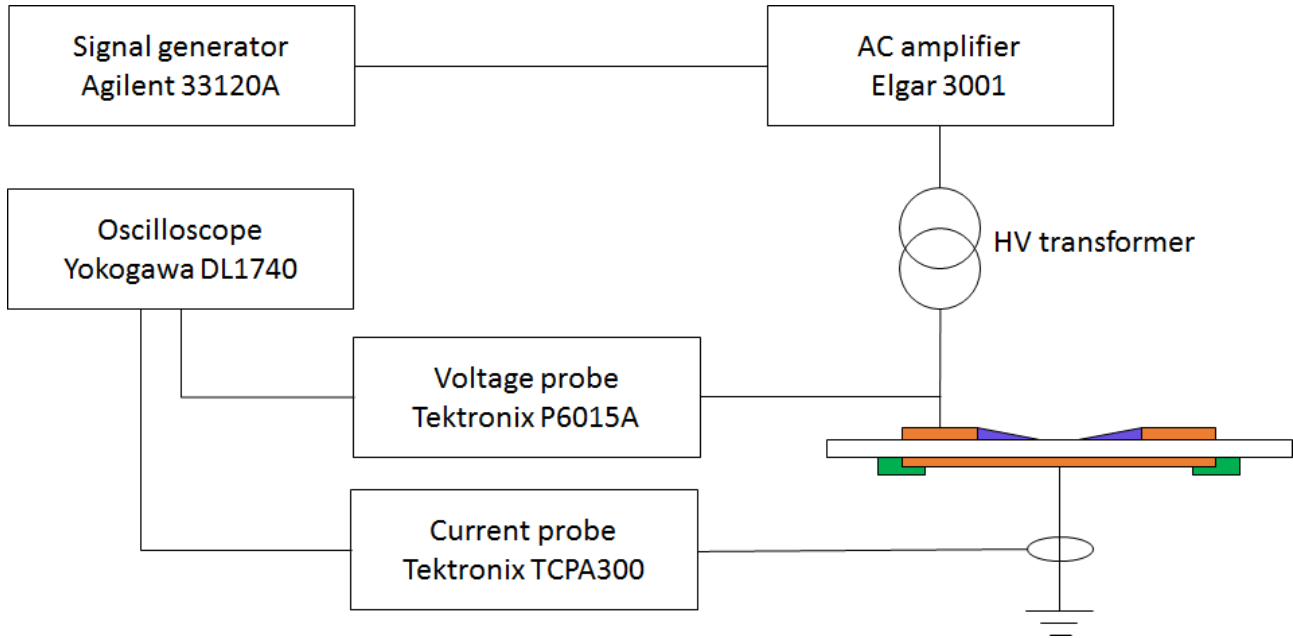


Figure 23 - High frequency, high voltage power supply and measurement setup.

#### 6.3.1 Power measurement

Instantaneous active power measurements have been evaluated by means of the following expression:

$$p(t) = v(t) \cdot i(t)$$

where  $v(t)$  and  $i(t)$  are the measured voltage and current,  $t$  is time<sup>28</sup>. A graph showing the actuators' voltage and current in time is shown in Figure 24. The mean power values reported in this work are obtained by averaging over 25 AC periods.

<sup>27</sup> An HP-Agilent 33120-A signal generator produced a low voltage (2-4 V) AC signal with a frequency of 5 kHz that was delivered to an Elgar Model 3001 AC amplifier. A high voltage ferrite transformer was used to increase the voltage to the desired value of 11.5 kV<sub>p</sub>.

<sup>28</sup> Voltage and current applied to the electrodes have been measured by means of two probes connected to a Yokogawa DL1740 4-channel, 500 MHz bandwidth, 1 GS/s oscilloscope. A capacitively compensated high voltage probe with a bandwidth up to 75 MHz Tektronix P6015 was used to measure the voltage. An AC/DC Hall current probe with a bandwidth up to 100 MHz Tektronix TCP312 is utilized to measure the current.

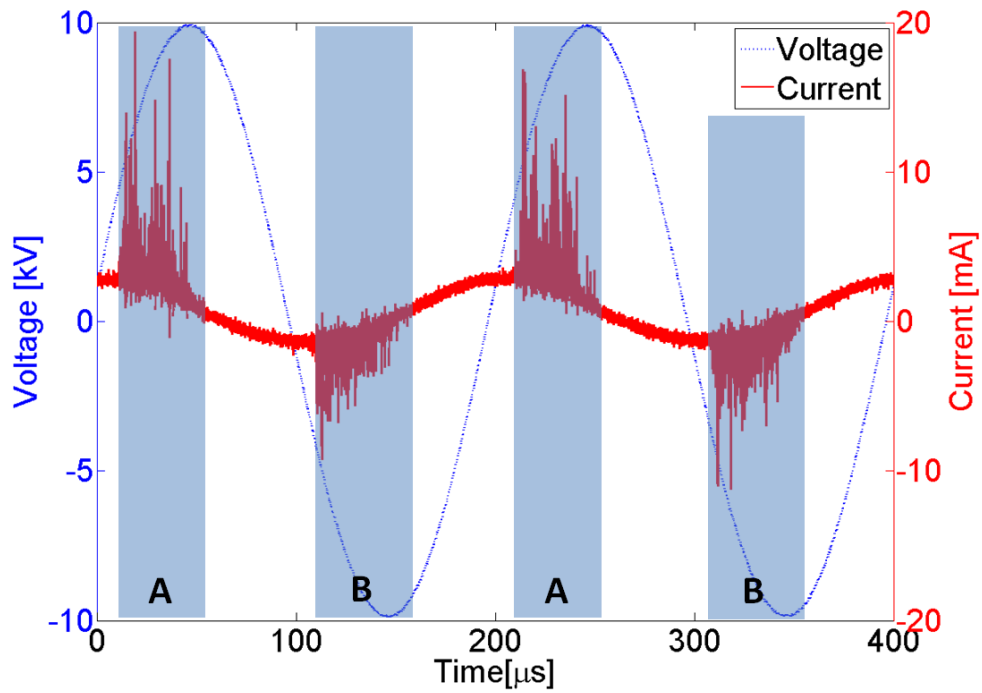


Figure 24 - Voltage and current trends over time.

As one can notice from Figure 22, the production of plasma on the bottom side of the DBD actuator is prevented by the application of a generous amount of epoxy resin at the periphery of the ground electrode. The formation of plasma in this region would not have affected velocity measurements of the induced air flow, but any evaluation on power would be influenced by the additional quota needed to ignite this extra plasma.

In Figure 25 the average electrical power absorbed by the actuators is plotted. The standard deviation value observed is limited to 3%.

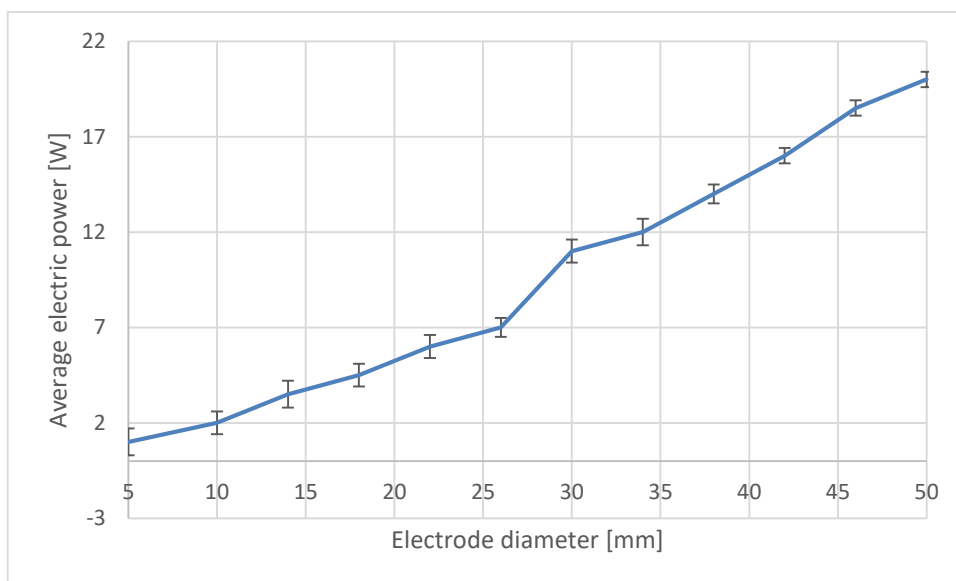


Figure 25 - Average electric power delivered to the plasma as a function of the upper electrode diameter.

The electric power increases by increasing the electrode diameter. In fact, the plasma surface linearly grows with increasing diameters. This is due to the geometry of the actuator.

### 6.3.2 Streamers length and plasma area

In order to further investigate the nature of those power trends, separate images of streamers coming from the upper electrode supplied with positive and negative voltages have been taken by means of an ICCD camera<sup>29</sup>. Images have been taken using an 80  $\mu\text{s}$  exposure time interval. This value ensures only positive or negative voltage streamers are imaged, since the time period of a semi-cycle for the applied 5 kHz AC voltage is 100  $\mu\text{s}$  (Figure 24).

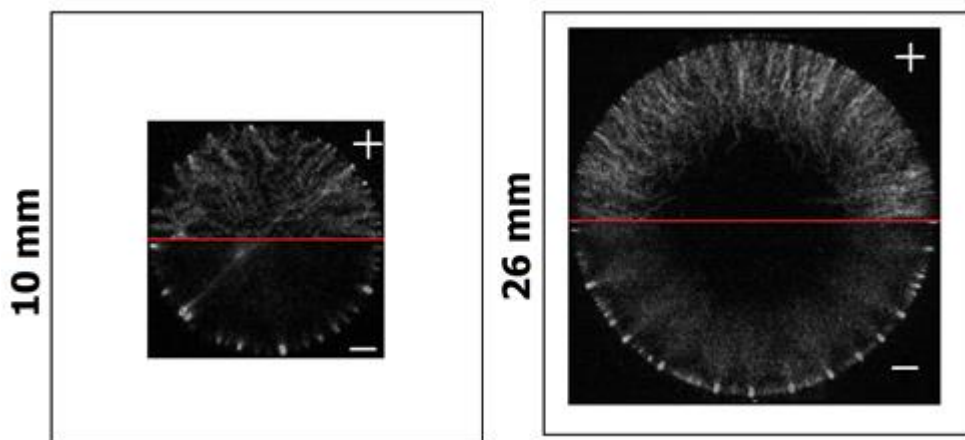


Figure 26 - ICCD images of streamers from 10 and 26 mm annular electrodes.

Figure 26 shows the plasma produced on the annular actuators with diameters of 10 and 26 mm. The upper part of the images show plasma streamers generated from a positive voltage (A in Figure 24). The lower part of the images show streamers generated from a negative voltage (B in Figure 24)<sup>30</sup>.

For the 10 mm diameter it appears that streamers are completely covering the inter-electrode area. With a gap of 26 mm, streamers are covering only a part of the inter-electrode surface in both cases. The average length in x-direction crossed by a streamer and the dielectric surface covered by plasma has been then determined from the ICCD plasma images. These quantities are plotted in Figure 27 as function of the diameter.

<sup>29</sup> ICCD images have been taken using a 4-Picos-dig S20 UV camera equipped with a Nikkor 35-80 f1/4-f1/5.6 lens and an 80  $\mu\text{s}$  exposure time interval. Separate images of streamers coming from the upper electrode supplied with positive and negative voltages have been taken triggering the camera when the AC voltage crosses the zero with a rising edge (positive voltage streamers) or a falling edge (negative voltage streamers).

<sup>30</sup> It is well known from the literature [Benard, Nicolas, and Eric Moreau. "Electrical and mechanical characteristics of surface AC dielectric barrier discharge plasma actuators applied to airflow control." *Experiments in Fluids* 55.11 (2014): 1-43.] that AC driven DBD actuators streamers are longer, brighter and more spatially separated during positive voltage slopes, while more diffused and limited during the negative ones.

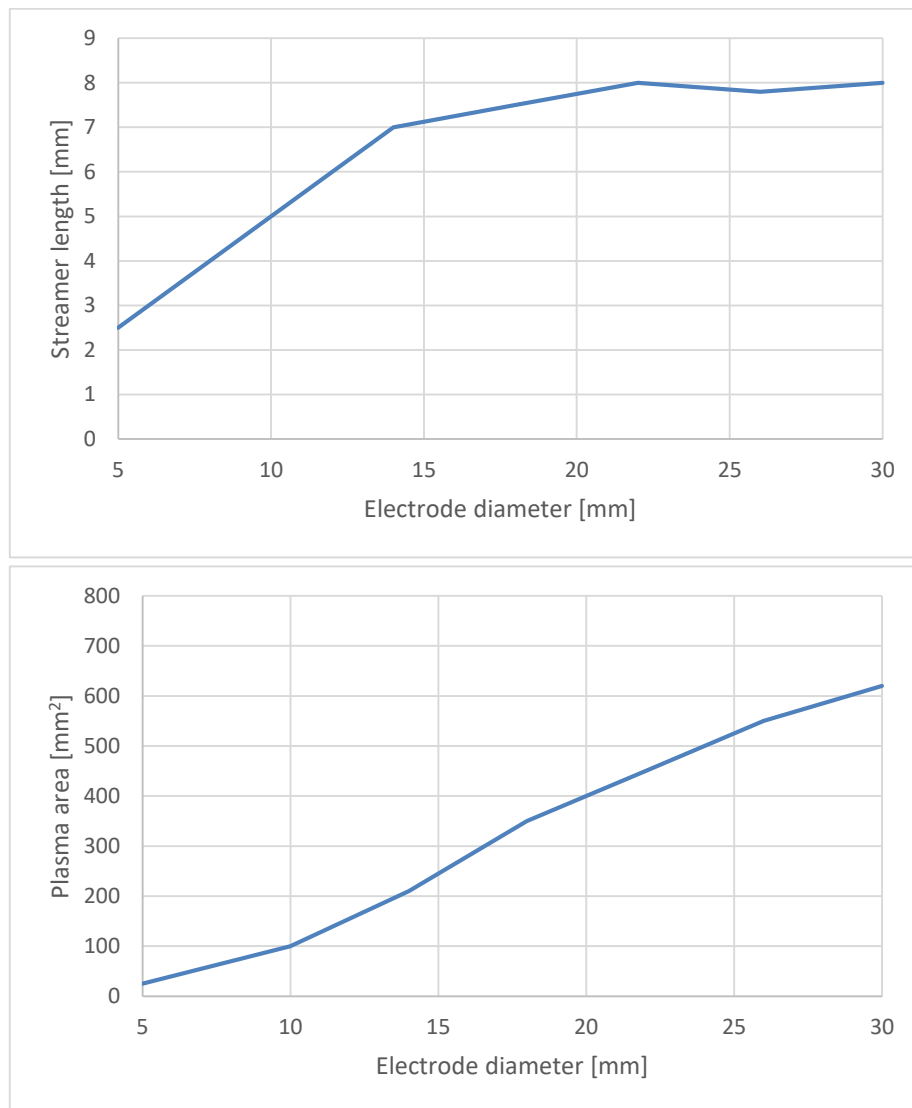


Figure 27 - Streamer length and plasma area for different electrode diameters.

Figure 27 shows how in annular actuators the streamer length is increasing for growing gaps from 10 to 22 mm. With gaps larger than 22 mm, the streamer length remains about equal to 8 mm. Correspondingly, the plasma surface goes from 25 mm<sup>2</sup> to about 620 mm<sup>2</sup>. With larger gaps (corresponding to a constant streamer length), plasma surface has an almost linear dependence to the electrode inner diameter, due the azimuthal symmetry of the electrode.

We can deduce that when the streamer is free to completely develop from an upper electrode along the x-direction, it crosses a distance of about 8 mm; this is what happens for gaps larger than 22 mm. For shorter gaps, the length travelled is smaller, as another streamer is coming from the opposite upper electrode. Streamers heads are characterized by a high charged particle density with the same polarity, as seen in section 2.1. Two streamers coming from opposite electrodes will therefore tend to repel each other, limiting their development and reducing the distance they can cover.

The electrical power increases when the streamer length and the plasma surface increase. We can correlate the plasma surface area to the electrical power feeding the annular actuators, completely justifying the results described in Figure 25.

### 6.3.3 Schlieren investigation

In order to visualize the jets during their development, Schlieren images were taken.

Schlieren imaging is used to photograph the flow of fluids of varying density. The classical implementation of an optical schlieren system uses light from a single collimated source shining on a target object.

Variations in refractive index caused by density gradients in the fluid distort the collimated light beam following the Snell's law:

$$n_1\theta_1 = n_2\theta_2$$

$$\frac{n_1}{n_2} = \frac{v_1}{v_2}$$

Where  $v_1$  and  $v_2$  are the phase velocities of light in the different mediums (Figure 28).

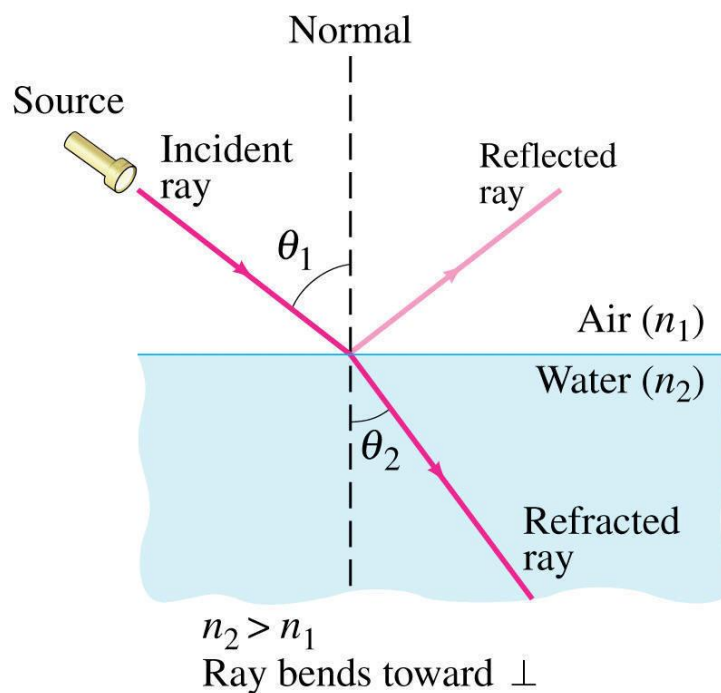


Figure 28 – Modification of the refractive index due to changes in the medium density.

This distortion creates a spatial variation in the intensity of the light, which can be visualised directly with a shadowgraph system. In classical schlieren photography, the collimated light is focused with a converging optical element (usually a lens or curved mirror), and a knife-edge is placed at the focal point, positioned to block about half the light. In flow of uniform density this will simply make the photograph half as bright. However, in flow with density variations the distorted beam focuses imperfectly, and parts which have been focused in an area covered by the knife-edge are blocked. The result is a set of lighter and darker patches corresponding to positive and negative fluid density gradients in the direction normal to the knife-edge.

Schlieren images have been taken using a Z-type configuration setup shown in Figure 29. The light source is a tungsten halogen low voltage lamp equipped with a rear reflector. The condenser of the optical system is a 40 mm double Gauss lens with an  $f=1.9$  focal ratio. The light beam is reflected by two off-axis parabolic mirrors 138 mm in diameter and with an  $f=3.5$  focal ratio. The light beam is along the z-direction (Figure 22). The knife edge is parallel to the actuator surface (the x-direction in Figure 22) so that the Schlieren

diagnostic can record density gradients perpendicular to it (the y-direction in Figure 22). The images are detected by a CCD camera equipped with a super-video-graphics array resolution with a pixel size of  $6 \times 6 \mu\text{m}^2$  and an exposure time of 1 ms [56].

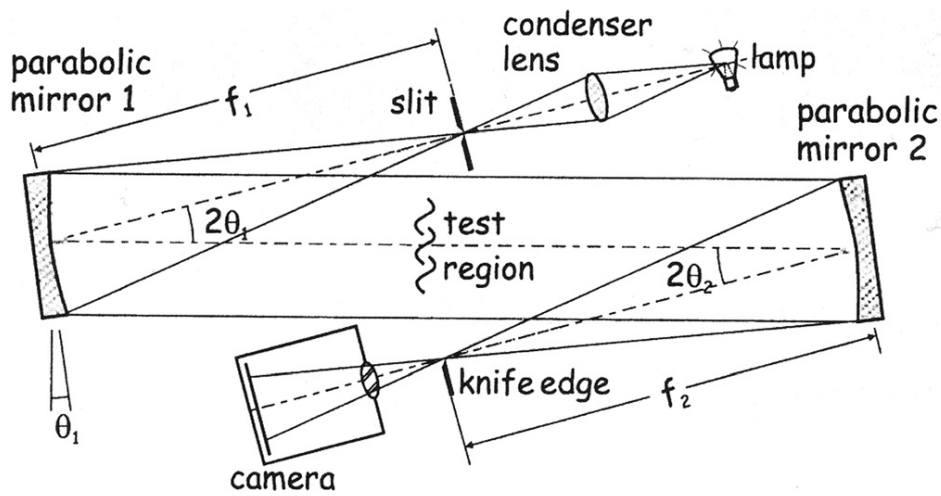


Figure 29 - Z-type configuration Schlieren setup.

The CCD camera was triggered with increasing delay times after the discharge ignition, obtaining a complete picture of the jets' development. The validity of this procedure has been checked acquiring several pictures with the same delay and condition, obtaining the same results.

Schlieren images of annular actuators after 30 ms from discharge ignition are shown in Figure 30.

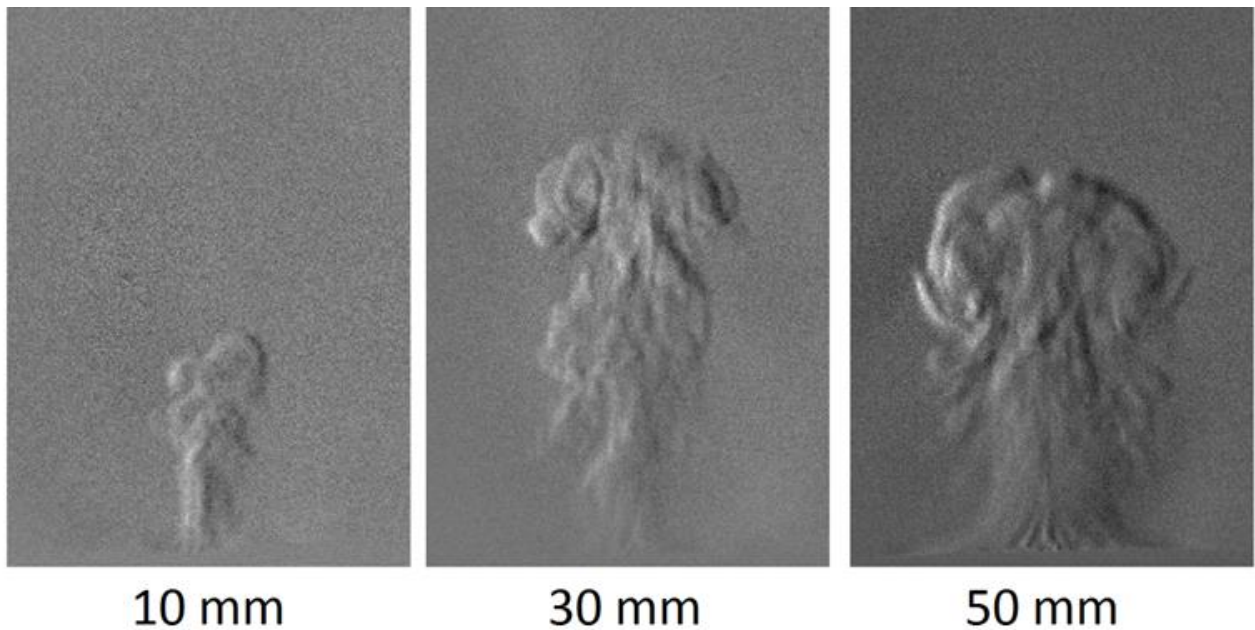


Figure 30 - Schlieren images showing the induced air flow after 30 ms from plasma ignition.

The picture clearly shows geometry's influence on EHD effect. In particular, smaller diameters have been found the least effective to induce any fluid motion, up to its complete prevention for the 5 mm case, therefore they are more desirable in this particular work.

#### 6.3.4 Velocity profiles

Normal component (y-direction in Figure 22) of the induced velocity along the x-direction has been measured by using a Pitot tube positioned at a distance of 5 mm from actuator surface.

The Pitot tube was connected to a DCAL401 Sursense ultra-low pressure sensor with a sensitivity of 32 mV/Pa and the measurements have been averaged over 5 different tests. All the measurements have been filtered by using a first order RC low pass filter with a cut off frequency of 100 Hz. Negative pressures detected from the sensor have been set to zero, since only positive pressures can be correlated to air velocities when using a Pitot tube. The Pitot tube was moved along the x-direction by a step motor with a linear resolution of 0.03 mm. All velocity measurements reported in this work were characterized by relative standard deviations within 10%.

Results from the measurements confirm the results previously anticipated by the Schlieren imaging, and are shown in Figure 31. Data for the 5 mm diameter have been neglected since they didn't overcome the minimum sensitivity of the setup used for this experiment, which is 1 m/s.

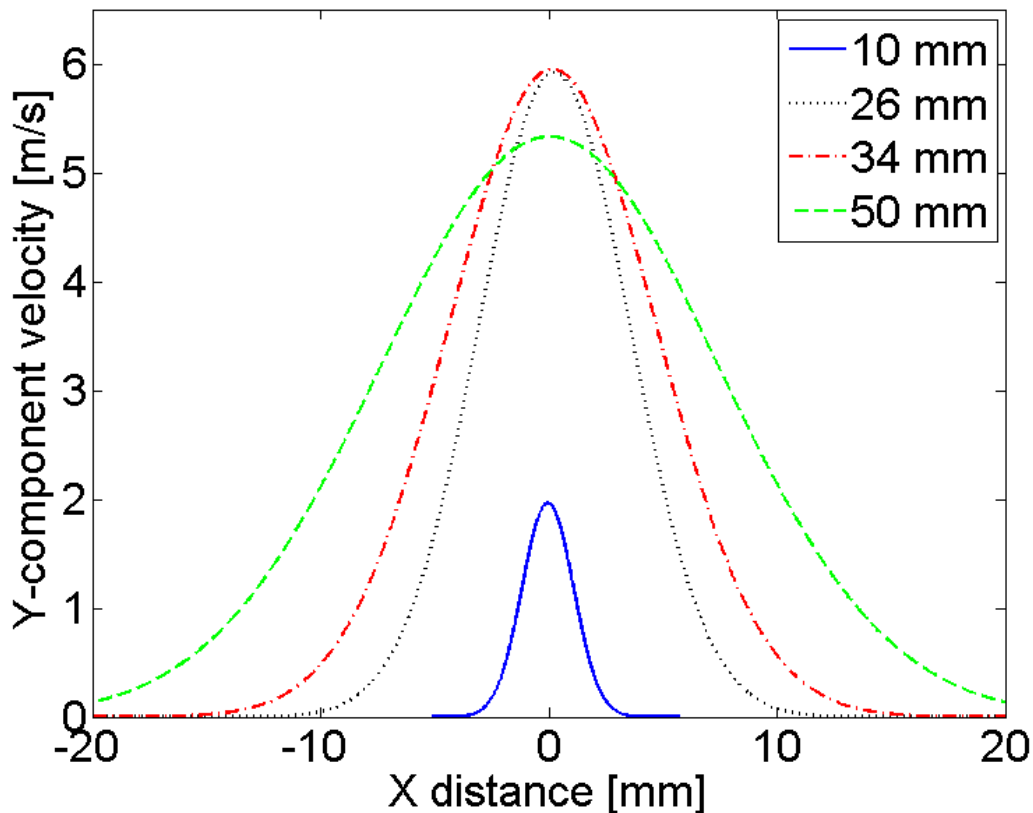


Figure 31 - Normal component of the induced velocity along the x-direction for different electrode diameters.

Maximum velocities achieved at a height of 5 mm above the actuators are shown in Figure 32. In the annular actuator the maximum velocity is observed at the centre of the circular electrode, where the  $x = 0$  coordinate has been imposed. The maximum velocity increases with larger inner diameters of the upper electrode, until a diameter of 30 mm is reached. With this diameter the maximum velocity measured at 5

mm above the actuator surface is 6.1 m/s. For diameters larger than 30 mm, maximum velocities are decreasing.

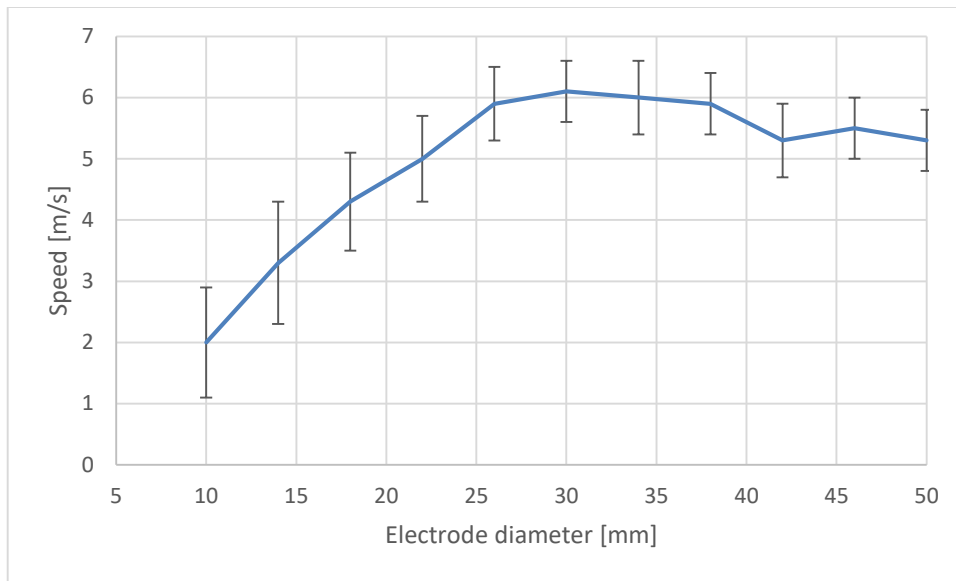


Figure 32 - Maximum induced speeds for different actuators diameters.

#### 6.4 Conclusions

This investigation clearly shows how geometry is a crucial variable of an EHD plasma actuator. In order to reduce or even remove the EHD effect from the variables of my experiment, electrodes inner diameter is not only a simple design choice, but also an effective parameter to be tuned for optimal performance. In my case, 5 mm diameter holes are the best choice to completely eliminate any EHD effect influence on the following experiments. A Schlieren image of an array of ten 5-mm actuators close to each other is pictured in Figure 33 confirming that not even an array of annular actuators has any EHD capabilities.

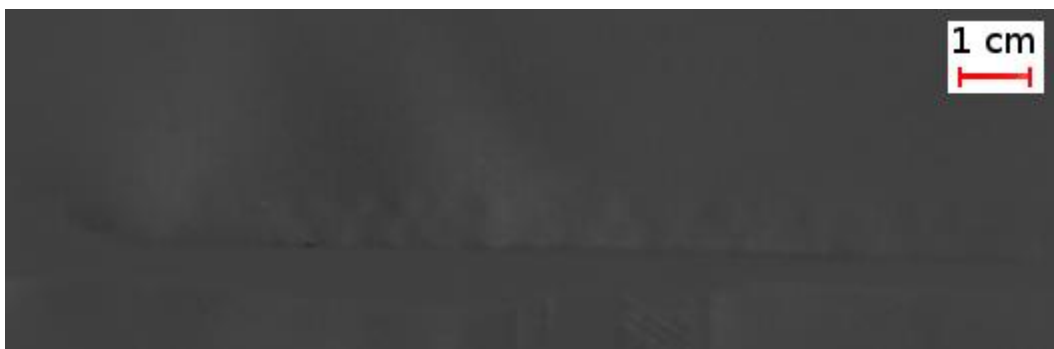


Figure 33 - Schlieren imaging of an array of 10 actuators with 5 mm diameter upper electrodes. Since the amount of EHD effect is practically negligible, the picture's quality cannot be enhanced.

The design of choice will be composed of a 2-layer PCB as previously stated, with a circular, 20 mm diameter, high voltage electrode on one side, and a ground electrode featuring an array of 13, 4 mm diameter holes on the other, as shown in Figure 34.

This study also shows that for the materials and power input levels used, annular electrodes with a 30 mm diameter outperform other designs. Different boundary conditions are however likely to influence the optimal diameter.

### 6.5 Final reactor's geometry

A custom-built surface dielectric barrier discharge (DBD) plasma device was fabricated. The plasma source consists of a 1.6 mm thick dielectric substrate (glass reinforced epoxy FR-4) with a powered copper plane on one side and a ground mesh-like copper electrode on the other, matching the discussed geometrical needs. The DBD plasma device that will be used in this work is composed by an array of several annular actuators, as shown in Figure 34.

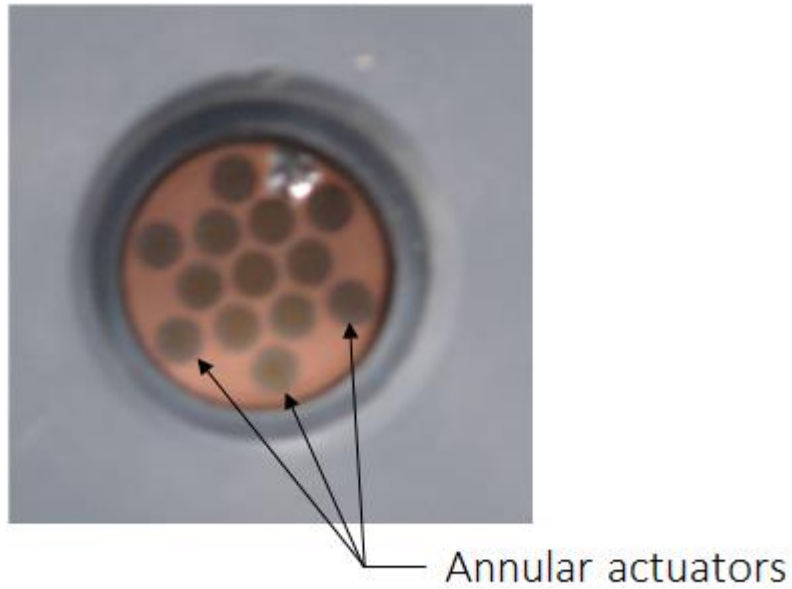


Figure 34 - Design of the ground annular actuators array used in this work.

## CHAPTER 7

### 7 A REFERENCE PROTOCOL

The objective of the present chapter is to propose a *biological* protocol for assessing the biocidal efficacy of the gas plasma device designed in the previous section so as to enable meaningful comparisons to be made between different operating conditions.

This chapter will propose a comparison between the consistency of results obtained with two organisms, and two forms in which the biological agents in question are presented to the plasma. Besides plasma treatment, irradiation of bacteria-laden membranes with UV light at a wavelength of 254 nm was also conducted in order to facilitate interpretation of the results on the basis that emission from simple UV sources is intrinsically reproducible and that it remains stable over time.

#### 7.1 Reference biological agent

Spores of the Gram positive bacterium *Bacillus subtilis* (ATCC 6633) are proposed as the reference biological agent. The advantages of using this particular bacterium are that it is non-pathogenic and therefore it can be widely used without high biological safety requirements, and once produced, spores stocks can be kept for many years with only a negligible reduction in viability. Although a new stock was prepared for this work in order to document precisely all the preparation steps, spores stocks in the lab that were prepared almost a decade ago were present and have over this period exhibited negligible loss of viability. This is hardly surprising given the intrinsic resistance of spores to radiation, heat and chemicals [81]. In fact, spores of the genus *Bacillus* (albeit *B. sphaericus* rather than *B. subtilis*), have been revived after more than 25 million years [82].

Using spores from a stock obviates the need to produce micro-organisms at a particular phase of growth for each experimental trial, which reduces variability between experiments and speeds up experimental procedures. Since spores are likely to be present in most practical applications and they are more resistant to external stresses than are vegetative bacteria, the use of spores would also add relevance to the inactivation results obtained in the proposed reference test.

Notwithstanding such considerations, it is important to ensure that the conditions under which the spores are generated is consistent as otherwise this will affect their resistance to gas plasma treatment [83]. This fact explains the exceedingly detailed procedures described for generating spore stocks and why it is necessary to adhere to them.

As a means of assessing the benefits of using *B. subtilis* spores as a reference biological micro-organism, inactivation tests with another bacterium have also been conducted for comparison. Methicillin resistant *Staphylococcus aureus* (MRSA PM64) was used in this case for its clinical relevance. Experiments involving MRSA required a Class II biological laboratory and to minimise the sources of variability between experiments with spores of *B. subtilis* and those with MRSA, all the experiments reported in this work were performed in the same Class II facility. Besides the additional biological safety demands and the longer preparation time required to prepare mid-log phase bacteria for each separate experiment, MRSA is also more liable to form cell clusters. As colonies formed from cell agglomerates cannot be differentiated from those originating from single cells, clustering is a source of variability that affects plate counts.

Furthermore, cell clustering also affects the consistency in which a monolayer of cells can be deposited (see section 7.2 below).

Although the plasma gas temperature can be actively controlled [84], most plasma treatments reported in the literature are conducted at room temperature without tight control over the temperature at which the cells are being treated. The resistance of vegetative cells to external stressors, however, can be quite sensitive to small temperature variations, and only a few degree difference can drastically change the cell response. For example, it has been documented that the antibiotic resistance of MRSA can change significantly depending on the temperature (30-37°C) at which this is measured [85, 86].

Therefore, the use of a less temperature sensitive biological agent, such as spores of *B. subtilis*, provides a more robust reference test and will enable meaningful comparisons between plasma devices in different labs without the need to exercise tight control over temperature during cultivation and subsequent processing.

#### 7.1.1 Preparation of the *B. subtilis* spores stock

The method employed to generate spores was essentially that described by Harnulv and Syngg [87] with minor variations to their procedures. Nutrient agar<sup>31</sup> slopes of *Bacillus subtilis* (NCIMB 8054/ATCC 6633) were prepared from a lyophilised culture obtained from the National Collection of Industrial and Marine Bacteria<sup>32</sup> using standard microbiological procedures. A loopful of cells from one such slope was used to inoculate 100 ml of Nutrient Broth<sup>33</sup> in a 500 ml Erlenmeyer flask which was then incubated at 37 °C for 24 hours in a rotary shaker at 130 rpm. Aliquots (200 µL) of this culture were pipetted onto the surface of 140 mm diameter petri dishes containing Sporulation Agar prepared as described by Harnulv and Syngg [87], which were then incubated at 30 °C for 14 days. After this period of time, de-ionised water (5 mL) was gently pipetted onto the surface of the agar and the bacterial growth was gently suspended into the water using a sterile loop. The accumulated spore suspensions from 5 petri dishes were then combined and centrifuged<sup>34</sup> at 8,000 x g for 20 minutes. The supernatant was then poured off and 10 mL of de-ionised water were pipetted into the centrifuge tube. The tube was then vigorously agitated to resuspend the pellet on a vortex mixer. This procedure of centrifugation and washing was repeated a further two times. The suspension was then transferred to a thin walled glass vial of 82 mm height and 27 mm dia<sup>35</sup>. The vial was then placed in water bath containing 20 L of water at ambient temperature<sup>36</sup> and the temperature of the bath was increased to 70°C at a rate of 2°C/min. Once the water bath had reached the set point (70 °C), it was maintained at this temperature for 30 minutes. The vial containing the spore suspension was removed from the water bath and stored at 4°C until needed. The spore concentration was measured to be  $1.5 \times 10^{10}$  spores per ml.

#### 7.1.2 Preparation of MRSA cultures

A clinical isolate of MRSA (PM64) was kindly donated by Dr Julie Morrissey of the Department of Genetics, University of Leicester, UK. The culture was maintained on Luria Agar slopes and stored in a refrigerator for no more than one month before subculturing. In order to prepare cultures for experiments, a loopful of cells from a slope were used to inoculate 100 ml of Luria Broth in a 500 ml Erlenmeyer flask which was

---

<sup>31</sup>Oxoid Ltd, Basingstoke, Berks

<sup>32</sup>Aberdeen, UK

<sup>33</sup> Oxoid

<sup>34</sup> Centrifuge model Z383K, Hermle Labortechnik GmbH, Wehningen, Germany

<sup>35</sup> Ref. 14823562, Fisher Scientific UK Ltd, Loughborough, UK

<sup>36</sup> Clifton NE2-22D, Fisher Scientific UK Ltd, Loughborough, UK

incubated on a rotary shaker at 37 °C and 130 rpm for 17 hours. Following this a 1 mL aliquot of this culture was used to inoculate a fresh flask of Luria broth incubated as described above for 4 hours in order to generate a mid-log phase culture ( $9.8 \times 10^8$  CFU/ml). A 10 mL aliquot of this culture was transferred to a sterile centrifuge tube and centrifuged<sup>37</sup> at 1750 x g for 30 minutes. The supernatant was poured off and 10ml of sterile Ringer's solution<sup>38</sup> was added to the tube. After vortexing to resuspend the pellet, the broth was centrifuged under identical conditions to those described above a further two times to yield a suspension of MRSA for deposition on membranes.

## **7.2 Comparison of results from filtration and pipetting procedures**

The physical state in which the micro-organisms are presented to the gas plasma influences their resistance to the treatment and therefore, in order to achieve meaningful comparisons between plasma devices it is important that not only the same microorganism be used, but also that the micro-organisms are presented in a consistent and repeatable form. To accomplish this, it is proposed that membranes loaded with a monolayer of bacteria are used. The membranes provide a consistent substrate for the deposition and recovery of micro-organisms and by depositing a monolayer of microorganisms, variability and problems associated with shadowing and stacking of bacteria are overcome [88].

### **7.2.1 Filtering protocol**

The B.Subtilis spore stock suspension was highly concentrated, and it was found necessary to dilute it in two stages in order to obtain a homogeneous suspension of disaggregated spores. To do this, 100 µl of spore stock was added to 900 µL of Ringers solution in an Eppendorf tube which was then vigorously agitated using a vortex mixer. A 90 µl aliquot of this suspension was added to 10 mL of Ringers solution. This suspension was then drawn into a 10 mL syringe which was mounted onto an autoclave-sterilised Swinnex filter holder with a Lauer fitting<sup>39</sup>. A 25 mm diameter Nucleopore track-etched polycarbonate hydrophilic membrane with a pore size of 0.2 µm<sup>40</sup> was loaded into the filter holder. The assembly was inserted through a rubber bung which was used to seal a heavy-walled glass conical flask of 2 L capacity and fitted with a side arm which was connected to a vacuum pump<sup>41</sup>. The arrangement is similar to that used by Bayliss et al [88] and a schematic is shown in Figure 35.

---

<sup>37</sup> Heraeus Labofuge 400R, Fisher Scientific UK Ltd, Loughborough, UK

<sup>38</sup> Oxoid

<sup>39</sup> SX0002500, Millipore Limited, Watford, UK

<sup>40</sup> GE Healthcare Life Sciences, Little Chalfont, UK

<sup>41</sup> Model N810FF-18, KNF Neuberger Inc, Trenton, USA

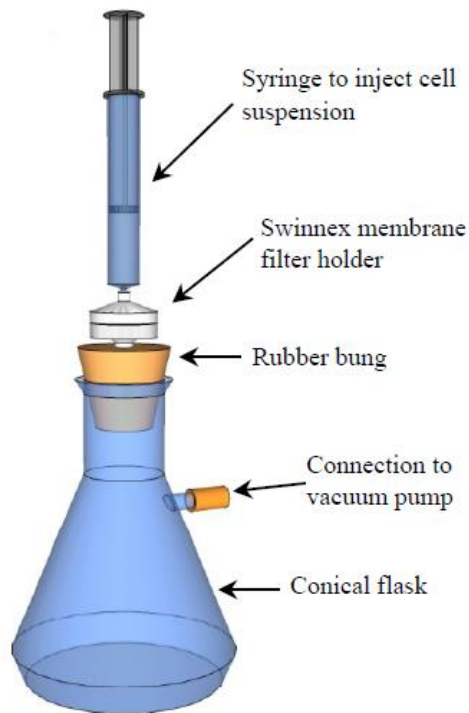


Figure 35 - Schematic of the arrangement used to filter-deposit cells onto membranes.

Filtration was conducted at 66kPa. Following this, the membrane holder was removed from the system and disassembled to permit the membrane to be carefully removed using fine-tipped forceps and then placed in an open petri dish to dry.

The procedure employed to deposit a layer of isolated bacteria on a membrane with MRSA was identical to that described above for *B.subtilis* with the exception that 220  $\mu\text{L}$  of the working suspension was pipetted into 10ml of Ringers solution for filtration.

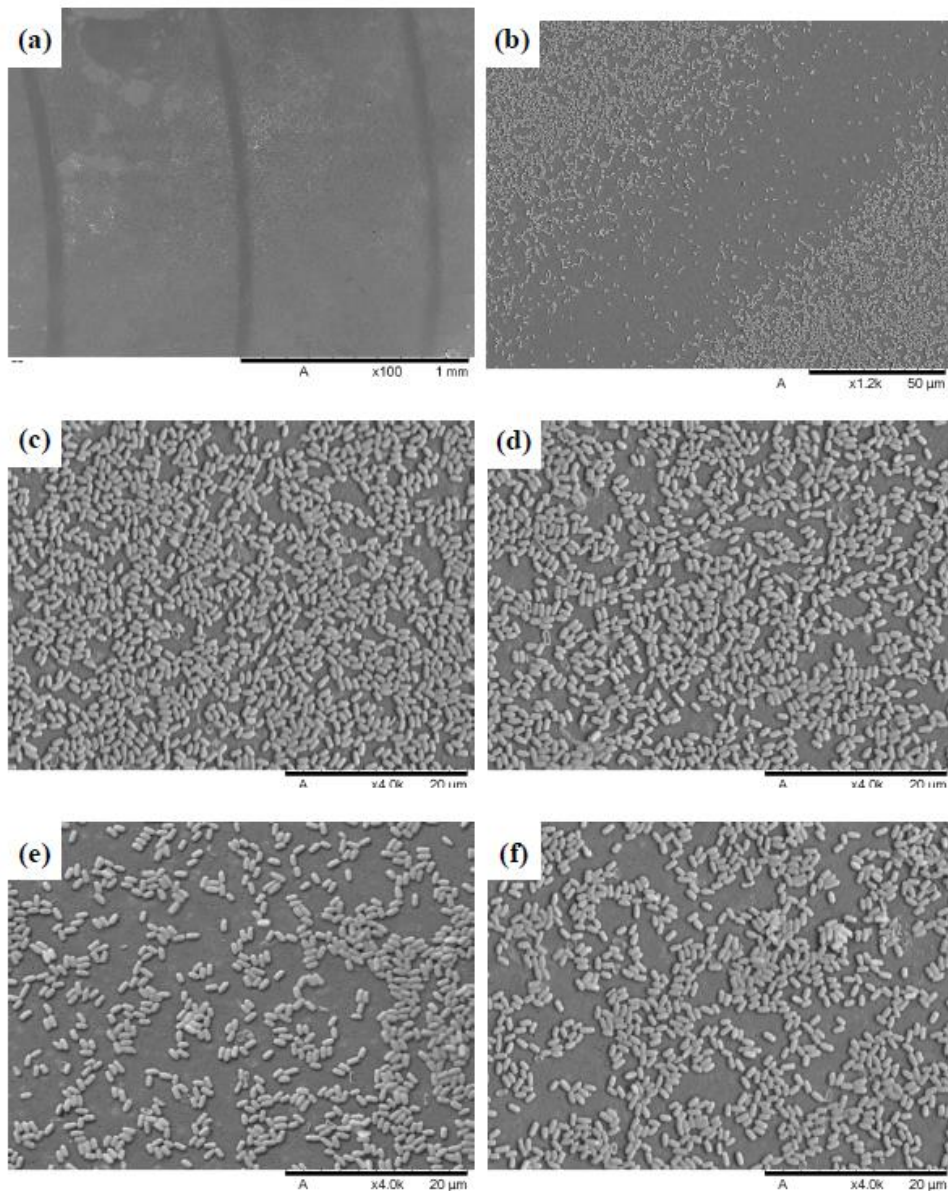


Figure 36 - SEM images of a *Bacillus subtilis* spore laden membrane. (a) Low magnification image showing concentric rings where spores are not deposited due to the geometric configuration of the membrane holder used during the filtration. (b) Close up view at one of the rings. (c-d) Close up view at two regions with high concentration of spores. (e-f) Close up view at two regions with low concentration of spores.

Most significantly, the distribution of spores across the entire membrane is fairly uniform. This is shown in the SEM images<sup>42</sup> of Figure 36 taken at four different locations across the same membrane. Two of these images were taken at regions which displayed a relatively high spore concentration (Figure 36 c, d) and two at regions with a relatively low spore concentration (Figure 36 e, f). These images clearly show that stacking of spores did not occur.

### 7.2.2 Pipetting protocol

<sup>42</sup> The procedure for preparing MRSA laden membranes for SEM imaging was identical to that described by Bayliss et al. [28]. Following the washing and dehydrating procedure, samples were coated with gold palladium using a sputter-coater for 90s at 25mA. The SEM images were obtained using a SEM microscope. For *B. subtilis* laden membrane, the protocol was modified to avoid washing off spores during the fixation and dehydrating procedure. In particular, the first 1% glutaraldehyde and the ethanol washing stages were omitted and samples were left to dry overnight to avoid having to pour off excess solutions which had a tendency to remove “rafts” of spores.

The pipetting protocols were designed to deliver the same number of cells per unit area of membrane as for filtration. An aliquot (98  $\mu$ L) of the working *B. Subtilis* spore stock suspension was pipetted directly onto a sterile membrane placed in a petri dish. The petri dish was then placed on a hot plate<sup>43</sup> at 40° C until all the liquid had evaporated. With MRSA the procedure outlined above was followed with the exception that 270  $\mu$ L of the working suspension was pipetted onto each membrane.

In the calculations conducted, account was made of the effective area of the membrane upon which the cells are deposited. This was because it was observed that in the case of filtration, contact of the membrane with the underlying supporting rings reduced the available area where cell could be deposited. The dimensions of these rings depend on the specific membrane holder used. These concentric rings formed on a *B. subtilis* spore-laden membrane are shown in Figure 36 a,b.

The stacking and the extent of the unpopulated regions observed in the pipette-deposited membranes of Figure 37 appears to be random as these are driven by surface tension forces acting during the drying process.

---

<sup>43</sup> 11-102-50SH Fisher Scientific UK Ltd, Loughborough, UK

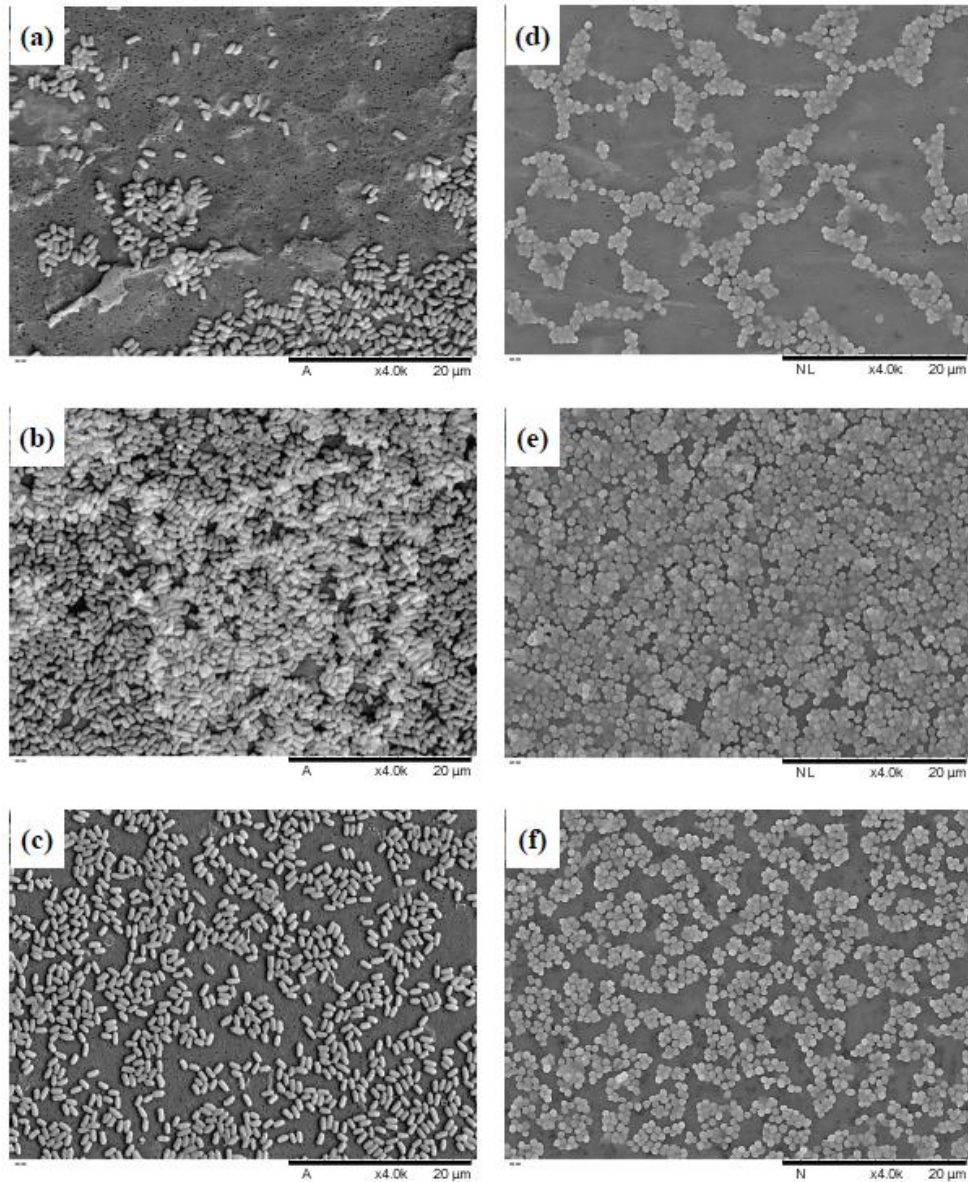


Figure 37 - SEM images of two regions of the same membranes laden with pipetted (a-c) *Bacillus subtilis* and (d-e) MRSA.

It is worth mentioning that even when the density of cells in the pipetted solution is lowered, agglomeration and stacking of cells persist. This random distribution of cells affects the inactivation tests because bacteria shielded in regions where stacking occurs will be more resistant to plasma than bacteria directly exposed to the plasma in regions where few cells have been deposited. Therefore, pipetting would inevitably contribute to variability in the results of inactivation tests, preventing meaningful comparison between different plasma operating conditions.

### 7.2.3 Comparison of the filtering and pipetting procedures

Figure 38 shows a comparison between the two deposition methods considered in this study, namely the proposed membrane filtering technique and the widely-used method of pipetting cell suspensions directly onto membranes.

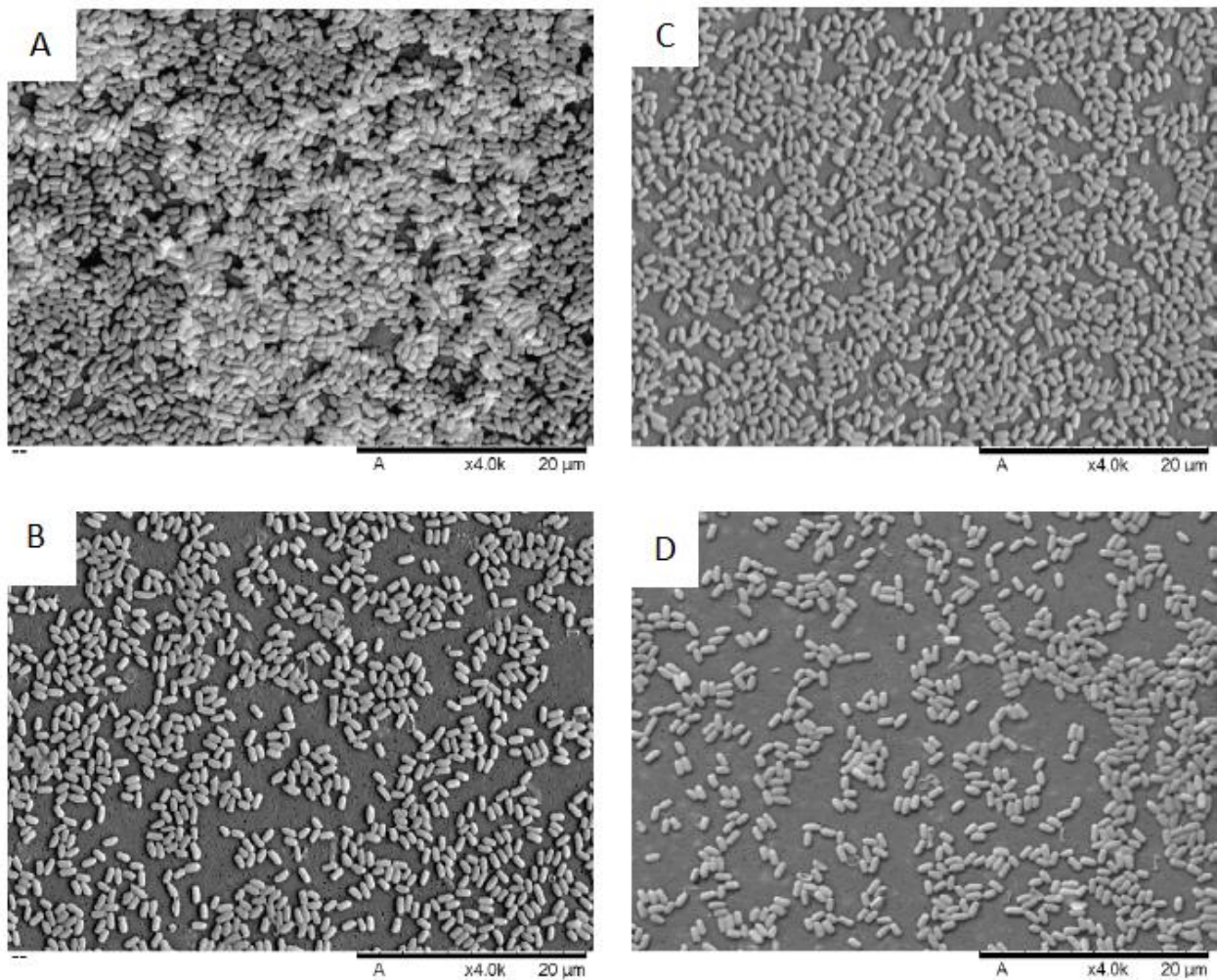


Figure 38 – SEM images of two regions of membranes laden with (a, b) pipetted and (c, d) filtered *B. subtilis* spores

Whereas pipetting cell suspensions onto membranes results in large variations in the way cells are deposited across the same membrane (see Figure 38 a, b for spores of *B. subtilis* and Figure 37 d-f for MRSA), the proposed filtering technique deposits cells uniformly across the whole membrane (with the exception of the ring regions as described above where no cells are deposited – see Figure 36 c-f).

### 7.3 Cells recovery

Besides sample preparation for inactivation tests, it is also imperative to assess the recovery of cells from the membranes following the exposure to the biocidal agent. To recover cells, the micro-organism laden membranes were transferred to sterile glass Universal bottles containing 10ml Ringers solution and five 3 mm glass Ballotini beads<sup>44</sup>. The contents of the bottle were then vigorously agitated for 45 seconds using a vortex mixer. Serial dilutions in Ringers solution were carried out prior to plating 100  $\mu$ L aliquots onto LB agar plates and incubating overnight at 37° C prior to counting the colonies formed. Counts were performed in triplicate.

<sup>44</sup> VWR International Ltd, Lutterworth, UK

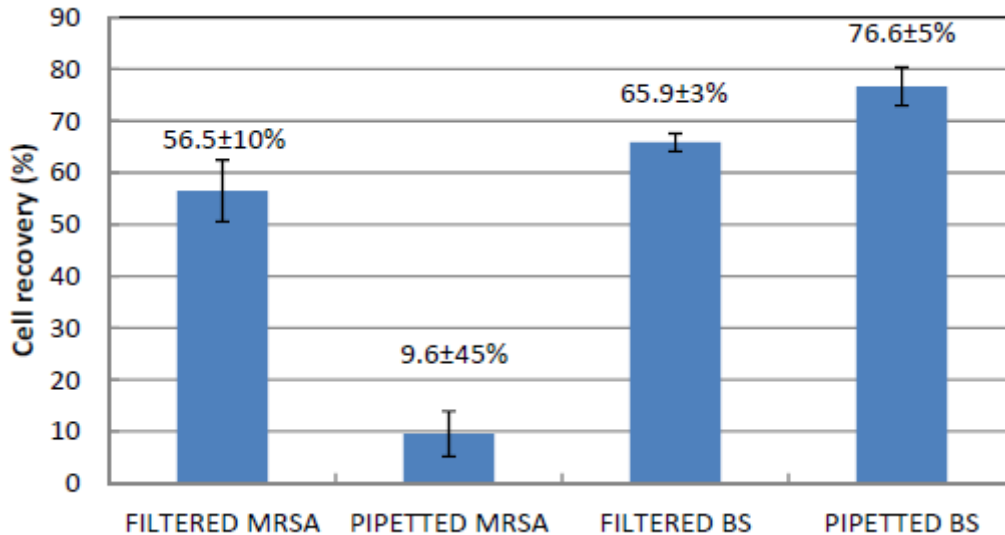


Figure 39 - Cell recovery from *B. subtilis* and MRSA laden membranes. Error bars represent standard deviation based on 4 experimental replicates.

Figure 39 shows the percentage of cells recovered from membranes laden with *B. subtilis* and MRSA using the proposed filtering technique and the conventional pipetting method. The percentage of cells recovered is dependent both upon the identity of the micro-organism and the deposition method employed, and in the case of pipetted MRSA only 9% of the deposited bacteria was recovered whereas in the case of pipetted *B. subtilis* 76% of the spores were retrieved. The very low MRSA recovery for pipetted samples is attributed to the tendency of MRSA bacteria to form clusters which, as explained above, in relation to plate counting will result in an underestimation of the actual number of viable cells. Although a low recovery is not a problem in itself, small variations in the low recovery rates translate into large relative errors (45% for the recovery of pipetted MRSA) and these would introduce large uncertainties in the inactivation tests.

It is worth noting that for both micro-organisms, recovery from filtered samples results in smaller error bars, i.e. better reproducibility, than for pipetted samples. This improved consistency in the recovery of filtered samples is attributed to the more reproducible deposition of cells across the membrane and in the reduction in the number of cell clusters present when the filtering technique is used. Although recovery of *B. subtilis* from filtered membranes is less effective than from pipetted membranes (probably due to some spores becoming trapped in the membrane after the pressure driven deposition), it is evident that the smallest error bars in the recovery data (3%) were obtained for the proposed protocol of filter-deposited *B. subtilis* spores.

#### 7.4 UV inactivation of *B. subtilis* and MRSA

Inactivation tests of *B. subtilis* and MRSA, both filtered and pipetted, were conducted by irradiating bacteria-laden membranes with UV light at 254nm. The goal of these tests was to demonstrate that more repeatable results are obtained when the proposed protocol (i.e. filtered membranes with *B. subtilis* spores) is used.

Membranes were placed inside open petri dishes for UV treatment. The petri dish was placed on a platform which rotated at 4 rpm directly underneath a 5W mercury vapour UV source<sup>45</sup>. The lamp was housed in a fixture which had a 2x9cm aperture. The distance between the source and the base of the petri dish being

<sup>45</sup> TUV 5W-F, Philips Belgium N.V., Brussels, BE

210 mm. For irradiating MRSA-laden membranes a tightly woven stainless steel mesh was placed immediately beneath the aperture to reduce the UV intensity. This was measured using a radiometer<sup>46</sup>. The UV intensity for irradiating *B. subtilis* laden membranes was 25.01  $\mu\text{W}/\text{cm}^2$ , whilst that for MRSA was 1.16  $\mu\text{W}/\text{cm}^2$ .

Figure 40 shows the results of these inactivation tests. Each curve shown in Figure 40 corresponds to the average of triplicate experiments. These triplicate experiments were conducted on the same day and from the same initial spore stock or cell suspension. Triplicate experiments were then repeated a further three times on different days and the average of all these experiments is shown in Figure 40 using solid black lines. Error bars represent the standard deviation from the mean. For both micro-organisms considered in this study, inactivation results determined from filtered samples are more reproducible than results obtained using pipetted samples (compare Figure 40 a and c for *B. subtilis* and Figure 40 b and d for MRSA).

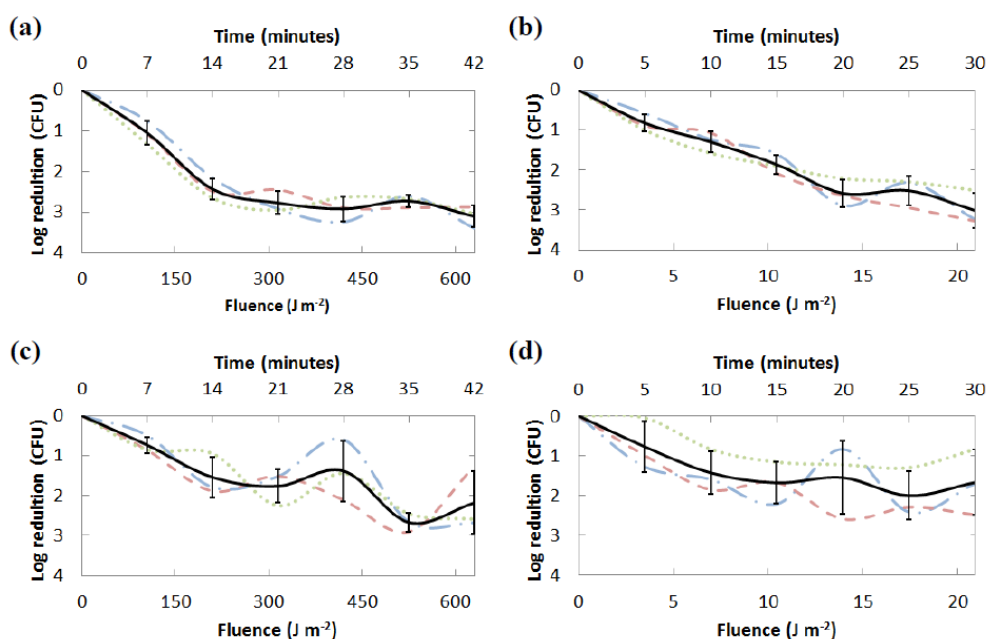


Figure 40 - Inactivation kinetics of (a) filtered *B. subtilis* spores, (b) filtered MRSA, (c) pipetted *B. subtilis* spores and (d) pipetted MRSA by 254nm UV irradiation.

Unsurprisingly, it is evident that micro-organisms filtered onto membranes can be inactivated more readily than those that were pipetted. For the present conditions, a further 1-log reduction is obtained for the longest treatment times. The lower inactivation efficacy against pipetted micro-organism is attributed to the protective shielding that occurs in regions where stacking takes place in pipette-prepared membranes (see Figure 37 b and e). When comparing the inactivation curve of *B. subtilis* spores with that of MRSA, it is evident that the *B. subtilis* spores are more resistant to UV irradiation, requiring about 15 times higher UV dosage to achieve the same log reduction. It is also noted that for both, the pipetting technique and the filtering method, inactivation of *B. subtilis* spores were found to be more reproducible than their MRSA counterparts (compare errorbars in Figure 40 a and c for MRSA cells and Figure 40 b and d for *B. subtilis* cells). In summary, of the four sample preparation methods considered, *B. subtilis* spores filtered onto membranes provides the most reproducible results.

<sup>46</sup> Model UVX, UVP Ltd., Cambridge, UK

## 7.5 Plasma inactivation of *B. subtilis* and MRSA

Inactivation tests of *B. subtilis* and MRSA, both filtered and pipetted, were also conducted by exposing bacteria-laden membranes to an atmospheric pressure air DBD discharge. As for the UV inactivation experiments, the goal of these tests was to demonstrate that more repeatable results are obtained when the proposed protocol is used.

### 7.5.1 DBD reactor design

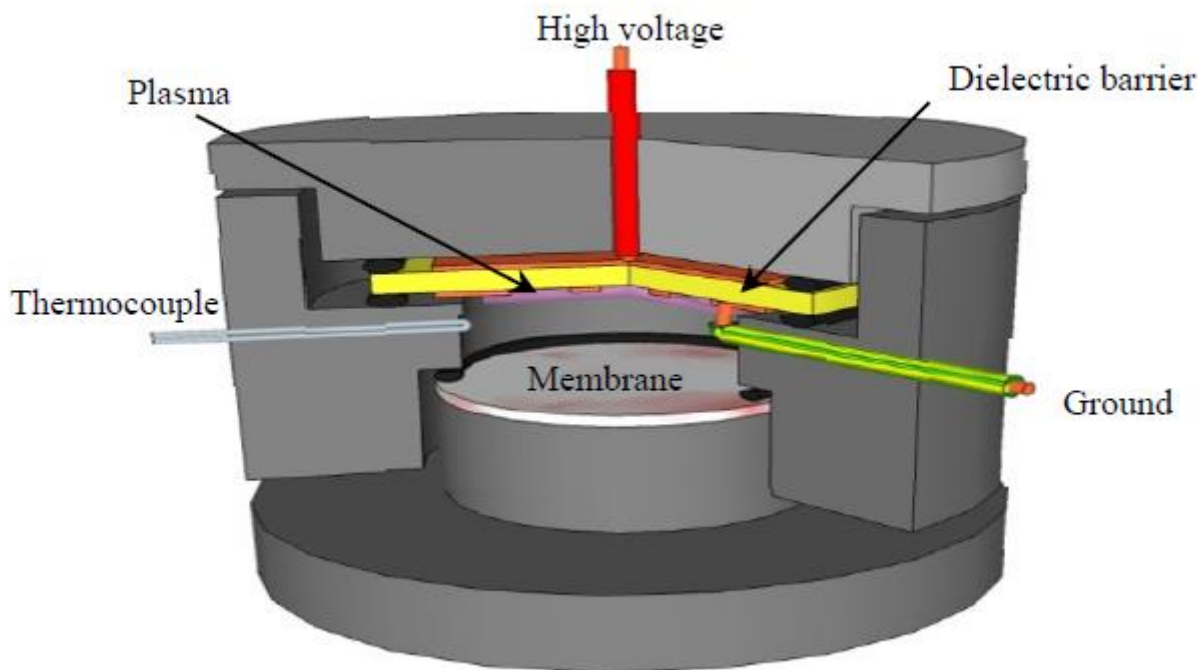


Figure 41 - Schematic of the plasma device used to treat the spore/cell laden membranes. The membrane is clamped by an O-ring onto the base of the device.

The custom-built surface DBD plasma device described in section 6.5 was fabricated to treat the membranes (Figure 41). In this configuration of the actuator's electrodes polarity is the reverse of the one seen in Figure 22. This is a fundamental safety precaution that keeps the high voltage side of the actuator hidden from the operator, exposing the ground side only. This choice does not influence the validity of the previous discussion, since the electrodes are fed with symmetrical, sinusoidal current. The bacteria-laden membranes were transferred from petri dishes to the plasma device sample holder using sterile thin tipped forceps making sure to only contact the outer edge of the membrane where no cells were present.

The system is operated in its closed modality and operates in ambient air.

### 7.5.2 Plasma source and electric measurements

The membranes were kept at a distance of 9mm from the plasma source. The plasma source was powered by an in-house built half-bridge resonant power supply that delivered a sinusoidal voltage of 5.25kV at 20.5kHz. The applied voltage was modulated by a square signal of 2Hz with a duty cycle of 5%, i.e. plasma on-time of 25ms every half second. The time averaged power delivered to the plasma was 850mW, as determined by the analysis of the charge vs voltage (Q-V) Lissajous diagram [89].

### 7.5.3 Reactor's temperatures

The maximum temperature reached during a plasma treatment was monitored using a K-type thermocouple<sup>47</sup> placed 2mm below the plasma source. A second set of data has been acquired by means of thermal imaging<sup>48</sup> on the exposed dielectric layer, confirming the following results. The plasma system was left to cool down to room temperature after each run. Figure 42 shows that the temperature in the system is increased by 7 degrees above ambient temperature after 1h of operation, but for the much shorter treatments employed for the MRSA inactivation tests, the increase in temperature was less than 2°C above the room temperature.

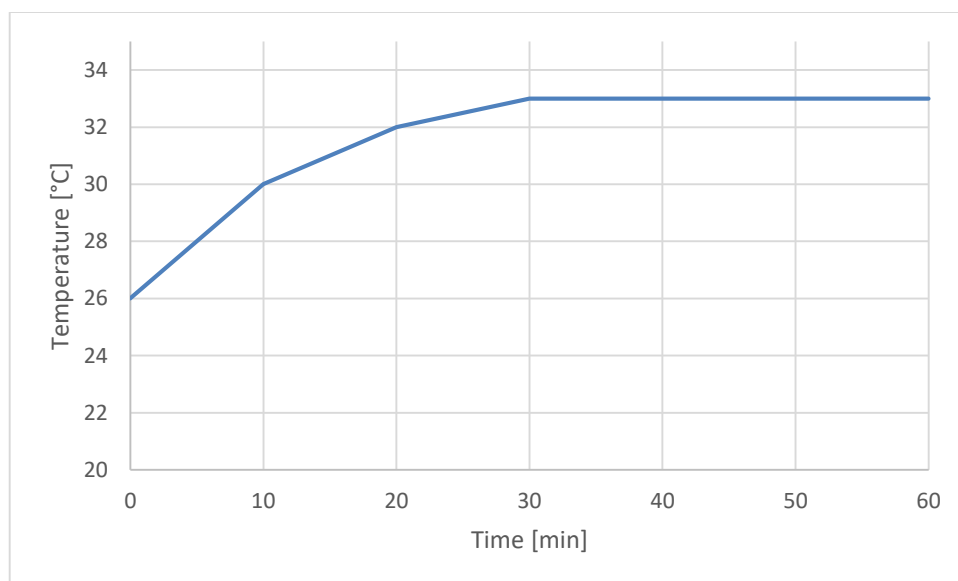


Figure 42 – Temperature measurements of the plasma DBD reactor operating at 20.5 kHz, 5% duty cycle.

### 7.5.4 Results of the plasma inactivation tests

Figure 43 shows the results of these inactivation tests. As before, each curve shown in Figure 43 corresponds to the average of a triplicate experiment. These triplicate experiments were conducted on the same day and from the same initial spore stock or cell suspension. Triplicate experiments were then repeated a further three times on different days and the average of all these experiments is shown in Figure 43 using solid black lines. The error bars represent the standard deviation.

<sup>47</sup> 307P, CIE test instruments, Kolkata, IN

<sup>48</sup> FLIR E30

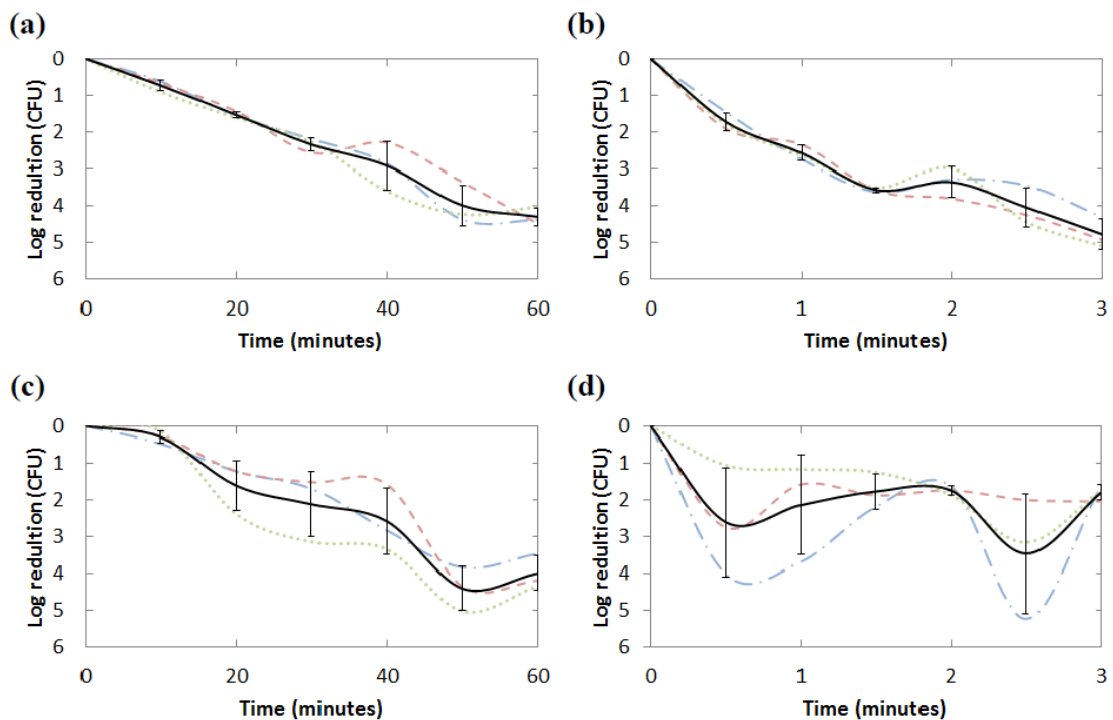


Figure 43 - Inactivation curves of (a) filtered *B. subtilis* spores, (b) filtered MRSA, (c) pipetted *B. subtilis* spores and (d) pipetted MRSA by exposure to air plasma.

For both microorganisms considered in this study, inactivation results determined from filtered samples are more reproducible than results from pipetted samples (compare Figure 43 a and c for *B. subtilis* and Figure 43 b and d for MRSA).

## 7.6 Conclusions

Of the four sample preparation methods considered in the plasma inactivation tests described in section 7.2, *B. subtilis* spores filtered onto membranes yielded the most reproducible results.

It is interesting to note that the inactivation kinetics of filtered *B. subtilis* spores undergoing UV irradiation (Figure 40) or plasma exposure (Figure 43) are distinct from one another. The UV inactivation kinetics show a bi-phasic characteristic whereas the plasma inactivation curve shows only a log-linear phase. This suggests that a different inactivation mechanism is at play when the cells are exposed to plasma.

The tailing of the inactivation curve has been attributed to a number of factors including an intrinsic lack of precision in the enumeration of low concentration of survivors, the presence of cell aggregates, heterogeneity of the population of micro-organisms, heterogeneity of treatment, and shielding from direct exposure to the biocidal agent. It is possible that the tailing phase in the plasma-treated samples is not observed at the doses considered in this work because plasma exposure comprises diffusible gaseous agents that can exhibit lethality even against stacks of cells for which UV irradiation is ineffective.

Spores of the Gram positive bacterium *Bacillus subtilis* (ATCC 6633) are proposed as a suitable reference biological agent for arriving at a valid assessment of the biocidal potential of gas plasma-generating devices. The advantages of using this particular bacterium are that it is non-pathogenic, and once produced, spores stocks can be kept for many years with only a negligible reduction in viability. Using spores from a stock obviates the need to produce micro-organisms at a particular phase of growth for each experimental trial, which reduces variability between experiments and speeds up the experimental procedures. In addition,

consistency in the form in which the biological agent is presented to the plasma was achieved by filtering under vacuum spore suspensions of known concentration through a polycarbonate membrane. This sample preparation technique was demonstrated to repeatedly minimise random cell stacking, a known source of variability in experimental tests. To demonstrate the advantages of the proposed protocol, we conducted inactivation tests using another micro-organism (methicillin resistant *Staphylococcus aureus* - MRSA) combined with the widely used sample preparation technique of pipetting cells suspensions onto membranes. Micro-organism laden membranes were exposed to either UV light at 254 nm or atmospheric pressure air plasma. In all cases, the proposed protocol required much shorter preparation time and resulted in greater reproducibility.

## CHAPTER 8

### 8 INFLUENCE OF DIFFERENT PRODUCTS ON ATMOSPHERIC AIR DBD PLASMA STERILIZATION

Ozone and NO<sub>x</sub> are, as previously described, the most important components found in the atmospheric pressure DBD discharge, when sterilization is the aim of the process. Ozone's role in this process have already been mentioned. It is a highly oxidative molecule that can easily damage the structure of a cell's membrane, undermining also the cellular breathing mechanisms. Ozone sterilization has been studied for decades and is industrially used for water sanitization, sterilization of medical instruments and food decontamination.

As previously said, it is clearly understood and most of the authors agree that air DBD plasmas' chemical compounds active in the sterilization process, especially for an indirect treatment, are ROS and RNS.

Choi, et al. [90] measured a D-value of 15.2 seconds for their sterilization of E. Coli using a symmetrical DBD device, claiming that "ozone molecules were the dominant germicidal species".

Despite the lower reduction potentials, NO<sub>x</sub> are also capable of enhancing the efficacy of a sterilization treatment. Other authors and inventors have developed and investigated sterilizing devices, claiming the usage of NO<sub>x</sub> compounds.

Mastanaiah, Navya, et al. [91] tried to understand the role of ozone in the process of plasma sterilization, with little success. The author showed that while ozone plays a primary role in the process of plasma sterilization of E. Coli, it is not the only agent responsible for sterilization, without any clear indication on the relative importance of those other components, suggesting that "future work should involve trying to understand which other factor complements ozone production and enhances the sterilization process."

Yoshino, et al. [92] developed a sterilization device using low-temperature atmospheric pressure plasma with circulating airflow. Using this device, they were able to sterilize G. steartothermophilus and B. atrophaeus spores completely in 25 min with 5,400 ppm and in 35 min with 7,600 ppm of plasma-generated NO<sub>x</sub>, respectively, at around 25 °C. "The developed device has the operating rapidity of sterilization equivalent to an autoclave, and it can operate sterilization process at much lower temperature than the commercial devices."

Pavlovich, et al. [93] studied the antimicrobial properties of a spark discharge in air. The main products of this device are 90% NO<sub>2</sub> and 10% NO. Other major species detected include N<sub>2</sub>O<sub>4</sub>, HNO<sub>2</sub> and HNO<sub>3</sub>. "Approximately 3000 ppm NO<sub>2</sub>, created within the first 3min of operation, is sufficient for rapid surface or water disinfection using E. coli as a model target microorganism."

Noxilizer, Inc. [94] have also patented a system or device for sterilizing a material using a mixture of NO and NO<sub>2</sub> as a sterilant gas. They claim compatibility with a variety of materials as stainless steel, polyethylene, silicone, aluminum... In this device, cylinders of liquid NO<sub>2</sub> is used as a convenient source for the sterilant gas. Paskalov, G [95] also developed an RF plasma-generated NO<sub>x</sub> sterilization device.

However, no other previous studies have clearly shown the relative importance O<sub>3</sub> and NO<sub>x</sub> have in an air plasma sterilization device. Now that a reactor design has been defined and a methodology to properly

estimate the microbiological effects of a plasma has been developed, it is time to investigate the influence and synergies  $O_3$  and  $NO_x$  have on plasma sterilization.

### 8.1 Reactor's discharge characterization

A study on the reactor's chemical yield could be performed. In this chapter, the bioreactor's chemical capabilities will be characterized by means of UV absorption spectroscopy, FTIR analysis and thermal measurements. The system will always operate in.

The setup of this experiment is shown in Figure 44. The custom-built surface DBD plasma device described in section 7.5.1 was fabricated (Figure 41). The system is operated with 2 l/min flowing ambient air provided by a gas flow controller<sup>49</sup> regulating the facility's filtered compressed air system flow. The afterglow of the discharge was then fed to an FTIR<sup>50</sup> for the chemical species identification. Additional information on the levels of  $O_3$  production rates were withdrawn from UV absorption spectroscopy of 254 nm photons inside the afterglow chamber<sup>51</sup>. The flow exiting the FTIR was filtered by an activated carbon filter and finally exhausted into the atmosphere.

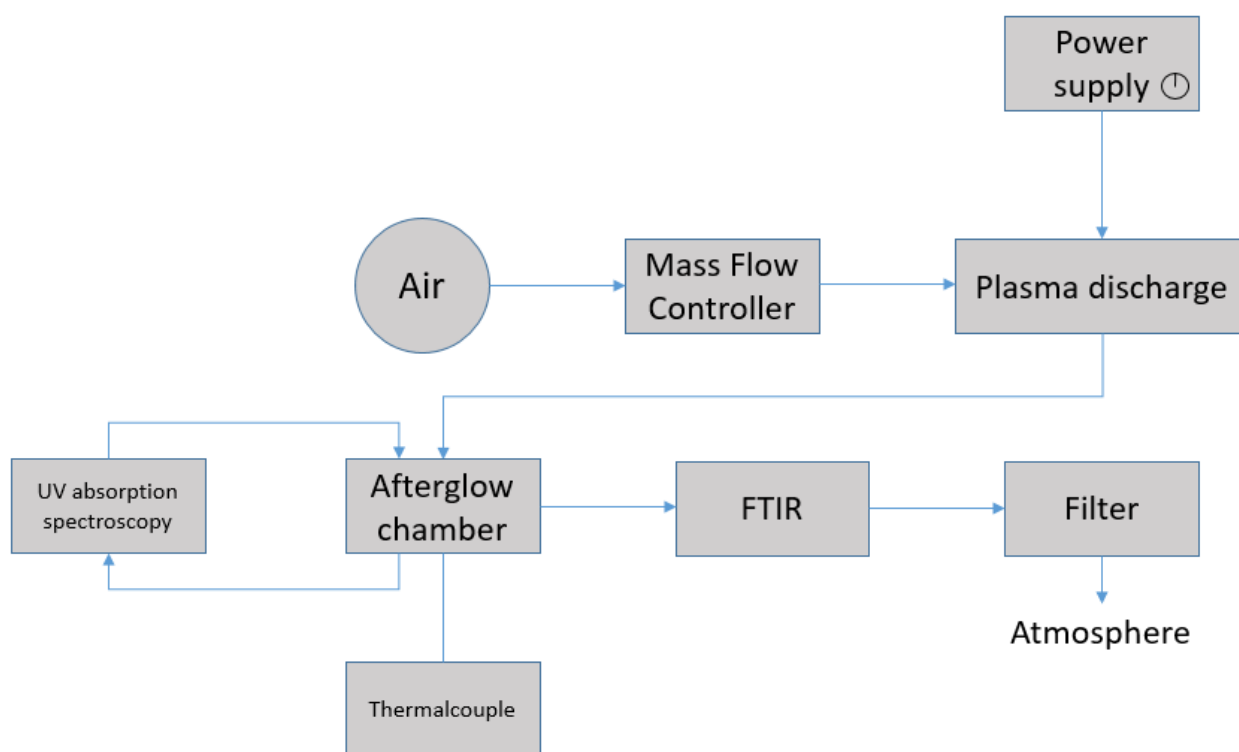


Figure 44 – Experimental setup.

The plasma source was powered by an in-house built half-bridge resonant power supply that delivered a sinusoidal voltage, two voltages were supplied to the reactor's electrodes: 10 kV and 11.5 kV. For those conditions, power was measured as 13 W and 17 W respectively. Additionally, the applied voltage could be modulated by a square signal of 2 Hz with a duty cycle set to 20% and 85%, reducing the power delivered to

<sup>49</sup> Bronkhorst F-201AI

<sup>50</sup> Jasco FT/IR 6600

<sup>51</sup> Ocean Optics LLS-250

the reactor accordingly. The time averaged power delivered to the plasma was determined by the analysis of the charge vs voltage (Q-V) Lissajous diagram [89].

### 8.1.1 Definition of two operating conditions

Different power levels not only results in a more intense discharge, but also a higher thermal contribution both from more energetic electrons and their slightly higher contribution to the macroscopic temperature, and joule heating effect.

We can then define two different operating conditions: the condition A, with the reactor powered by a 10 kV voltage, 20% duty cycle and an average power of 2.6 W. On the other hand, condition B will see the reactor powered by an 11.5 kV voltage, 85% duty cycle and an average power of 14.5 W<sup>52</sup>.

### 8.1.2 Influence of power on temperature

The maximum temperature reached during the reactor's operation in time was monitored using two K-type thermocouples<sup>53</sup> placed 2 mm below the plasma source (reactor temperature) and 10 cm downstream (afterglow chamber) during a 1 hour continuous operation. The plasma system was left to cool down to room temperature after each run.

Results are in Figure 45. They clearly show how the reactor's temperature increases by 1°C in the A condition and 14°C for the B one. Inside the afterglow chamber such variations are more limited: no changes are noticed in the case A, and a 3°C change for the case B is measured. A limited temperature variation is one of the reasons behind our decision to investigate only the indirect treatment effect on micro-organisms, since placing cells in direct contact with plasma could also result in thermal inactivation process triggering, which are not interesting from this work's perspective and should be avoided as much as possible.

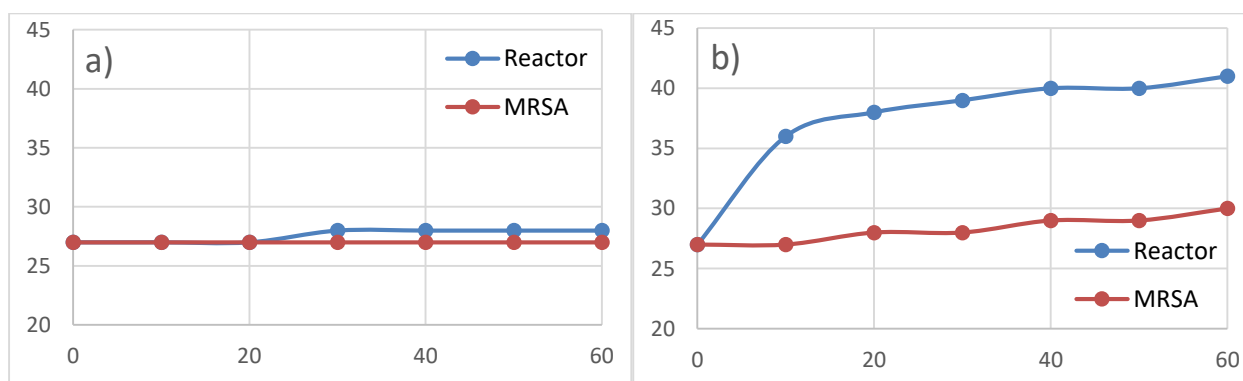


Figure 45 – Temperature measurements inside the plasma reactor (blue line) and for a 20% duty cycle (a) and 85% duty cycle (b).

### 8.1.3 Influence of power on chemistry

A study on the reactor's chemical yield was necessary to determine the typology of reactive species involved in the sterilization mechanism and to quantify their amount. The effects of a power increase on

<sup>52</sup> Those conditions were carefully selected by a trial and fail process. Their purpose was to try and identify two power levels that could be suitable for the peculiar method of investigation on the discharge chemistry employed later in this chapter (see section 8.1.3).

<sup>53</sup> 307P, CIE test instruments, Kolkata, IN. The thermocouple is profoundly influenced by the plasma due to the intense electromagnetic noise coupled with its ignition. In order to have an accurate readout, only values during the off-times of the discharge operated with a duty cycle were considered.

the chemistry of this specific setup were investigated, focusing on Ozone and NO<sub>x</sub> concentrations trends in time.

Power surely influences any plasma's intensity. This does not however mean that chemical reactions dynamics will surely increase as well. As previously seen in Table 1, chemical reactions' coefficients are deeply influenced by the macroscopic temperature. Previous studies on Ozone generation from a DBD discharge [15] pointed out how operating a reactor at higher voltages (therefore higher power levels) would benefit from the gas discharge intensity point of view, as a result of a higher electric field. However, "elevated temperature would decrease the ozone generation rate significantly". The mechanism responsible for this effect is discharge poisoning, and have already been extensively discussed in section 3.3.

#### 8.1.4 FTIR measurements

In order to measure O<sub>3</sub> and NO<sub>x</sub>, Fourier Transform Infrared Spectroscopy (FTIR)<sup>54</sup> have been used. UV absorption spectroscopy<sup>55</sup> was also implemented as shown in Figure 44, to confirm FTIR results on O<sub>3</sub>. Both instruments are based off the capability of a certain molecule to absorb photons of known wavelengths.

Ozone concentration has been evaluated from the absorption peaks at 1055 and 2122 cm<sup>-1</sup>, NO<sub>2</sub> at 1580 cm<sup>-1</sup>, N<sub>2</sub>O at 2237 cm<sup>-1</sup>, N<sub>2</sub>O<sub>5</sub> at 1240 and 1720 cm<sup>-1</sup> and HNO<sub>3</sub> at 1315 cm<sup>-1</sup>.

Experiments were performed in triplicate and the standard deviation between experiments was <10%. Results for O<sub>3</sub> concentration with 20% and 85% duty cycles are shown in Figure 46.

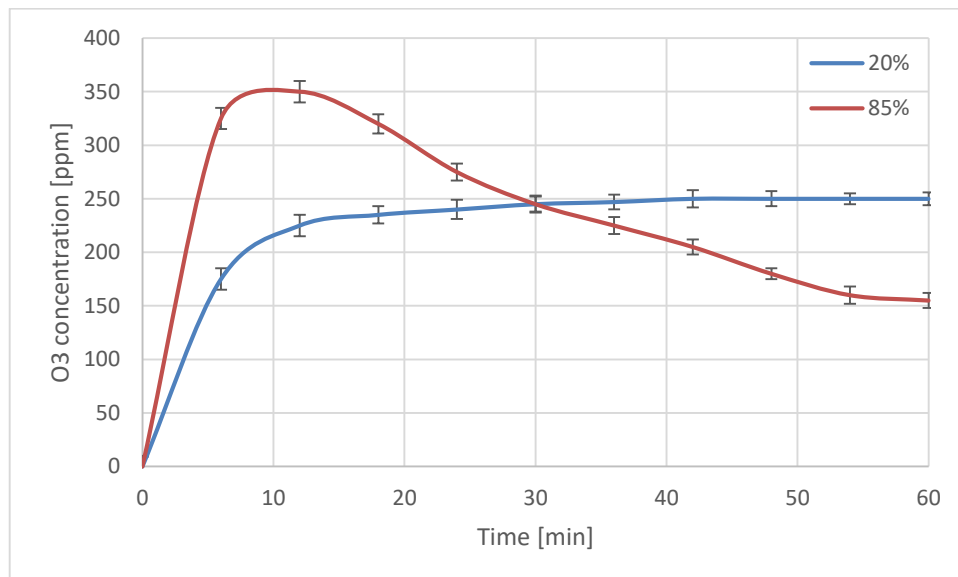


Figure 46 – Ozone concentration trends over time for 20% duty cycle operating condition (blue line) and 85% duty cycle operating condition (red line).

<sup>54</sup> Data gathered from Jasco FT/IR 6600 with 4 cm<sup>-1</sup> resolution and 1 mm/s scan speed.

<sup>55</sup> Two Ocean Optics 74-UV/VIS collimating lenses were mounted facing each other on the walls of the reactor to transmit and receive light emitted by an Ocean Optics LLS-250. An optical length of X mm was used. The time evolution of the light intensity at 254 nm was measured by means of an Ocean Optics USB2000+ spectrometer. Calculations were made on the average of 100 acquisitions with 1 ms exposure time.

Results for NO<sub>x</sub> concentration with 20% and 85% duty cycles are shown in the following figures.

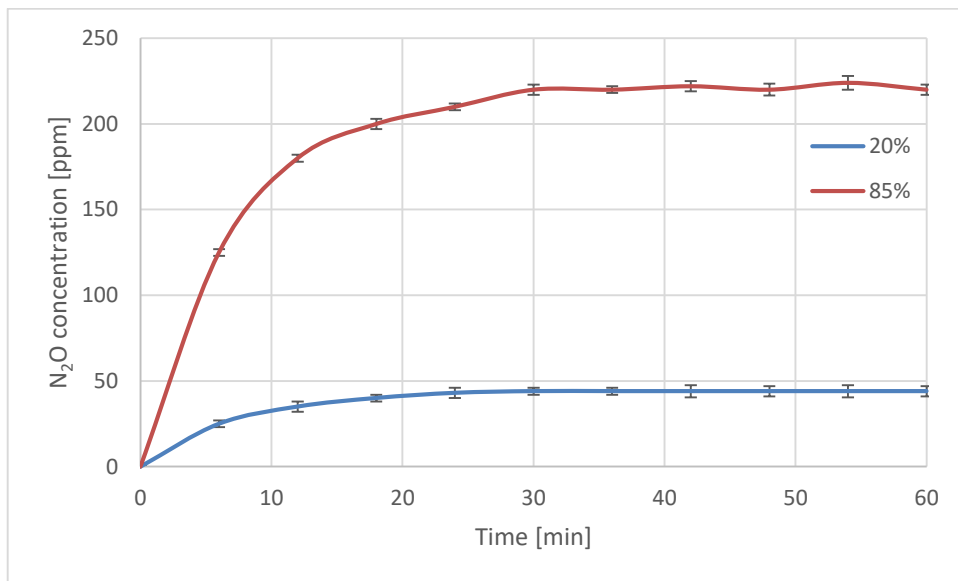


Figure 47 – N<sub>2</sub>O concentration trends over time for 20% duty cycle operating condition (blue line) and 85% duty cycle operating condition (red line).

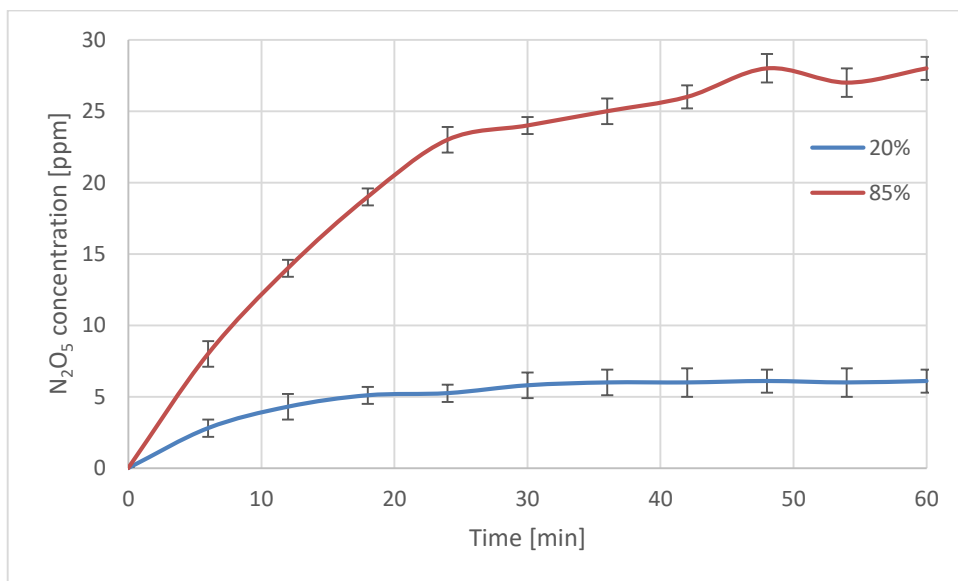


Figure 48 – N<sub>2</sub>O<sub>5</sub> concentration trends over time for 20% duty cycle operating condition (blue line) and 85% duty cycle operating condition (red line).

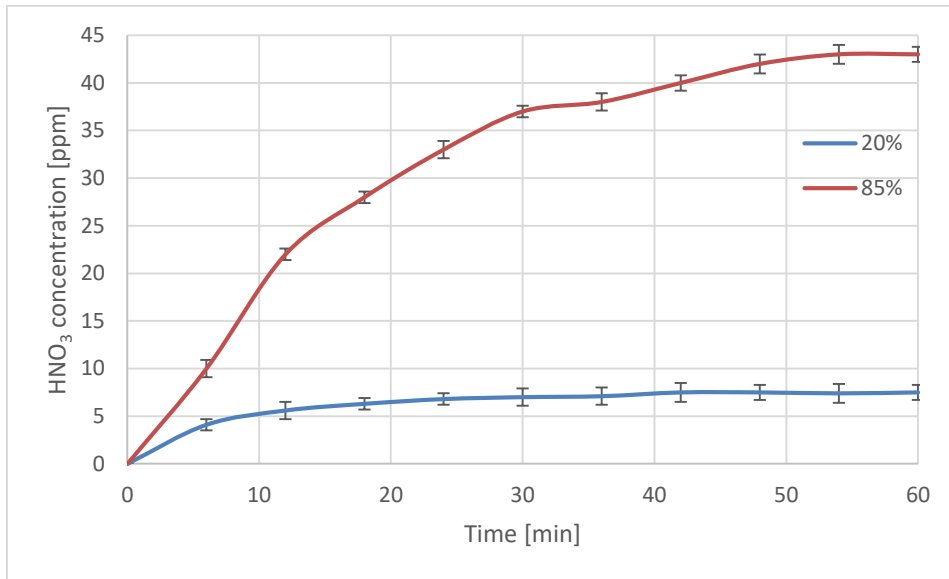


Figure 49 – HNO<sub>3</sub> concentration trends over time for 20% duty cycle operating condition (blue line) and 85% duty cycle operating condition (red line).

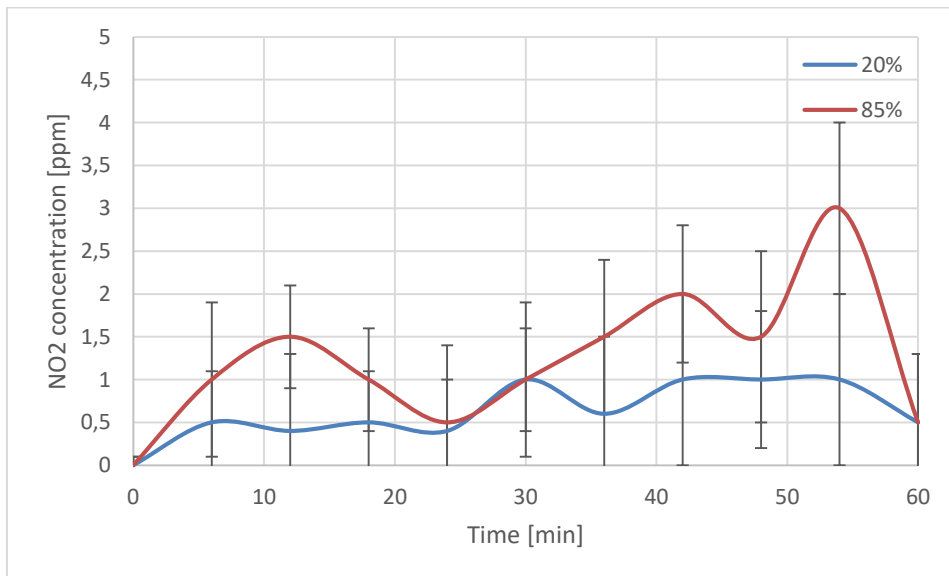


Figure 50 – NO<sub>2</sub> concentration trends over time for 20% duty cycle operating condition (blue line) and 85% duty cycle operating condition (red line).

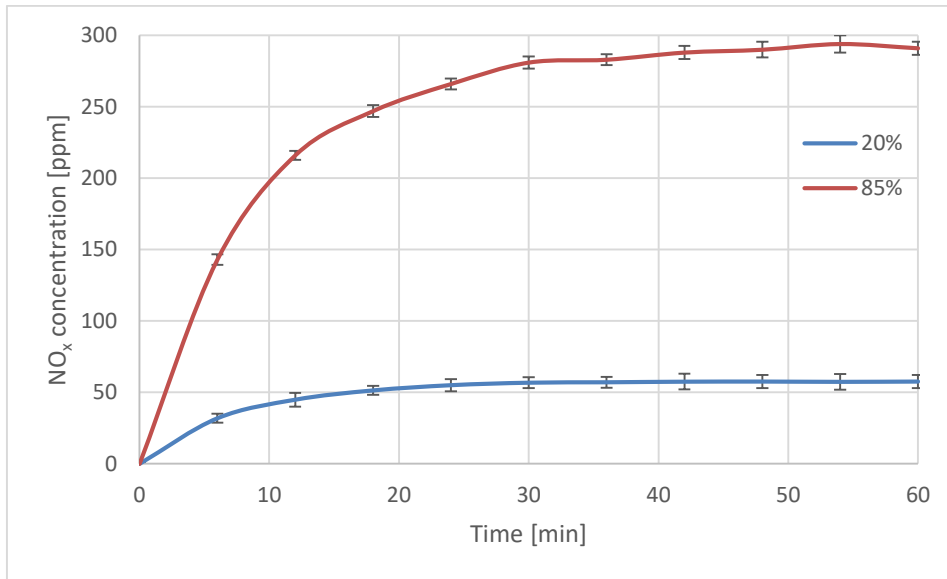


Figure 51 - NO<sub>x</sub> concentration trends over time for 20% duty cycle operating condition (blue line) and 85% duty cycle operating condition (red line).

Since a net increase in power should only increase the rate of all the reactions inside a plasma, and the thermal effects takes several minutes to reach a non-negligible level, we can see how ozone generated with a 20% duty cycle is steadily rising, eventually reaching a steady state concentration of 250 ppm. NO<sub>x</sub> in this case have a similar trend, reaching a maximum value of 45 ppm for N<sub>2</sub>O.

At higher power level (85% duty cycle), ozone is initially produced at a higher rate, as one would expect from a more intense plasma. 350 ppm is reached after 10 minutes only. After this, discharge poisoning mechanisms becomes prevalent. Ozone concentration drops to 200 ppm, while NO<sub>x</sub> concentration is increased up to 5 times the concentrations seen in the 20% duty cycle power setting.

Pavlovich, et al. [93] suggests that NO<sub>x</sub> compounds formation from plasmas in air is influenced by the discharge morphology and development: “NO is formed primarily in an initial transient spark regime and NO<sub>2</sub> forms later as NO is oxidized in various subsequent reactions. On a relative basis, NO is the first species to appear in the volume after initiating the discharge and when the plasma is extinguished, it disappears most rapidly. A discharge with predominantly, but not entirely, glow-like character appears to create the greatest concentration of NO<sub>2</sub> on the basis of the amount of energy expended.”

The very little presence of NO<sub>2</sub> can be explained by the relatively long residence time of the afterglow gases in the instrument and piping. Gentile, et al. [96] showed how N<sub>x</sub>O<sub>y</sub> compounds mixtures in plasmas have the tendency to drift their concentrations towards the most stable products, such as N<sub>2</sub>, N<sub>2</sub>O, NO<sub>2</sub>, HNO<sub>3</sub> and N<sub>2</sub>O<sub>5</sub>. Following the chemical reactions patterns pictured in Figure 52, one can see how during the long residence times inside the tubing and instruments of the experimental setup, most of the NO<sub>2</sub> can be converted into HNO<sub>3</sub> and N<sub>2</sub>O<sub>5</sub>, which is the end products found in those tests.

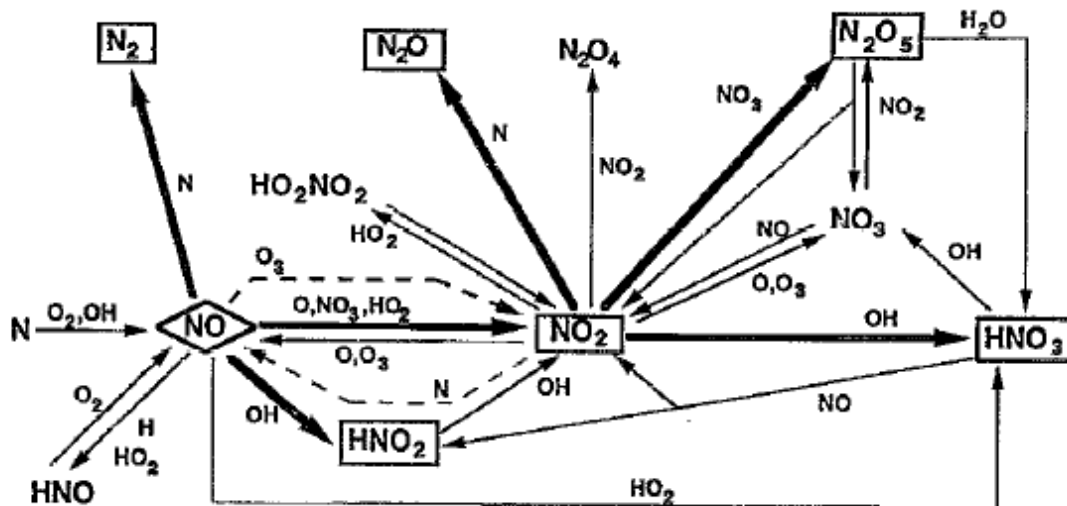


Figure 52 – Chemical reactions patterns involved in the formation of N<sub>x</sub>O<sub>y</sub>. Gentile, et al. [96]

### 8.1.5 Chemical doses

Power increase is clearly influencing chemistry in two opposite directions: it enhances the chemical yield and rate of production of reactive species, but on the other hand the increase in temperature that also comes with it will trigger the discharge poisoning and the partial removal of ozone from the produced afterglow air stream.

This typical behaviour of the discharge with increasing power was exploited in an uncommon manner to reliably perform two sterilizing regimes. Condition A can be used to provide a certain “dose” of O<sub>3</sub> with little amounts of NO<sub>x</sub>. On the other hand, condition B can provide the same dosage of O<sub>3</sub>, with higher NO<sub>x</sub> percentages. Doses coming from one hour treatments are provided by the following graphs:

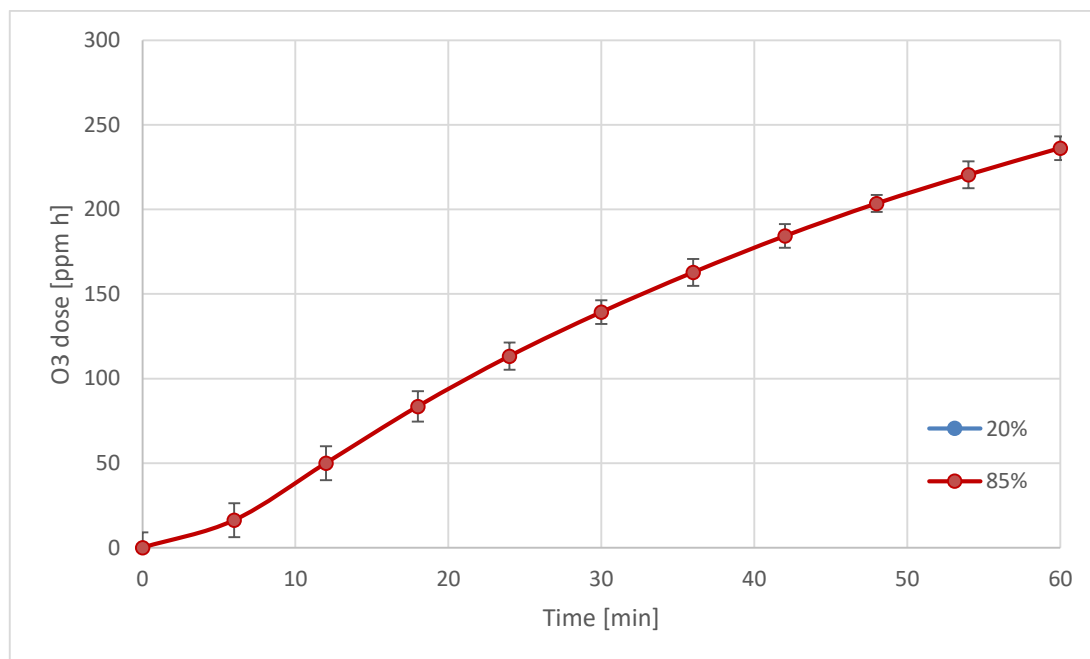


Figure 53 –Ozone dose delivered to the target sample over time for 20% duty cycle operating condition (blue line) and 85% duty cycle operating condition (red line).

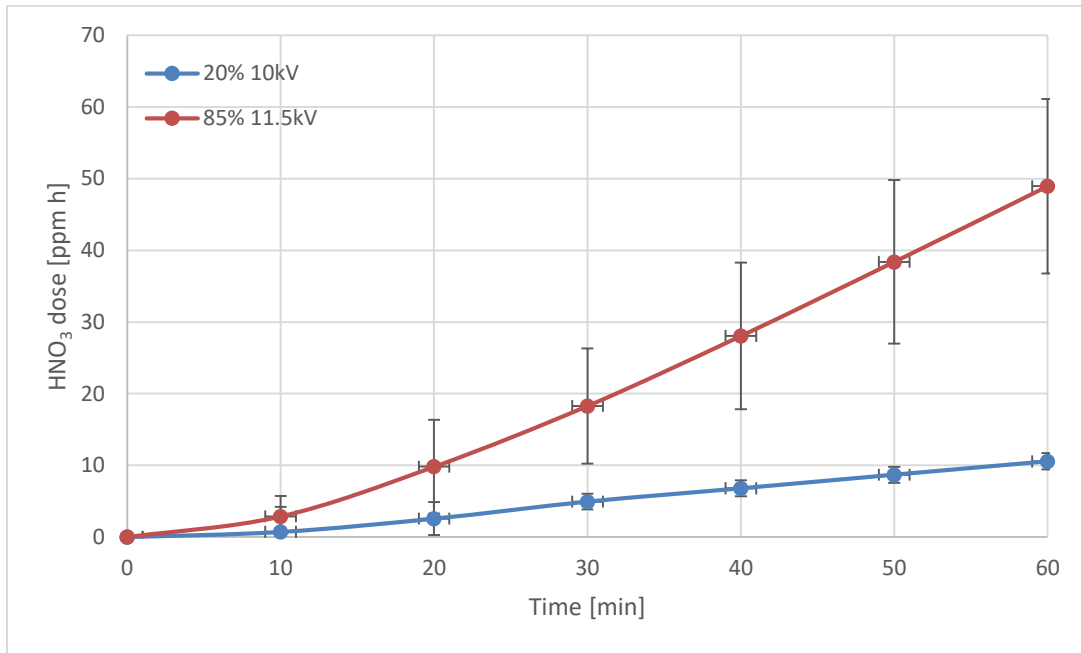


Figure 54 – HNO<sub>3</sub> dose delivered to the target sample over time for 20% duty cycle operating condition (blue line) and 85% duty cycle operating condition (red line).

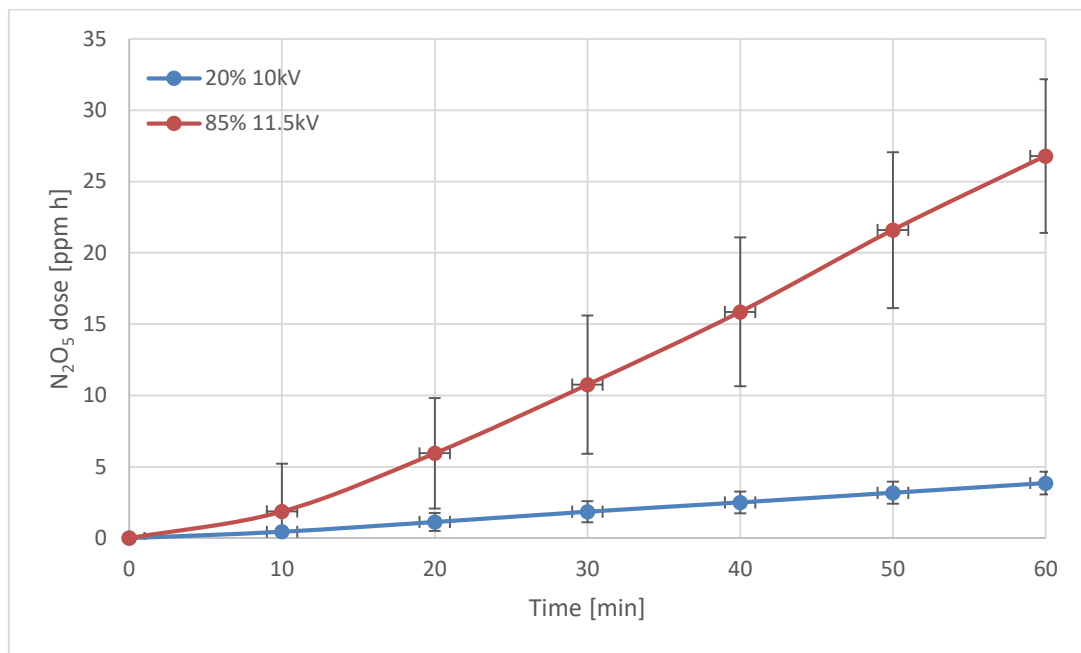


Figure 55 – N<sub>2</sub>O<sub>5</sub> dose delivered to the target sample over time for 20% duty cycle operating condition (blue line) and 85% duty cycle operating condition (red line).

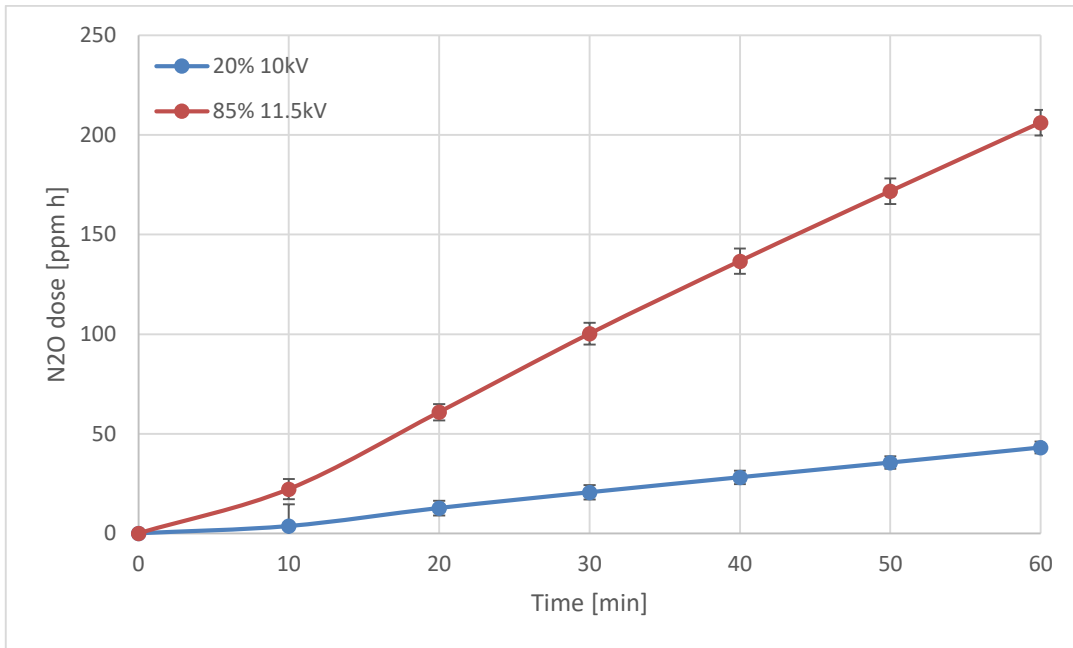


Figure 56 – N<sub>2</sub>O dose delivered to the target sample over time for 20% duty cycle operating condition (blue line) and 85% duty cycle operating condition (red line).

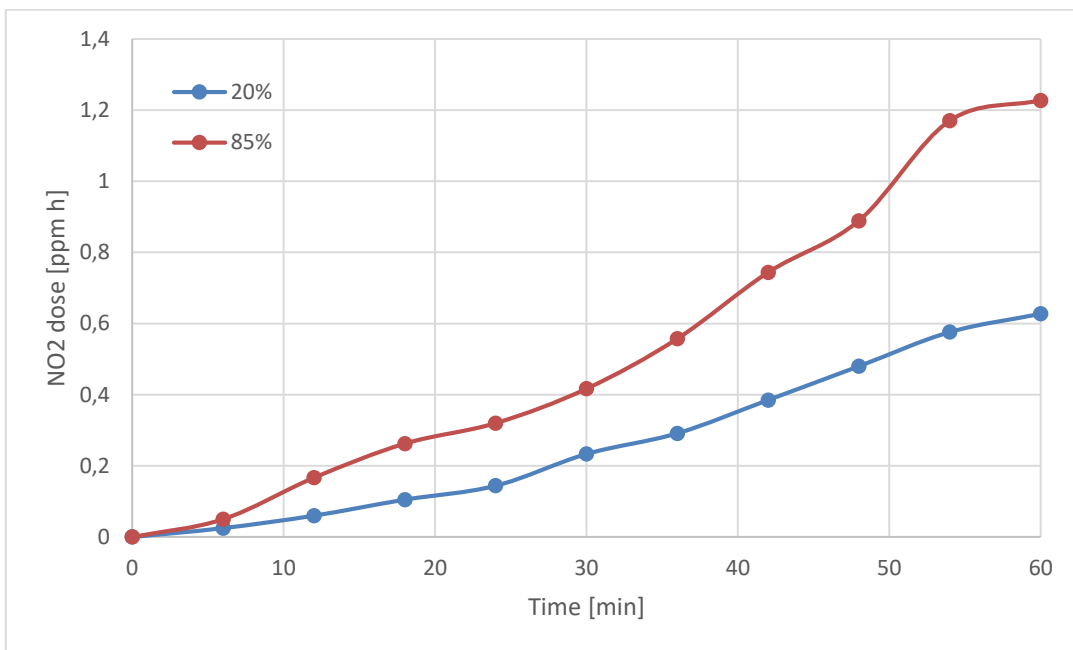


Figure 57 – NO<sub>2</sub> dose delivered to the target sample over time for 20% duty cycle operating condition (blue line) and 85% duty cycle operating condition (red line).

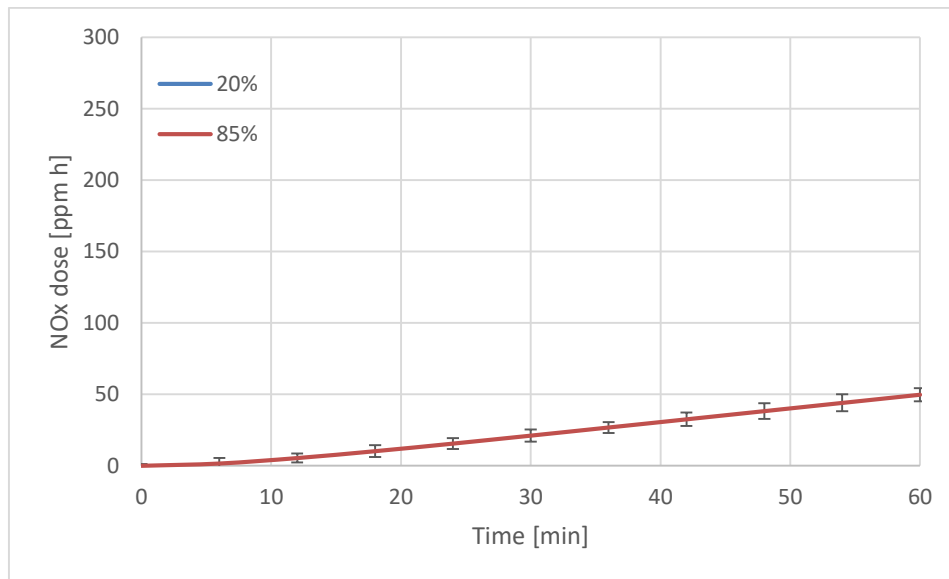


Figure 58 – Total NO<sub>x</sub> dose delivered to the target sample over time for 20% duty cycle operating condition (blue line) and 85% duty cycle operating condition (red line).

Any clear difference on plasma sterilization's efficacy when operating the discharge in those two conditions will surely and reliably provide the answer to this investigation: the importance and role of O<sub>3</sub> and NO<sub>x</sub> have on sterilization processes.

## 8.2 Plasma sanitization process

Since both O<sub>3</sub> and NO<sub>x</sub> are both stable products of the DBD discharge, an indirect treatment is a wise choice. This way no radicals or any other non-stable oxidizing species, or UV emission will influence the results of this experiment. Only the chemical species measured in section 8.1.3 will be in contact with the spores<sup>56</sup>.

Plasma is produced in a reactor chamber, in 2 l/min flowing ambient air. The plasma source was powered by with the setup and conditions seen above. The afterglow of the discharge is transported by a 10 cm PTFE tube into another chamber, where the spore-laden membranes are placed. The methodology to prepare *B. subtilis* laden membranes is the one described in section 7.2.1. Inside the afterglow chamber, *B. subtilis* spores will be inactivated by the stable chemical reactive species produced by the s-DBD plasma reactor with 1 hour treatments.

The air flow, still rich in reactive species, and potentially loaded with residual spores from the membrane surface<sup>57</sup>, is then filtered in an active carbon filter, and then released into the atmosphere.

Experiments were performed in triplicate and the standard deviation between experiments was less than 10%. Results from those treatments have been gathered with the same procedure shown in section 7.3, and are shown in Figure 59.

<sup>56</sup> In the case of this experiment to be reproduced on a different micro-organism, an additional reason to choose an indirect treatment instead of a direct one is temperature. According to section 8.1.2, while operating in the condition A, the reactor chamber reaches temperatures as high as 27°C, condition B would reach 41°C, potentially inactivating microbiological life by thermal mechanisms.

<sup>57</sup> Potential mechanical removal of spores from the air flow has been separately investigated. No appreciable spore reduction has been observed.

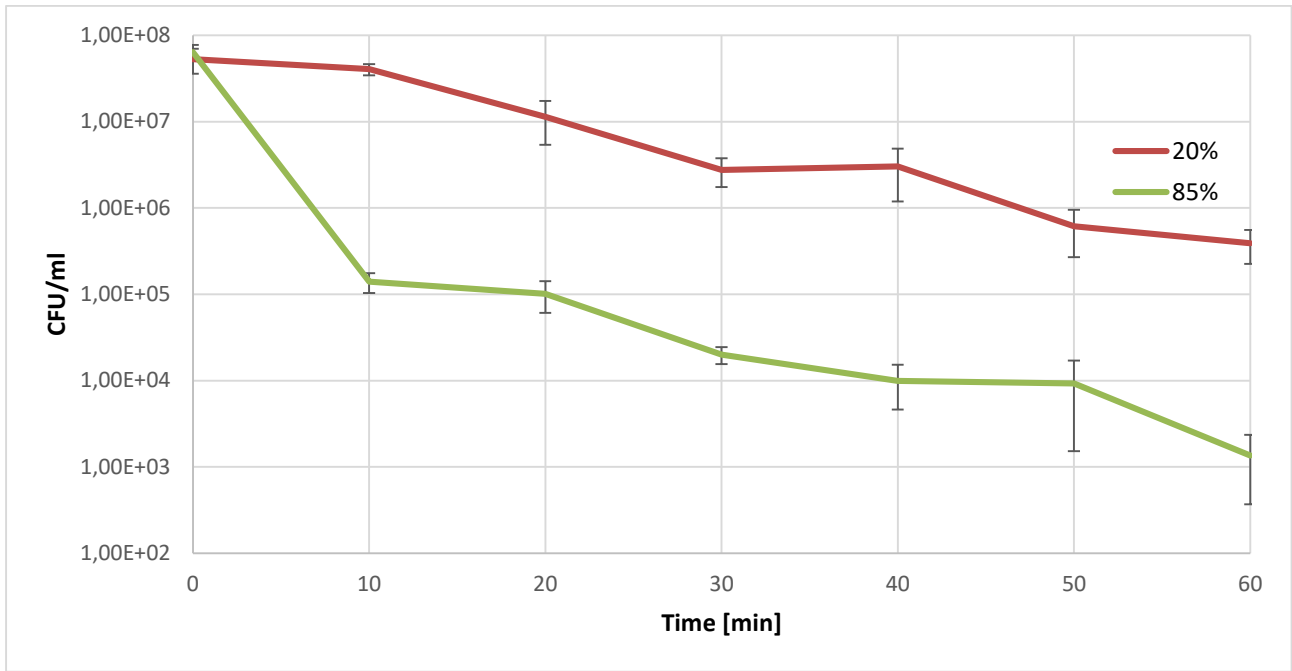


Figure 59 – Inactivation efficacies for the different treatment conditions: 20% duty cycle, 10 kV (blue line) and 85% duty cycle, 11.5 kV (red line).

### 8.3 Conclusions

Results clearly expose a difference in between the two operating conditions. A 2-log reduction and 18 minutes  $D_{10}$  value is observed after 1 hour treatment for the condition with high  $O_3$  and low  $NO_x$  concentrations. On the other hand, an increase in  $NO_x$  provided the same result after only 10 minutes. For this second condition, a 5-log reduction of spores viability is achieved after 1 hour treatments ( $D_{10} = 4$  minutes). The increase in  $NO_x$  concentration is therefore responsible for the 3-log increase with this particular treatment procedure.

The addition of a dose of  $NO_x$  comparable to the dose of  $O_3$  produced by the discharge contributes to reduce the inactivation times roughly to half. This means that among other reactive products of a cold DBD plasma devices, half of the inactivation processes *efficacy* on microbiological life has to be ascribed to  $NO_x$  species. A reduction of  $O_3$  dose,  $\Delta D_{O_3}$ , due to the discharge poisoning when increasing the device's power levels is compensated when an increase in  $NO_x$  dose,  $\Delta D_{NO_x}$ , is also verified. A complete compensation fits the next empirical equation:

$$\Delta D_{O_3} \approx \Delta D_{NO_x}$$

However, one should also not forget that the increase in performances verified with a high- $NO_x$  concentration condition also implies a high power delivery to the electrodes. Power consumption for the 85% duty cycle case is circa 5 times higher than the 20% duty cycle case. This can represent a problem since materials get more stressed over time and thermal or reliability problems may arise as a consequence.

## 9 CONCLUSIONS

Given the numerous uncertainties regarding the products of a cold atmospheric plasma, understanding the importance of each one of those components is a top research priority in plasma medicine.

In this work, the role reactive nitrogen species have on plasma sterilization has been studied. This Ph. D. thesis focuses in particular on the indirect plasma sterilization of two micro-organisms and two operating conditions. A specific design and procedure have been developed prior to the microbiological investigation, in order to increase the precision and reliability of the results.

Fluid-dynamics influence on final results were suppressed after an investigation regarding the impact of geometrical parameters on annular EHD actuators. The influence of electrodes diameters on EHD effect was evaluated and characterized through velocity profiles measurements and schlieren imaging. Other studies suggested that EHD effect can play a big role in delivering chemical species onto a target [40]. This analysis eventually suggested the correct design for a good optimization of annular actuators that could entirely prevent the formation of ionic winds from the electrode surfaces of our DBD reactor (or maximize it, when the effect is needed for different applications).

Part of the obscurity surrounding the results gathered from different authors testing the inactivation efficacy of the same plasma devices and similar operating conditions on microbiological life must be ascribed to the different procedures used for the preparation and treatment of their samples.

Spores of *Bacillus subtilis* (ATCC 6633) are proposed as a suitable reference biological agent for arriving at a valid assessment of the biocidal potential of gas plasma-generating devices. This bacterium is non-pathogenic, and once produced, spores stocks can be kept for many years with only a negligible reduction in viability. This obviates the need to produce micro-organisms at a particular phase of growth for each experimental trial, which reduces variability between experiments and speeds up the experimental procedures.

In addition, consistency in the form in which the biological agent is presented to the plasma was achieved by filtering under vacuum spore suspensions of known concentration through a polycarbonate membrane. The presence of random cells or spores aggregates and the subsequent shielding from direct exposure to the biocidal agent that the common pipetting deposition provides is adding an additional source of noise to the results found in the literature. The sample filtering technique developed in this work was demonstrated to repeatedly minimise random cell stacking, a known source of variability in experimental tests.

This was demonstrated testing four preparation methods, using two different microbiological agents (MRSA cells and *B. subtilis* spores), two deposition methods (filtering and the more common pipetting) and two inactivation treatments (254 nm UV light and DBD plasma). Results showed how the inactivation dataset of filtered *B. subtilis* spores was the most reliable for both UV and plasma treatments efficacy estimations.

The final estimation of reactive nitrogen species' role in plasma inactivation mechanisms has been made studying the efficacy of a DBD plasma reactor equipped with an array of annular actuators providing no EHD effect, using the most reliable samples preparation procedure previously developed. After the characterization of the discharge products via FTIR measurements, two operating conditions were selected providing the target with the same dose ozone but different NO<sub>x</sub> levels (a low and a high level one).

Half of the inactivation processes *efficacy* was credited to NO<sub>x</sub> species. Clear different results from the two operating conditions suggest that a higher concentration of NO<sub>x</sub> provides better inactivation performances

of the discharge. Ozone remains a main player involved during inactivation of micro-organisms, but higher NO<sub>x</sub> concentrations are also desirable, when the discharge poisoning or thermal problems are not triggered.

In conclusion, the results gathered from those experiments can seriously influence the design choices of any DBD air plasma device and the optimization of its operating conditions during the sterilization process. A properly optimized device should be operated with the highest NO<sub>x</sub> yield, as soon as this does not reduce the O<sub>3</sub> delivery rate by the following empirical formula:

$$\Delta D_{O_3} \leq \Delta D_{NO_x}$$

Where  $\Delta D_{O_3}$  and  $\Delta D_{NO_x}$  are respectively the decrease and increase of O<sub>3</sub> and NO<sub>x</sub> doses after a change in the plasma operating conditions.

## 10 Bibliography

1. Michelmore, Andrew, et al. "Nanoscale deposition of chemically functionalised films via plasma polymerisation." *RSC Advances* 3.33 (2013): 13540-13557.
2. Fridman, Alexander. *Plasma chemistry*. Cambridge university press, 2008.
3. Bruggeman, P. J., et al. "Gas temperature determination from rotational lines in non-equilibrium plasmas: a review." *Plasma Sources Science and Technology* 23.2 (2014): 023001.
4. Siemens, Werner. "Ueber die elektrostatische Induction und die Verzögerung des Stroms in Flaschendrähnen." *Annalen der Physik* 178.9 (1857): 66-122.
5. Machala, Z., et al. "Emission spectroscopy of atmospheric pressure plasmas for bio-medical and environmental applications." *Journal of Molecular Spectroscopy* 243.2 (2007): 194-201.
6. Kogelschatz, Ulrich, Baldur Eliasson, and Walter Egli. "From ozone generators to flat television screens: history and future potential of dielectric-barrier discharges." *Pure and Applied Chemistry* 71.10 (1999): 1819-1828.
7. Chirokov, A., A. Gutsol, and A. Fridman. "Atmospheric pressure plasma of dielectric barrier discharges." *Pure and applied chemistry* 77.2 (2005): 487-495.
8. Fridman, A., A. Chirokov, and A. Gutsol. "Non-thermal atmospheric pressure discharges." *Journal of Physics D: Applied Physics* 38.2 (2005): R1.
9. Orlov, Dmitri M., Gabriel I. Font, and Daniel Edelstein. "Characterization of discharge modes of plasma actuators." *AIAA journal* 46.12 (2008): 3142-3148.
10. Enloe, C. L., et al. "Surface potential and longitudinal electric field measurements in the aerodynamic plasma actuator." *AIAA journal* 46.11 (2008): 2730-2740.
11. Kogelschatz, Ulrich. "Filamentary, patterned, and diffuse barrier discharges." *IEEE Transactions on plasma science* 30.4 (2002): 1400-1408.
12. Kogelschatz, Ulrich. "Atmospheric-pressure plasma technology." *Plasma Physics and Controlled Fusion* 46.12B (2004): B63.
13. B. Eliasson and S. Straessler, *Bull. Am. Phys. Soc.* 28, 183 (1983)
14. Macchi, Andrea. "Appunti su scariche di plasma per applicazioni tecnologiche." CNR-INFM, Dipartimento di Fisica E. Fermi, Università di Pisa (2007).
15. Chang, Moo Been, and Shi-Jia Wu. "Experimental study on ozone synthesis via dielectric barrier discharges." (1997): 241-254.
16. Stefanovic, I., et al. "Kinetics of ozone and nitric oxides in dielectric barrier discharges in O<sub>2</sub>/NO<sub>x</sub> and N<sub>2</sub>/O<sub>2</sub>/NO<sub>x</sub> mixtures." *Plasma Sources Science and Technology* 10.3 (2001): 406.
17. Hadj-Ziane, S., et al. "Ozone generation in an oxygen-fed wire-to-cylinder ozonizer at atmospheric pressure." *Journal of Physics D: Applied Physics* 25.4 (1992): 677.
18. Atkinson, R., et al. "Evaluated kinetic and photochemical data for atmospheric chemistry: Supplement IV: IUPAC subcommittee on gas kinetic data evaluation for atmospheric chemistry." *Atmospheric Environment. Part A. General Topics* 26.7 (1992): 1187-1230.
19. Campbell, I. M., and C. N. Gray. "Rate constants for O (3P) recombination and association with N (4S)." *Chemical Physics Letters* 18.4 (1973): 607-609.
20. Atkinson, R., et al. "Evaluated kinetic, photochemical and heterogeneous data for atmospheric chemistry: Supplement V. IUPAC Subcommittee on Gas Kinetic Data Evaluation for Atmospheric Chemistry." *Journal of Physical and Chemical Reference Data* 26.3 (1997): 521-1011.

21. Atkinson, R., et al. "Evaluated kinetic and photochemical data for atmospheric chemistry: Part 1? gas phase reactions of Ox, HOx, NOx and SOx species." *Atmospheric Chemistry and Physics Discussions* 3.6 (2003): 6179-6699.
22. Mericam-Bourdet, Nicolas, et al. "Effect of voltage waveform on dielectric barrier discharge ozone production efficiency." *The European Physical Journal Applied Physics* 57.3 (2012): 30801.
23. Nester, Eugene W., et al. *Microbiology*. No. 2nd edition. Holt, Rinehart and Winston., 1978.
24. Shintani, Hideharu, et al. "Gas plasma sterilization of microorganisms and mechanisms of action (Review)." *Experimental and therapeutic medicine* 1.5 (2010): 731-738.
25. Laroussi, Mounir. "Low temperature plasma-based sterilization: overview and state-of-the-art." *Plasma processes and polymers* 2.5 (2005): 391-400.
26. Moisan, M., et al. "Low-temperature sterilization using gas plasmas: a review of the experiments and an analysis of the inactivation mechanisms." *International journal of Pharmaceutics* 226.1 (2001): 1-21.
27. Shaw, Alex, Gilbert Shama, and Felipe Iza. "Emerging applications of low temperature gas plasmas in the food industry." *Biointerphases* 10.2 (2015): 029402.
28. Niemira, Brendan A. "Cold plasma decontamination of foods\*." *Annual review of food science and technology* 3 (2012): 125-142.
29. Misra, N. N., et al. "Nonthermal plasma inactivation of food-borne pathogens." *Food Engineering Reviews* 3.3-4 (2011): 159-170.
30. Von Woedtke, Th, et al. "Plasmas for medicine." *Physics Reports* 530.4 (2013): 291-320.
31. Kong, Michael G., et al. "Plasma medicine: an introductory review." *New Journal of Physics* 11.11 (2009): 115012.
32. Fridman, Gregory, et al. "Applied plasma medicine." *Plasma Processes and Polymers* 5.6 (2008): 503-533.
33. Kim, Yun-Jung, et al. "Plasma apparatuses for biomedical applications." *IEEE Transactions on Plasma Science* 43.4 (2015): 944-950.
34. Weltmann, K-D., et al. "Plasma processes and plasma sources in medicine." *Contributions to Plasma Physics* 52.7 (2012): 644-654.
35. Iza, Felipe, et al. "Microplasmas: sources, particle kinetics, and biomedical applications." *Plasma Processes and Polymers* 5.4 (2008): 322-344.
36. Xingmin, Shi, et al. "Experimental research of inactivation effect of low-temperature plasma on bacteria." *Plasma Science and Technology* 8.5 (2006): 569.
37. Miao, Hu, and Guo Yun. "The sterilization of Escherichia coli by dielectric-barrier discharge plasma at atmospheric pressure." *Applied Surface Science* 257.16 (2011): 7065-7070.
38. Sun, Yanzhou, et al. "Experimental research on inactivation of bacteria by using dielectric barrier discharge." *IEEE Transactions on Plasma Science* 35.5 (2007): 1496-1500.
39. Ma, Yue, et al. "Chemical mechanisms of bacterial inactivation using dielectric barrier discharge plasma in atmospheric air." *IEEE transactions on plasma science* 36.4 (2008): 1615-1620.
40. Taglioli, Matteo, et al. "EHD-driven mass transport enhancement in surface dielectric barrier discharges." *Plasma Sources Science and Technology* 25.6 (2016): 06LT01.
41. Pavlovich, Matthew J., Douglas S. Clark, and David B. Graves. "Quantification of air plasma chemistry for surface disinfection." *Plasma Sources Science and Technology* 23.6 (2014): 065036.
42. European Cooperation in Science and Technology (COST) Action MP1101: "Biomedical Applications of Atmospheric Pressure Plasma Technology"  
[http://www.cost.eu/COST\\_Actions/mpns/Actions/MP1101](http://www.cost.eu/COST_Actions/mpns/Actions/MP1101)

43. Wassmann, Marko, et al. "Growth phase-dependent UV-C resistance of *Bacillus subtilis*: data from a short-term evolution experiment." *Archives of microbiology* 193.11 (2011): 823-832.
44. Yu H, Perni S, Shi JJ, Wang DZ, Kong MG, and Shama G 2006 *J. Appl. Microbiol.* 101 1364
45. Link, L., et al. "Extreme spore UV resistance of *Bacillus pumilus* isolates obtained from an ultraclean spacecraft assembly facility." *Microbial ecology* 47.2 (2004): 159-163.
46. Bayliak, M., H. Semchyshyn, and V. Lushchak. "Effect of hydrogen peroxide on antioxidant enzyme activities in *Saccharomyces cerevisiae* is strain-specific." *Biochemistry (Moscow)* 71.9 (2006): 1013-1020.
47. Kossakowska, Monika, et al. "Discovering the mechanisms of strain-dependent response of *Staphylococcus aureus* to photoinactivation: oxidative stress toleration, endogenous porphyrin level and strain's virulence." *Photodiagnosis and photodynamic therapy* 10.4 (2013): 348-355.
48. Perni S, Shama G, Hobman J L, Lund P A, Kershaw C J, Hidalgo-Arroyo G A, Penn C W, Deng X, Walsh J L and Kong M G 2007 *Appl. Phys. Lett.* 90 073902
49. Noriega, Estefanía, et al. "Cold atmospheric gas plasma disinfection of chicken meat and chicken skin contaminated with *Listeria innocua*." *Food microbiology* 28.7 (2011): 1293-1300.
50. Laroussi, M., and F. Leipold. "Evaluation of the roles of reactive species, heat, and UV radiation in the inactivation of bacterial cells by air plasmas at atmospheric pressure." *International Journal of Mass Spectrometry* 233.1 (2004): 81-86.
51. Choi, Jai Hyuk, et al. "Analysis of sterilization effect by pulsed dielectric barrier discharge." *Journal of electrostatics* 64.1 (2006): 17-22.
52. Mastanaiah, Navya, et al. "Examining the role of ozone in surface plasma sterilization using dielectric barrier discharge (DBD) plasma." *Plasma Processes and Polymers* 10.12 (2013): 1120-1133.
53. Laroussi, Mounir. "Low temperature plasma-based sterilization: overview and state-of-the-art." *Plasma processes and polymers* 2.5 (2005): 391-400.
54. M. Gad-El-Hak. *Flow Control*. Cambridge: Cambridge University Press; 2000.
55. Benard, N., et al. "Airflow control by non thermal plasma actuator: application to control of separation of an air jet naturally attached along the bevel of an axisymmetric diffuser." 42ème Colloque d'Aérodynamique Appliquée AAAF, Sofia-Antipolis, 19-21 Mars 2007. 2007.
56. Cristofolini, A., et al. "Schlieren imaging in a dielectric barrier discharge actuator for airflow control." *Journal of Applied Physics* 111.3 (2012): 033302.
57. Martina Fabbri et al., "The effect of plasma surface modification on the biodegradation rate and biocompatibility of a poly(butylene succinate)-based copolymer" *Polymer Degradation and Stability* 09/2015; 121. DOI:10.1016/j.polymdegradstab.2015.09.015.
58. Amano, Isamu, et al. "Sterilization using a wide-gap discharge formed by dielectric barrier discharge coupled with surface discharge under atmospheric pressure." *Industry Applications Conference, 2007. 42nd IAS Annual Meeting. Conference Record of the 2007 IEEE. IEEE, 2007.*
59. Wang, Chin-Cheng, and Subrata Roy. "Three-dimensional simulation of a microplasma pump." *Journal of Physics D: Applied Physics* 42.18 (2009): 185206.
60. Ouyang, Chien. "Plasma cooling heat sink." U.S. Patent Application No. 12/157,233.
61. Cristofolini, Andrea, Carlo A. Borghi, and Gabriele Neretti. "Charge distribution on the surface of a dielectric barrier discharge actuator for the fluid-dynamic control." *Journal of Applied Physics* 113.14 (2013): 143307.
62. Borghi, Carlo A., et al. "A plasma aerodynamic actuator supplied by a multilevel generator operating with different voltage waveforms." *Plasma Sources Science and Technology* 24.4 (2015): 045018.

63. Cristofolini, A., et al. "Experimental and numerical investigation on a DBD actuator for airflow control." AIAA Paper (2011): 2011-3912.
64. Benard, Nicolas, and Eric Moreau. "Electrical and mechanical characteristics of surface AC dielectric barrier discharge plasma actuators applied to airflow control." *Experiments in Fluids* 55.11 (2014): 1-43.
65. Nishida, Hiroyuki, and Takashi Abe. "Validation study of numerical simulation of discharge plasma on DBD plasma actuator." 42nd AIAA Plasmadynamics and Lasers Conf. 2011.
66. Mamunuru, Meenakshi, et al. "Plasma actuator simulation: Force contours and dielectric charging characteristics." AIAA Paper 1221 (2010): 1-9.
67. Neretti, Gabriele, et al. "Experimental results in DBD plasma actuators for air flow control." *Plasma Science, IEEE Transactions on* 40.6 (2012): 1678-1687.
68. Lai, Koon Chun. Performance analysis of a dielectric barrier discharge (DBD) plasma actuator. Diss. Universiti Malaysia Sarawak, UNIMAS, 2009.
69. Debien, A., N. BenardP, and E. Moreau. "Single and multi-DBD plasma actuators based on wire HV electrode." 30th ICPIG, August 28th–September 2nd (2011).
70. Riherd, Mark, and Subrata Roy. "Serpentine geometry plasma actuators for flow control." *Journal of applied physics* 114.8 (2013): 083303.
71. M. Kotsonis, S. Ghaemi. Performance improvement of plasma actuators using asymmetric high voltage waveforms. *Journal of Physics D: Applied Physics*. 2012;45(045204). DOI: 10.1088/0022-3727/45/4/045204.
72. Santhanakrishnan, Arvind, and Jamey D. Jacob. "Flow control with plasma synthetic jet actuators." *Journal of Physics D: Applied Physics* 40.3 (2007): 637.
73. Debien, Antoine, Nicolas Benard, and Eric Moreau. "Streamer inhibition for improving force and electric wind produced by DBD actuators." *Journal of Physics D: Applied Physics* 45.21 (2012): 215201.
74. Tirumala, Rakshit, et al. "Temperature characterization of dielectric barrier discharge actuators: influence of electrical and geometric parameters." *Journal of Physics D: Applied Physics* 47.25 (2014): 255203.
75. Borghi, Carlo A., et al. "A plasma aerodynamic actuator supplied by a multilevel generator operating with different voltage waveforms." *Plasma Sources Science and Technology* 24.4 (2015): 045018.
76. G Correale, T Michelis, D Ragni, M Kotsonis, F Scarano. Nanosecond-pulsed plasma actuation in quiescent air and laminar boundary layer . *Journal of Physics D: Applied Physics*, 2014 44 (4), 045204.
77. F. A. Dragonas, G. Neretti, P. Sanjeevikumar, G. Grandi, "High-Voltage High-Frequency Arbitrary Waveform Multilevel Generator for DBD Plasma Actuators", *IEEE Transactions on Industry Applications*, Volume PP, Issue 99, 2015, DOI 10.1109/TIA.2015.2409262.
78. Riherd, Mark, and Subrata Roy. "Serpentine geometry plasma actuators for flow control." *Journal of applied physics* 114.8 (2013): 083303.
79. M. Kotsonis, S. Ghaemi. Performance improvement of plasma actuators using asymmetric high voltage waveforms. *Journal of Physics D: Applied Physics*. 2012;45(045204). DOI: 10.1088/0022-3727/45/4/045204.
80. Santhanakrishnan, Arvind, and Jamey D. Jacob. "Flow control with plasma synthetic jet actuators." *Journal of Physics D: Applied Physics* 40.3 (2007): 637.
81. Setlow, Peter. "Spores of *Bacillus subtilis*: their resistance to and killing by radiation, heat and chemicals." *Journal of applied microbiology* 101.3 (2006): 514-525.

82. Cano, Raul J., and Monica K. Borucki. "Revival and identification of bacterial spores in 25-to 40-million-year-old Dominican amber." *Science* 268.5213 (1995): 1060.
83. Perni S, Deng X T, Shama G and Kong M G 2006 *IEEE Trans. Electron Devices* 34 1297–303
84. Oshita, Takaya, et al. "Temperature Controllable Atmospheric Plasma Source." *IEEE Transactions on Plasma Science* 43.6 (2015): 1987-1992.
85. Thornsberry, Clyde, J. Q. Caruthers, and Carolyn N. Baker. "Effect of temperature on the in vitro susceptibility of *Staphylococcus aureus* to penicillinase-resistant penicillins." *Antimicrobial agents and chemotherapy* 4.3 (1973): 263-269.
86. Welch, WILLIAM D., and PAUL M. Southern. "Unusual susceptibility of methicillin-resistant *Staphylococcus aureus* to erythromycin, clindamycin, gentamicin, and tetracycline at 30 degrees C but not at 35 degrees C." *Journal of clinical microbiology* 19.6 (1984): 831-833.
87. Härnult, B. G., and B. G. Snygg. "Heat resistance of *Bacillus subtilis* spores at various water activities." *Journal of applied bacteriology* 35.4 (1972): 615-624.
88. Bayliss, Danny L., et al. "Complex responses of microorganisms as a community to a flowing atmospheric plasma." *Plasma Processes and Polymers* 9.6 (2012): 597-611.
89. Manley, T. C. "The electric characteristics of the ozonator discharge." *Transactions of the electrochemical society* 84.1 (1943): 83-96.
90. Choi, Jai Hyuk, et al. "Analysis of sterilization effect by pulsed dielectric barrier discharge." *Journal of electrostatics* 64.1 (2006): 17-22.
91. Mastanaiah, Navya, et al. "Examining the role of ozone in surface plasma sterilization using dielectric barrier discharge (DBD) plasma." *Plasma Processes and Polymers* 10.12 (2013): 1120-1133.
92. YOSHINO, Daisuke, et al. "Development of low-temperature sterilization device using atmospheric pressure air plasma with circulating flow." *Mechanical Engineering Journal* 2.5 (2015): 15-00187.
93. Pavlovich, M. J., et al. "Air spark-like plasma source for antimicrobial NO<sub>x</sub> generation." *Journal of Physics D: Applied Physics* 47.50 (2014): 505202.
94. Vaughn, Ernst, et al. "Sterilization system and method." U.S. Patent No. 8,703,066. 22 Apr. 2014.
95. Paskalov, George. "Sterilization Using Plasma Generated NO<sub>x</sub>." U.S. Patent Application No. 13/712,373.
96. Gentile, Ann C., and Mark J. Kushner. "Reaction chemistry and optimization of plasma remediation of NxOy from gas streams." *Journal of applied physics* 78.3 (1995): 2074-2085.